Zircon U-Pb constraints on the timing of Sveconorwegian migmatite formation in the Western and Median Segments of the Idefjorden terrane, SW Sweden

Mimmi Ingered

Dissertations in Geology at Lund University,
Master's thesis, no 558
(45 hp/ECTS credits)

Department of Geology
Lund University
2019

Zircon U-Pb constraints on the timing of Sveconorwegian migmatite formation in the Western and Median Segments of the Idefjorden terrane, SW Sweden

Master's thesis

Mimmi Ingered

Department of Geology
Lund University
2019

Contents

Cover Picture: Garnet-bearing migmatized gneiss with amphibolite layers, north of Hälltorp. Author for scale. Photo by Anna Sartell.

Zircon U-Pb constraints on the timing of Sveconorwegian migmatite formation in the Western and Median Segments of the Idefjorden terrane, SW Sweden

MIMMI INGERED

Ingered, M., 2019: Zircon U-Pb constraints on the timing of Sveconorwegian migmatite formation in the Western and Median Segments of the Idefjorden terrane, SW Sweden. *Dissertations in Geology at Lund University*, No. 558, 36 pp. 45 hp (45 ECTS credits).

Abstract: The Western and Median Segments of the Idefjorden terrane have been metamorphosed and migmatized during the Sveconorwegian orogeny (ca. 1 Ga), but the timing of these events between the two segments remains unclear. Here I show that Sveconorwegian metamorphism and associated migmatite formation is not coeval between the Western and Median Segments and that there is a contrast between the segments in terms of strain, migmatite abundance and retrograde metamorphic overprint. Magmatic crystallization ages were determined through U -Pb spot dating on zircon using Laser Ablation Inductively Coupled Plasma Mass Spectrometry (LA-ICP-MS). Zircon cores with Th/U >0.2 yields an age of 1551±6 Ma for the Arsjön migmatite in the Western Segment, 1349±5 Ma for the Tösslanda migmatite within the Göta Älv Shear Zone, and 1601±3 Ma and 1581±8 Ma respectively for the Hälltorp migmatites in the Median Segment. Zircon in leucosome yield dates of 1073±31 Ma for the Arsjön migmatite, 1046±21 Ma for the Tösslanda migmatite and 1019±27 Ma for the Hälltorp migmatites. The dates of the zircon rims are interpreted to be ages of metamorphism and migmatization and are supported by Th/U values around 0.02. The metamorphic ages are coeval with Sveconorwegian metamorphism in the Idefjorden terrane (1.14 -0.90 Ga), but the results demonstrate that Sveconorwegian metamorphism and migmatite formation occurred earlier in the Western Segment than in the Median Segment.

Keywords: Geochronology, Sveconorwegian orogen, U-Pb, Zircon, Migmatite, Idefjorden terrane, Western Segment, Median Segment

Supervisor: Anders Scherstén

Subject: Bedrock Geology

Mimmi Ingered, Department of Geology, Lund University, Sölvegatan 12, SE-223 62 Lund, Sweden.
E-mail: mimmi.ingered@gmail.com

U-Pb-datering av zirkon från Svekonorvegiska migmatiter i Västra segmentet respektive Mediansegmentet i Idefjordenterrängen, sydvästra Sverige.

MIMMI INGERED

Ingered, M., 2019: Zirkon U-Pb datering av Svekonorvegiska migmatiter i Västra segmentet och Mediansegmentet i Idefjordenterrängen, sydvästra Sverige . *Examensarbeten i geologi vid Lunds universitet*, Nr. 558, 36 sid. 45 hp.

Sammanfattning: Det Västra segmentet och Mediansegmentet i Idefjordenterrängen omarbetades under metamorfos och migmatitbildning under den Svekonorvegiska orogenesen (ca. 1 Ga), men det råder fortfarande oklarheter kring tidpunkterna för dessa händelser inom och mellan de två segmenten. Denna studie visar att Svekonorvegisk metamorfos och associerad migmatitbildning inte är samtida i Västra segmentet och Mediansegmentet, samt att deformation, retrograd metamorf överprägling och mängden migmatiter kontrasterar mellan segmenten. Magmatiska kristallationsåldrar bestämdes med U-Pb-datering av zirkon genom laserablation och induktivt kopplad plasma masspektrometri (LA-ICP-MS). Zirkonkärnor med Th/U >0,2 ger en ålder av 1551±6 Ma för Arsjönmigmatiten i Västra segmentet, 1349±5 Ma för Tösslandamigmatiten i Göta Älv zonen, samt 1601±3 Ma respektive 1581±8 Ma för Hälltorpmigmatiterna i Mediansegmentet. Zirkon i leukosom ger 1073±31 Ma för Arsjönmigmatiten, 1046±21 Ma för Tösslandamigmatiten och 1019±27 Ma för Hälltorpmigmatiterna. Dateringarna av tillväxterna tolkas som åldern för metamorfos och migmatitbildning och stöds av Th/U runt 0,02. De metamorfa åldrarna är samtida med Svekonorvegisk metamorfos i Idefjordenterrängen (1.14-0.90 Ga), men resultaten visar att Svekonorvegisk metamorfos och migmatitbildning inträffade tidigare i Västra segmentet än i Mediansegmentet.

Nyckelord: Geokronologi, Svekonorvegiska orogenesen, U-Pb, Zirkon, Migmatit, Idefjordenterrängen, Västra Segmentet, Mediansegmentet.

Handledare: Anders Scherstén

Ämnesinriktning: Berggrundsgeologi

Mimmi Ingered, Geologiska institutionen, Lunds Universitet, Sölvegatan 12, 223 62 Lund, Sverige.
E-post: mimmi.ingered@gmail.com

1 Introduction

The Sveconorwegian orogen in southwestern Fennoscandia includes several tectonothermal terranes that are divided by major shear zones. The terranes were reworked in the Sveconorwegian orogeny at the end of the Mesoproterozoic (Bingen et al. 2005; Bingen et al. 2008b). The Sveconorwegian orogen is interpreted to have formed as a continent-continent collision between proto-Fennoscandia and another continent around 1.0 Ga (Bingen et al. 2005; Bingen et al. 2008b), although an accretionary orogen has also been suggested (Slagstad et al. 2013). The Idefjorden terrane, bound by the Mylonite Zone in the east and the Vardefjell Shear Zone in the northwest, was subdivided into the Western and Median Segments by Berthelsen (1980). These segments are structurally different from each other and might have been affected by the Sveconorwegian orogen to different extent in terms of deformation and preserved mineral assemblage. The segments are divided by the Göta Älv Shear Zone south of lake Vänern (Park et al. 1991). Migmatite gneisses are abundant within the Idefjorden terrane, but the age of these migmatites and the relative timing of migmatite formation between the different segments remain unclear. Since the available geochronological data on migmatites in the Idefjorden terrane is limited, it is uncertain if migmatite formation also occurred during the 1.64-1.52 Ga Gothian orogeny (Bingen et al. 2005). Recent results from radiometric dating of migmatite formation in the Median Segment determines the age to 1002±9 Ma (Ingered 2017). This result demonstrates that Sveconorwegian migmatite formation was associated with ductile isoclinal folding and that crustal melting did occur in the Idefjorden terrane. However, the regional extent of Sveconorwegian migmatites in the Idefjorden terrane remains unclear, and so far no Sveconorwegian migmatites have been recorded in the Western Segment. Here I present new zircon U-Pb data from migmatites around Lilla Edet from both the Western and Median Segments of the Idefjorden terrane. Electron imaging and zircon U-Pb dating through LA-ICP-MS (Laser Ablation Inductively Coupled Plasma Mass Spectrometry) analysis have been used to obtain ages of migmatite formation in the Idefjorden terrane. Field observations and petrography were also used to describe structural and textural differences of the migmatites on either side of the Göta Älv Shear Zone. The main research questions were:

1) Are Sveconorwegian migmatites widely spread in the Median Segment?
2) Are Sveconorwegian migmatites present in the Western Segment?
   A) If yes, are they equal in extent and style to those of the Median Segment?
   B) If yes, was migmatite formation coeval between the Western and Median Segments?

2 Background

2.1 Regional Geology

The 1.14-0.90 Ga Sveconorwegian orogen in southwestern Fennoscandia extends across southern Norway and through southwestern Sweden (Fig. 1) (Bingen et al. 2005; Bingen et al. 2008b). It is a tectonic counterpart to the Grenville Province in Canada and traditionally interpreted to have formed by a continent-continent collision with another craton, possibly Amazonia (Bingen et al. 2005; Bingen et al. 2008a,b ; Möller & Andersson 2018). This conventional collision theory was questioned by Slagstad et al. (2013) where the Sveconorwegian belt has rather been explained as an accretionary orogen with periodic compression and extension.

The Sveconorwegian orogen is bounded to the east by the Sveconorwegian Frontal Deformation Zone (SFDZ) and the Protogine Zone, and to the northwest by the Caledonides (Wahlgren et al. 1994; Bingen et al. 2008b). East of the Protogine Zone lies the Transscandinavian Igneous Belt and the Svecofennian Province (Gorbatschev & Bogdanova 1993). The Sveconorwegian orogen is made up of five large lithotectonic units, separated by roughly N-S trending shear zones. The units are in order from west to east; Telemarkia, Bamble, Kongsberg, Idefjorden and Eastern Segment (Bingen et al. 2008b).

Bingen et al. (2008b) divides the Sveconorwegian orogeny into four phases, named Arendal, Agder, Falkenberg and Dalane. The Sveconorwegian assembly is illustrated in Fig. 1 and the scenario works for both an indigenous and an exotic Telemarkia terrane (Bingen et al. 2008b).

The Arendal phase (1140-1080 Ma) is characterized by high-grade metamorphism in the Bamble and Kongsberg terranes. The lithologies in the terranes are similar to the lithologies in both the Telemarkia and Idefjorden terranes, and it is therefore believed that the Bamble and Kongsberg tectonic wedges were formed by a collision between the Idefjorden and Telemarkia terranes (Bingen et al. 2008b and references therein). According to Bingen et al. (2008b) the time between 1080 Ma and 1050 Ma marked a period of tectonic quiescence in the Sveconorwegian orogen followed by the main Sveconorwegian orogenic event, the Agder phase. As mentioned above, the Agder phase (1050-980 Ma) reflects the possible continent-continent collision between Fennoscandia and another craton, possibly Amazonia (Bingen et al. 2005; Bingen et al. 2008b). This led to crustal thickening and imbrication in the centre of orogen affecting both the Telemarkia and Idefjorden terranes (Bingen et al 2008b). High-pressure conditions (1.0-1.5 GPa) in the Idefjorden terrane took place at 1050 Ma due to underthrusting and burial beneath the Telemarkia terrane to a depth of at least 35 km (Bingen et al 2008b; Söderlund et al. 2008). At the same time granitoid plutons intruded the Telemarkia terrane, followed by tectonic imbrication of the terrane at 1035 Ma reaching medium-pressure

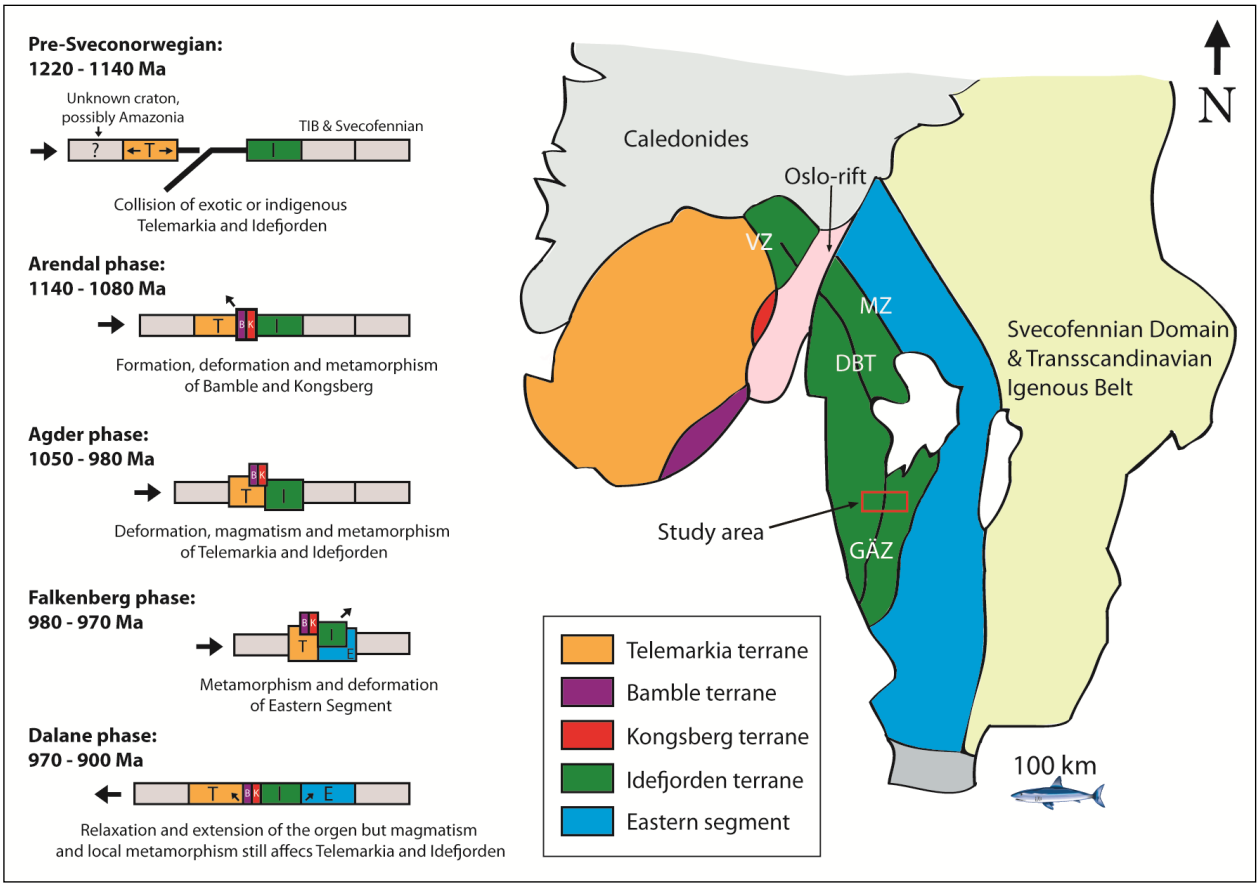

Fig. 1. *Left*: Schematic model of the four phases: Arendal, Agder, Falkenberg and Dalane of the Sveconorwegian orogeny, redrawn after Bingen et al. (2008b). *Right*: Illustration of the Sveconorwegian orogen showing the main lithotectonic units and shear zones. VZ = Vardefjell Shear Zone, MZ = Mylonite Zone, GÄZ = Göta Älv Shear Zone and DBT = Dalsland Boundary Thrust. Redrawn after Bingen et al. (2008b).

granulite facies metamorphism (Bingen et al. 2008b).

At 980-970 Ma, the Falkenberg phase represents the last step of convergence represented by high-grade metamorphism in the Eastern Segment (Bingen et al. 2008b). Eclogites in the Eastern Segment, dated at 988±6 Ma, provide evidence of burial of the segment to a depth of ~65 km, shortly followed by divergence and exhumation (Möller et al. 2015; Tual et al. 2017). Andersson et al. (2002) and Ahlin et al. (2006) also provide evidence of metamorphism and migmatization along the Mylonite Zone and the Göta Älv Shear Zone around 980-970 Ma. The orogen collapsed after 970 Ma and entered the Dalane phase (970-900 Ma). This period was characterized by extension and relaxation, associated with post-collisional magmatism in the Telemarkia and Idefjorden terranes peaking at 930-920 Ma (Bingen et al. 2008b and references therein).

2.1.1 Telemarkia terrane

The allochthonous Telemarkia terrane (Fig. 1) in southern Norway is characterized by voluminous 1.52-1.48 Ga magmatism which produced volcanic and plutonic suites interlayered with metasedimentary rocks. These rocks were intruded by magmatic suites and overlain by sediments between 1.28 and 1.13 Ga (Bingen et al. 2008b and references therein). Sveconorwegian plutonism and metamorphism started around 1.05 Ga during the Agder phase and continued to ca. 0.92 Ga (Bogdanova et al. 2008; Bingen et al. 2008b; Slagstad et al. 2013). The Sveconorwegian metamorphism in the Telemarkia terrane ranges from greenschist to granulite-facies (Bingen et al. 2008b; Bogdanova et al. 2008).

2.1.2 Bamle and Kongsberg terranes

The Bamble and Kongsberg terranes (Fig. 1) in southeast Norway consists of metamorphosed 1.57-1.46 Ga plutonic and volcanic rocks intercalated with metasedimentary rocks (Bingen et al. 2008b and references therein; Engvik et al. 2016). The terranes form two small wedges overlying the Telemarkia terrane and according to Bingen et al. (2005) the Bamble and Kongsberg terranes could have formed from a collision between the Telemarkia and Idefjorden terranes (Bingen et al. 2008b; Petersson et al. 2015). Several magmatic suites intruded both the Bamble and Kongsberg terranes at around 1.20-1.15 Ga (Bingen et al. 2008b; Robert & Slagstad 2014; Engvik et al. 2016). The terranes give evidence of two Sveconorwegian metamorphic phases reaching amphibolite to granulite-facies. The first phase is limited to the Bamble terrane and is dated 1.14-1.12 Ga (Arendal phase), while the

second phase affected both the Bamble and Kongsberg terranes at around 1.11-1.08 Ga (Arendal phase; Bingen et al. 2008b,c and references therein; Engvik et al. 2016).

2.1.3 Idefjorden terrane

The allochthonous Idefjorden terrane (Fig. 1) lies immediately to the west of Eastern Segment and is delimited to the east by the Mylonite Zone (Bingen et al. 2008b). The terrane is made up of 1.66-1.53 Ga granitoid plutons, volcanic rocks, gneisses and metagraywacke sequences assembled during the Gothian (1.66-1.52 Ga) accretionary event (Bingen et al. 2008b; Petersen et al 2015). Berthelsen (1980) divided the terrane into the Median and the Western Segment, originally termed the Östfold slab. This internal subdivision will be used in this study when discussing the Idefjorden terrane. The Median and Western Segments (Fig. 2) are separated by the Dalsland Boundary Thrust north of lake Vänern, continuing as the Ørje Shear Zone in Norway (Berthelsen 1980; Bingen et al. 2008b). The boundary between the segments south of lake Vänern corresponds to the Göta Älv Shear Zone (Park et al. 1991). The Median Segment is made up of 1.63-1.59 Ga plutonic granitoids, volcanic dacites and intercalated sedimentary rocks, belonging to the Göteborg-Åmål Suite (Åhäll & Connelly 2008; Austin Hegardt 2010). The segment also comprises the older 1.66 Ga Horred formation with metavolcanic rocks and the early Sveconorwegian (1.1 Ga) volcanic and sedimentary Dal formation (Brewer et al. 2002; Åhäll & Connelly 2008).

The Western Segment contains 1.58-1.52 Ga intrusive granitic rocks belonging to the Hisingen suite and 1.59-1.55 Ga metasedimentary graywackes with minor metabasalts, termed the Stora Le-Marstrand (SLM) formation (Åhäll & Connelly 2008). A large granite batholith, the Bohus granite, also intruded the northern coast of the Western Segment at ca. 0.92 Ga (Eliasson & Schöberg 1991). The Kungsbacka Bimodal Suite (1.34-1.30 Ga) overlaps both the Median and Western Segments and forms a belt of granitic plutons along the Göta Älv Shear Zone and the Dalsland Boundary Thrust (Austin Hegardt et al. 2007).

Sveconorwegian metamorphism in the Idefjorden terrane took place between 1.05 and 0.98 Ga, during the Agder phase, and the metamorphic grade ranged from greenschist-facies to amphibolite-facies (Bingen et al. 2008b). Local high-pressure granulite-facies in mafic granulite boudins have also been reported by Söderlund et al. (2008) east of the Göta Älv Shear Zone.

2.1.4 Eastern Segment

The parautochthonous Eastern Segment (Fig. 1) in Sweden forms the easternmost unit affected by the Sveconorwegian orogeny and is mostly comprised of metamorphosed and deformed rocks belonging to the Transscandinavian Igneous Belt (Söderlund et al. 1999; Söderlund et al. 2002; Andersson et al. 2002). The unit is delimited to the east by the Sveconorwegian Frontal Deformation Zone and the Protogine Zone, and to the west by the west-dipping Mylonite Zone (Wahlgren et al. 1994; Andersson et al. 2002). The majority of the rocks in the Eastern Segment are gneissic granitoids with protolith ages between 1.74-1.66 Ga, however overprinted by the 1.47-1.38 Ga Hallandian orogeny in the southern parts (Möller et al. 2007; Bingen et al. 2008b; Petersson et al. 2015; Ulmius et al. 2015). The Sveconorwegian metamorphism took place between 0.98-0.96 Ga, during the Falkenberg phase (Bingen et al. 2008b; Möller & Andersson 2018) in the Eastern Segment and reached upper amphibolite to high-pressure granulite-facies (Johansson et al. 1991; Andersson et al. 1999; Möller & Andersson 2018). Metamorphism also reached eclogite-facies conditions, limited to a tectonic unit southeast of the Mylonite Zone (Möller et al. 2015; Möller & Andersson 2018).

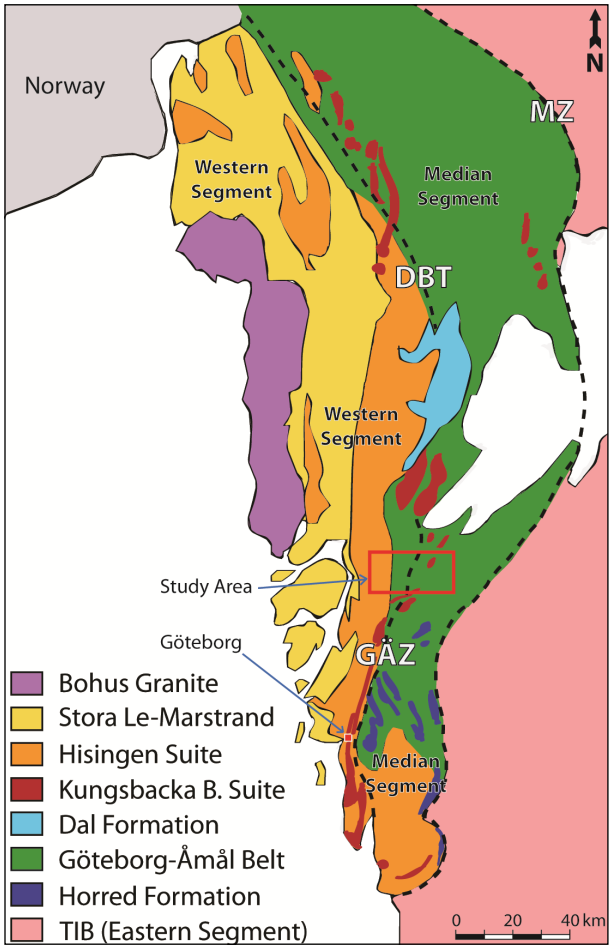

Fig. 2. Geological map of the Idefjorden terrane showing major bedrock units and shear zones. The Median and Western Segments are divided by GÄZ = Göta Älv Shear Zone and DBT = Dalsland Boundary Thrust. The Mylonite Zone (MZ) marks the boundary between the Idefjorden terrane to the west and the Eastern Segment to the east. TIB = Transscandinavian Igneous Belt, which in this case refers to the main composition of the Eastern Segment. Redrawn after Åhäll & Connelly (2008) and Austin Hegardt et al. (2005).

2.2 Locality Lilla Edet - field description

Lilla Edet lies 50 km north of Gothenburg, close to Trollhättan (Fig. 3) and by the river Göta Älv, within the Göta Älv Shear Zone. The bedrock in the area consists of north-south trending orthogneisses affected both by ductile and brittle deformation.

In the Western Segment (to the west of the Göta Älv Shear Zone) the bedrock is homogeneous and is made up of granitic to granodioritic gneisses and augen gneiss, of which some contain traces of muscovite. Garnet and hornblende have not been observed. Pegmatite bodies and dykes intrude the rocks and are rarely deformed. In one area around locality 3.1, small mafic lenses of amphibolite can be seen (Fig. 3c). Migmatitic rocks have been observed at locality 3.2 (Fig. 3c) where a granodioritic gneiss have been migmatized and folded (see section 4.1). Ductile deformation has been observed but not brittle deformation.

The bedrock in the Median Segment (to the east of the Göta Älv Shear Zone) is heterogeneous and consists of granitic to granodioritic gneisses, amphibolite and metamorphosed ultramafic rocks. The gneisses are often garnet-bearing and in some places contain hornblende and/or muscovite (see section 4.3). The mafic

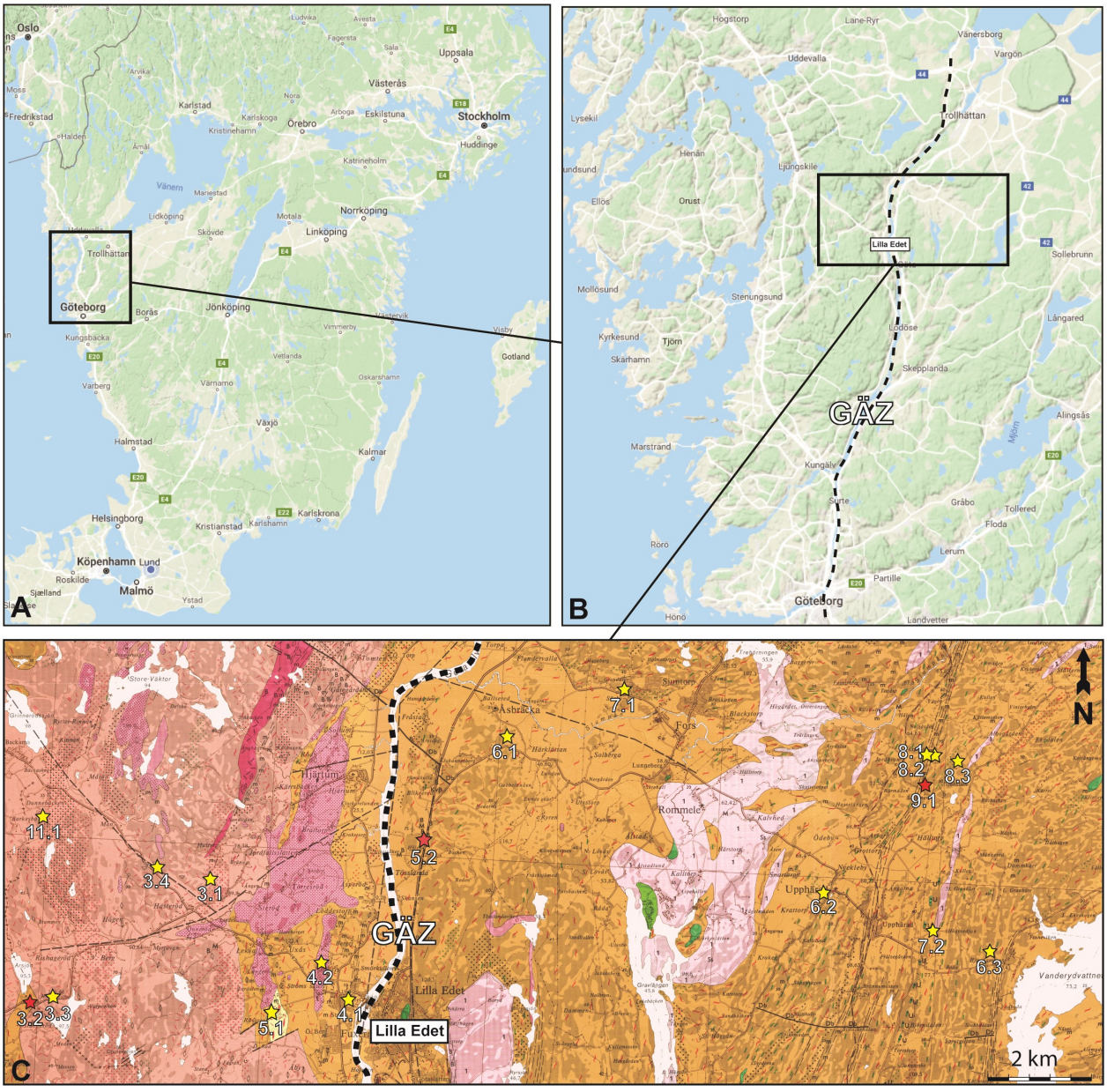

Fig. 3. (a) Situation map of southern Sweden, rectangle referring to map *b*. Map data © 2019 Google. (b) Map over the area between Göteborg and Trollhättan, showing the study area marked with a rectangle and the position of Lilla Edet. GÄZ = Göta Älv Shear Zone. Map data © 2019 Google. (c) Close-up bedrock map showing the study area, from the Swedish Geological Survey. Sample locations are marked with stars and numbers (see Table 1 for further information). Red stars refer to the analysed samples. Legend for the bedrock map can be found in Appendix I. Modified after Samuelsson & Lundqvist (1988).

rocks form larger bodies and layers which are often garnet-rich. The area has also been intruded by deformed pegmatite dykes. In the Median Segment the rocks are more ductilely deformed. Brittle deformation has also been observed adjacent to the Göta Älv Shear Zone. Folding and migmatization is common and has affected both the felsic and the mafic rocks.

In the middle of the Göta Älv Shear Zone the bedrock consists of granitic to granodioritic gneisses, some of which have been migmatized (see section 4.2). Layers of mafic rocks and pegmatite veins are also abundant. The bedrock adjacent to the Göta Älv Shear Zone have been subject to ductile deformation and brittle deformation, the latter which is evident from abundant faults and slickensides.

2.3 Migmatites

Sawyer (2008) defines a migmatite as ‘‘a rock found in medium- and high-grade metamorphic areas that can be heterogeneous at the microscopic to macroscopic scale and that consists of two, or more, petrographically different parts.’’ One of the parts must have been partially melted. The following section is based on Sawyer (2008). The partially melted part usually contains light-coloured minerals separated from dark-coloured minerals. The temperature must become sufficiently high for a rock to partially melt, above 650°C. Deformation also plays a role for the morphology of migmatites. The partial melt has a lower viscosity than the solid non-melted parts of the rock and will thus tend to deform to a greater extent. During deformation the melt is separated from the solids due to its viscosity and moves more rapidly down pressure gradients and collects in low pressure sites. Deformation continues in the weakest places, where the melt is situated, and the migmatites develop complex morphologies. Here I use the terminology from Sawyer (2008) when describing the constituents of a migmatite (Fig. 4):

Neosome: ‘‘The parts of a migmatite newly formed by, or reconstituted by, partial melting’’ - Sawyer, (2008).

Paleosome: ‘‘the non-neosome part of a migmatite that was not affected by partial melting and in which structures (such as foliations, folds, layering) older than the partial melting are preserved’’ - Sawyer (2008).

Residuum: the solid part of the neosome left after partial melting, e.g. melanosome.

Melanosome: the solid residual part (residuum) left after melt segregation, the melanosome constitutes the darker-coloured part of the neosome enriched in ferromagnesian minerals.

Leucosome: the segregated melt fraction of the neosome forming lighter-coloured parts of the neosome dominated by quartz and feldspars.

Selvedge: a narrow rim often situated around the leucosome, which is not part of paleosome or residuum and that is compositionally and mineralogically different from the host. This rim can consist of both light and dark minerals, but the more common type is a thin biotite-rich rim called a *mafic selvedge.*

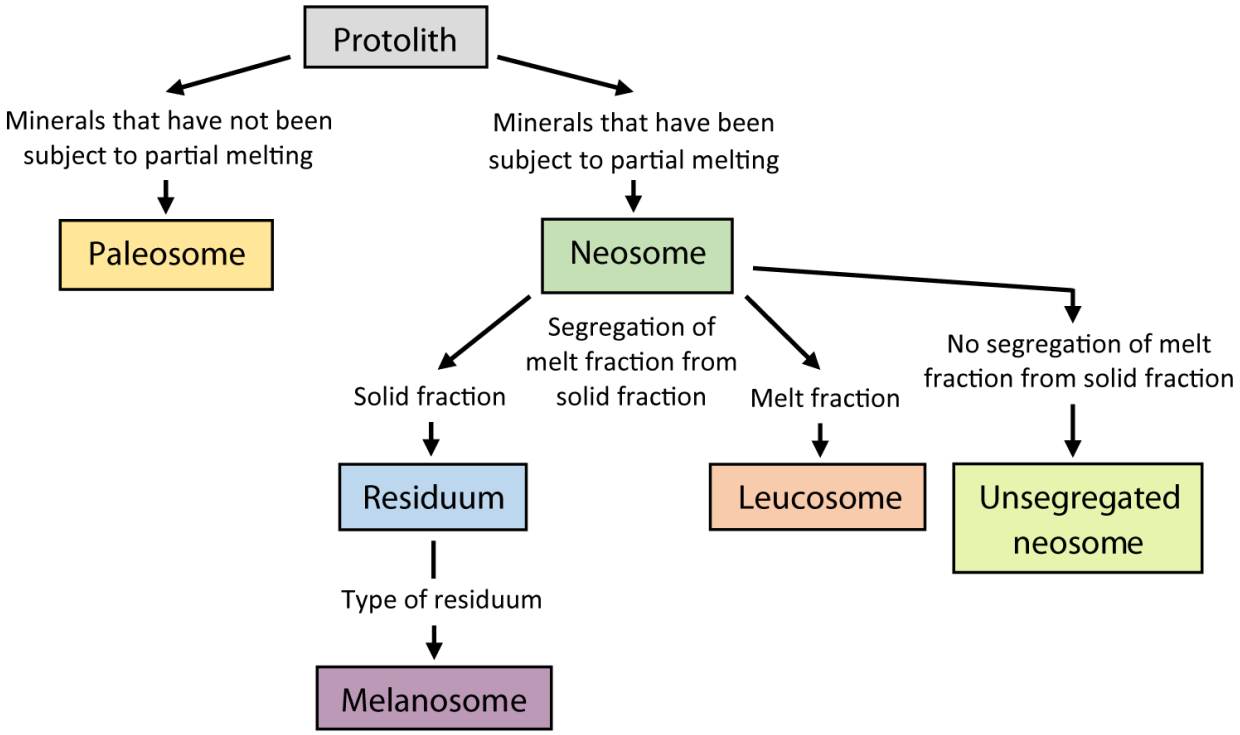

Fig. 4. Schematic illustration of the constituents of migmatites. Modified from Sawyer (2008).

2.4 Geochronology and visualization of U-Pb data

One of the most commonly used mineral for U-Pb dating is zircon ($ZrSiO_4$) which incorporates U in its structure through substitution of Zr, while Pb does not fit into the crystal structure at the time of crystallization (Sylvester 2001). Other minerals used for U-Pb geochronology are monazite, apatite, titanite, rutile, baddeleyite, allanite and perovskite (Sylvester 2001; Schoene 2014). U-Pb geochronology is based on the decay of ^{238}U to ^{206}Pb with the half-life 4.468 billion years and ^{235}U to ^{207}Pb with the half-life 0.704 billion years (Sylvester 2001). None of the parent isotopes decay directly to the stable Pb isotopes but follows a decay sequence through a series of intermediate daughter isotopes. The decay sequence always leads to the same stable Pb isotopes (Schoene 2014). The decay chains are illustrated in Fig. 5. The half-lives of the intermediate daughter isotopes are short, often less than 10 years (Schoene 2014). Concentrations of U and Pb and the isotopic composition of Pb in a sample yield two ages: $^{206}Pb/^{238}U$ and $^{207}Pb/^{235}U$ (Sylvester 2001).

The data is usually displayed in a Wetherill concordia diagram (Wetherill 1956) or a Tera-Wasserburg concordia diagram (Tera & Wasserburg 1972a,b). The concordia diagrams describe how the ratios of U and Pb isotopes change over time, determined by its decay constants. In a Wetherill concordia diagram $^{206}Pb/^{238}U$ is plotted against $^{207}Pb/^{235}U$ and in a Tera-Wasserburg concordia diagram $^{238}U/^{206}Pb$ is plotted against $^{207}Pb/^{206}Pb$. If a sample has remained a closed system since crystallization the sample will plot on the concordia curve and is therefore *concordant*. Samples plotting outside the concordia curve are called *discordant* and have gone through open-system behaviour (Schoene 2014; Sylvester 2001).

In geochronology, the result is usually assessed using the statistical relationship between the error of the population mean and the analytical error of each datum, which is expressed as the Mean Square of Weighted Deviates (MSWD; Wendt & Carl 1991). An MSWD value of 1 indicates that the scatter around the mean is due to analytical errors alone, while values >>1 can be the result of underestimated analytical errors, the presence of geological scatter or a combination of both. Geological causes for excess scatter in zircon U-Pb data can for example be Pb-loss or domain mixing. MSWD values <<1 indicate that analytical errors have been overestimated (Wendt & Carl, 1991; Schoene 2014; Ludwig 2012).

Discordant data can be due to gain or loss of U and/or Pb, or contamination of common Pb (Schoene 2014). In Fig. 6 the common causes of discordant data are illustrated in a Tera-Wasserburg concordia diagram. Episodic or ancient Pb-loss can be caused by an episode of metamorphism resulting in the point plotting off the concordia curve, on a line between the original crystallization age and the event of Pb-loss (Faure 2001; Schoene 2014). Mixing of different age domains in a complex zircon can also result in the point plotting off the concordia curve in the same man-

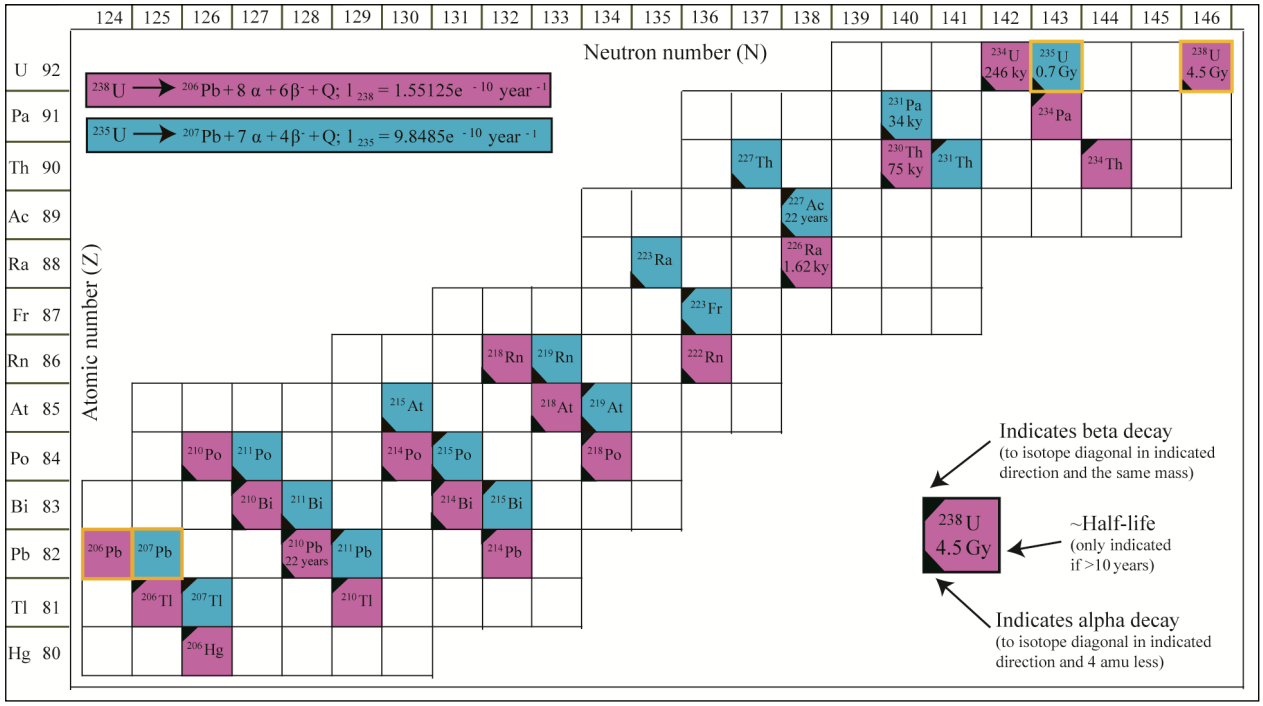

Fig. 5. Illustration of the U-Pb decay chains. Parent and stable daughter isotopes are outlined in orange. The blue boxes refer to the decay of ^{235}U and the purple boxes refer to the decay of ^{238}U. α = alpha decay, β = beta decay and Q = energy released during the decay. The inset shows further details of the symbols in each box. Redrawn after Schoene (2014).

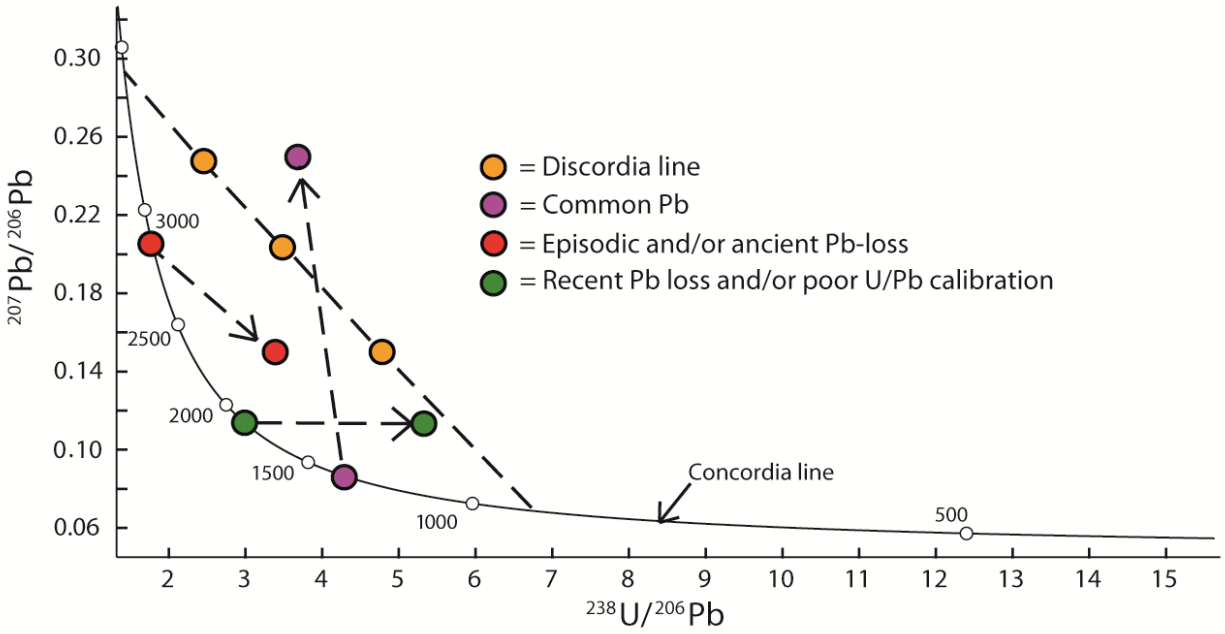

Fig. 6. Tera-Wasserburg concordia diagram showing the common reasons to why data plot discordant.

ner as in the case of episodic Pb-loss (Gehrels 2014). Recent Pb-loss, often caused by radiation damage, is illustrated by horizontal displacement of a point to the right of the concordia curve. Poor U/Pb calibration can also result in horizontal displacement (Linders 2016; Faure & Mensing 2005). Contamination of common Pb in a sample results in discordant points displaced towards high $^{207}Pb/^{206}Pb$ values (Schoene 2014). Interpretation of discordant data is inherently difficult as it can be near impossible to distinguish the cause for the discordance, and for this reason, data that is >5% discordant is discarded to avoid incorrect interpretation.

3 Methods

3.1 Sample collection

Sixteen rock samples were collected during fieldwork in April and in May 2018. Four of these were chosen for zircon geochronology, and rock chips were sawed for thin section preparation. (See section 4 for further information about the samples).

3.2 Preparation and extraction of zircon

The four selected samples were sawed into eight smaller pieces, consisting of leucosome and melanosome, respectively. The pieces were crushed and powdered in a steel swing mill. The rock powder was panned by hand to separate the heavier minerals. Magnetic minerals were removed with a hand magnet. Zircon from the eight subsamples were hand-picked under a binocular microscope. Around 80 zircon crystals from each subsample were picked and placed on double-sided tape and cast into three separate 1-inch epoxy mounts. The mounts were polished with diamond paste to expose flat cross sections through the grains.

3.3 Petrography

Eleven thin sections from three of the selected samples have been manufactured. The fourth sample was small, and the entire sample was used for zircon U-Pb analysis. The thin sections were investigated under a polarization microscope for mineral assemblage, texture and compositional and fluid alterations.

3.4 Scanning Electron Microscopy (SEM)

The epoxy mounts were carbon coated with a Cressington Carbon Coater 108Carbon/A before analysis in a Scanning Electron Microscope (SEM) of model Tescan Mira3 equipped with Oxford EDS and EBSD system, at the department of Geology, Lund University. The SEM was used to study internal structures of the zircons and to determine spot positions for the following Laser Ablation Inductively Coupled Plasma Mass Spectrometry (LA-ICP-MS) analysis. Inclusions in the zircons were also analysed for their composition. The following settings was used during the analysis: beam intensity of 12-16 nA, acceleration voltage of 10-13 kV and a working distance of 10 mm. In a SEM, a fine beam of high-energy electrons is scanned across the surface of a sample. The beam induces several secondary features, such as backscattered electrons (BSE), secondary electrons (SE) and cathodoluminescence (CL) etc. (Goldstein et al. 2018). The latter two were used in this study.

During BSE analysis beam electrons are scattered when they hit the sample and some of the electrons change their direction of travel to return and exit the sample. The electrons that escape are referred to as *backscattered electrons (BSE)* and give important information of the composition of the sample. The BSE

intensity changes with compositions which produces a compositional contrast, such that lighter domains correspond to heavier elements (Goldstein et al. 2018). *Secondary electrons (SE)* are produced when beam electrons enter the sample and interact with weakly bound outer-shell atomic electrons. The secondary electrons produced close to the surface may escape the sample and thus be detected. The SE image displays a topographical contrast (Egerton 2016). *Cathodoluminescence (CL)* is the process by which beam electrons collide with atomic electrons in a sample. The beam electron transfers energy to an atomic electron which then emits an x-ray photon (visible light) while returning to its lowest-energy state. CL images also display a contrast because the wavelength of the emitted photon is dependent on the element (Egerton 2016). In CL internal structures in zircons like cores and growth rims can be distinguished (Hanchar & Miller 1993).

3.5 Laser Ablation Inductively Coupled Plasma Mass Spectrometry (LA-ICP-MS)

Spot positions in the zircon grains were selected on the basis of the SEM images. A Laser Ablation Coupled Plasma Mass Spectrometry (LA-ICP-MS) analysis was used to obtain U-Pb ages of the zircons. The laser ablation model used is a Teledyne Photon Machines Analyte G2 and the laser system is connected to a Bruker Aurora M90 quadrupole inductively coupled plasma mass spectrometer. LA-ICP-MS is a fast and accurate analytical technique for U-Pb dating of zircons (Frei & Gerdes 2009). The instrument consists of two parts, the laser ablation system and the ICP-MS system (Schoene 2014). The epoxy mounts were placed in the sample cell together with primary reference zircon GJ-1 (Jackson et al. 2004) and secondary reference zircon 91500 (Wiedenbeck et al. 1995). The samples were ablated, and the particles were incorporated into a gas mixture of helium, argon and nitrogen. The gas carried the particles into an ICP torch where they were ionized (Schoene 2014). The ionized particles were then transported into the quadrupole mass spectrometer where the following isotopes were detected; ^{202}Hg, ^{204}Hg, ^{206}Pb, ^{207}Pb, ^{208}Pb, ^{232}Th and ^{238}U (See Appendix II for further descriptions). Ablation spots were put in cores and growth rims of the zircons, where a spot size of 18-20 μm was used with the laser running at 11-13 Hz and 2.5 J/cm^2. The geometry of the spots could be adjusted when necessary.

3.6 Data reduction

The raw data from the LA-ICP-MS analysis was imported into the program Iolite (Paton et al. 2011) where it was filtered and reduced. A baseline correction and a downhole fractionation correction was made. Mass discrimination was corrected using standard-sample bracketing where ^{207}Pb/^{206}Pb and ^{238}U/^{206}Pb are normalized to the primary standard GJ-1. Each spectra was manually analysed, and the most stable signal block was chosen for each spectra. The reduced data was then tabulated and plotted in Microsoft Excel 2003 using the add-in Isoplot 3.75 (Ludwig 2012) to create U-Pb concordia diagrams, weighted averages and histograms. Baseline corrected common Pb is insignificant in a vast majority of the analysed spots. Data with significant common Pb was discarded given the difficulty to make an appropriate correction due to ^{204}Hg interference on mass 204 and due to the unknown age of the common Pb component (e.g. ancient Pb in cracks or inclusions or recent Pb from lab contamination). Only data that do not require correction for common Pb and with a maximum discordance of 5% was used. All results are plotted in Tera-Wasserburg concordia diagrams with ellipses corresponding to 2 standard errors. Diagrams illustrating Th/U values were plotted in Igpet 2014.

4 Samples and petrography

Six out of sixteen samples collected in the field were selected for U-Pb zircon dating, sample localities are shown in Table 1. MISE1802 and MISE1805 were sampled in the Western Segment. MISE1813, MISE1814 and MISE1816 in the Median Segment, and MISE1806 within the Göta Älv Shear Zone. Sample MISE1805 and MISE1813 lack zircon and were discarded. A short field description and a petrographic description of the selected samples are summarized below.

4.1 Western Segment (Sample MISE1802)

Sample MISE1802, near Arsjön, is taken from a biotite-rich migmatitic granodioritic gneiss, at locality 3.2 west of the Göta Älv Shear Zone in the Western Segment (Fig. 3c and Fig. 7). The rock has 2-5 cm thick leucosome veins that are coarser-grained than the melanosome. Some veins are folded but only open folds were found. Sample MISE1802 was divided into three subsamples MISE1802a, MISE1802b and MISE1802c out of which the first two were analysed (Fig. 7c,d). MISE1802a consists of both a piece of leucosome and melanosome. MISE1802b consists of two pieces of leucosome.

There are four thin sections from this rock, MISE1802a leucosome, MISE1802a melanosome, MISE1802b leucosome 1 and MISE1802b leucosome 2 (Fig. 8). Quartz, K-feldspar, plagioclase, biotite, and epidote dominate the samples with accessory muscovite, titanite, apatite and zircon (Fig. 8e,f). The rock is inequigranular and the melanosome is slightly finer-grained than the leucosome. Minerals with euhedral to subhedral crystal habits are biotite, epidote, muscovite, titanite, apatite and zircon**.** The remaining minerals have a subhedral to anhedral crystal habit. The biotite is magnesium rich, which is indicated by its green colour and the biotite aggregates define a weak foliation in sample MISE1802a melanosome and is absent in the leucosome samples. The K-feldspar shows tartan

Arsjön, Western Segment

Fig. 7. (a) The Arsjön migmatite (locality 3.2) in the Western Segment, from which sample MISE1802 was taken. (b) Close-up of picture *a* where folded leucosome veins can be seen. (c) The left hand-specimen represents subsample MISE1802a melanosome and the right hand-specimen represents subsample MISE1802a leucosome. (d) Hand-specimen from which subsample MISE1802b leucosome was taken.

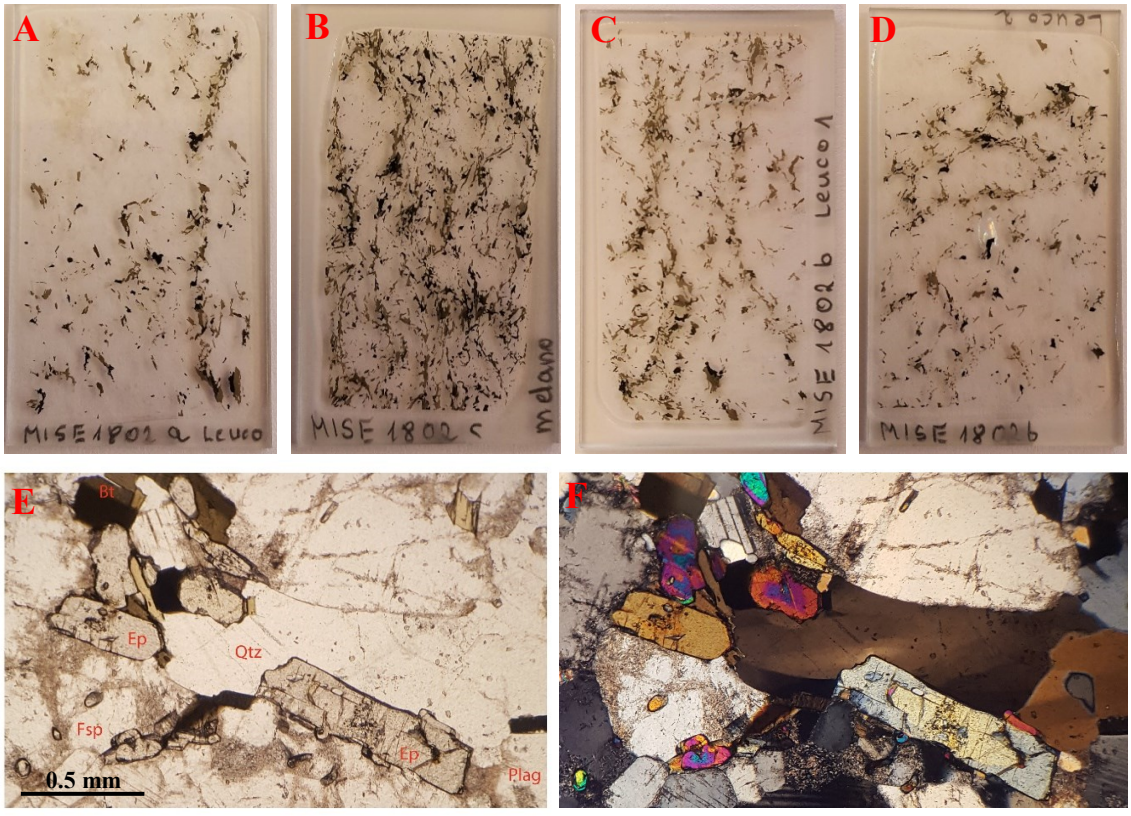

Fig. 8. (a) Thin section MISE1802a leucosome. (b) Thin section MISE1802a melanosome. (c) Thin section MISE1802b leucosome 1. (d) Thin section MISE1802b leucosome 2. (e) Photomicrograph (plane light) of MISE1802a leucosome. Several epidote grains can be seen. Bt = biotite, Ep = epidote, Qtz = quartz, Plag = plagioclase, Fsp = K-feldspar. (f) Same photomicrograph as *e* but in cross-polarized light.

twinning, perthitic and sieve texture. The MISE1802b samples have dustier K-feldspar crystals than the MISE1802a samples. Titanite crystals are small in the leucosome and occur as inclusions in biotite or adjacent to biotite crystals. In the melanosome the titanite crystals are larger. The muscovite grains lie adjacent to biotite and epidote, but it is not clear whether it is primary or secondary muscovite.

4.2 Göta Älv Shear Zone (Sample MISE1806)

Sample MISE1806, near Tösslanda is a migmatitic alkali granitic gneiss that was sampled at locality 5.2 within the Göta Älv Shear Zone, between the Western and Median Segments (Fig. 3c and Fig. 9) The rock is heavily fractured and metasomatized. It has 2-4 cm thick leucosome veins rimmed by distinct biotite selvedges (Fig. 9a). Thin leucosome-looking veins (<5 mm) are also present within the melanosome (Fig. 9a). At this locality, no fold structures were observed, and the leucosome is coarser-grained than the melanosome. The sample was divided into subsamples MISE1806 melanosome and MISE1806 leucosome (Fig. 9b).

Three thin sections were made from this rock; MISE1806 melanosome 1, MISE1806 melanosome 2 and MISE1806 leucosome (Fig. 10). Quartz, K-feldspar, plagioclase, biotite, hornblende and ilmenite dominate the samples with accessory apatite and zircon (Fig. 10a). The minerals are anhedral except for a few subhedral biotite grains. The rock is inequigranular and the leucosome is coarser-grained than the melanosome. Interstitial fine-grained quartz with sutured boundaries are present in both leucosome and melano-

Tösslanda, Göta Älv Shear Zone

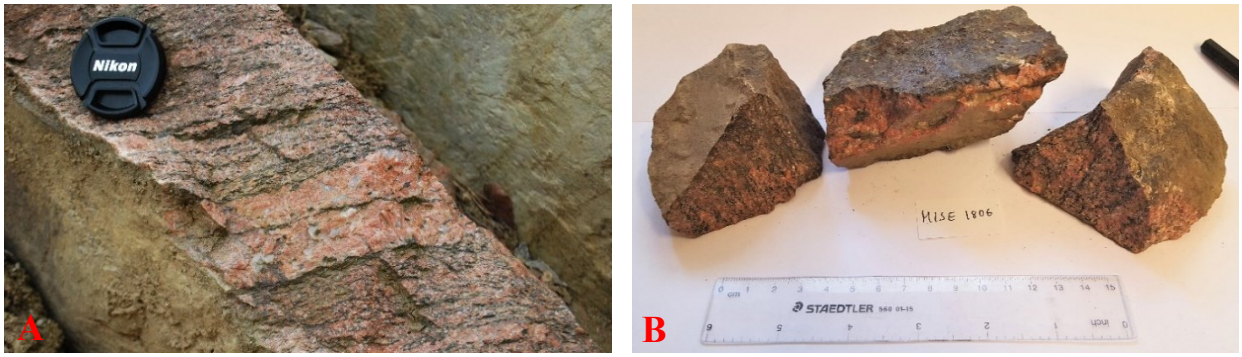

Fig. 9. (a) The Tösslanda migmatite at locality 5.2 within the Göta Älv Shear Zone, from which sample MISE1806 was taken. (b) The hand-specimens from which subsamples MISE1806 leucosome (the middle hand-specimen) and MISE1806 melanosome (the left and right hand-specimens) was taken.

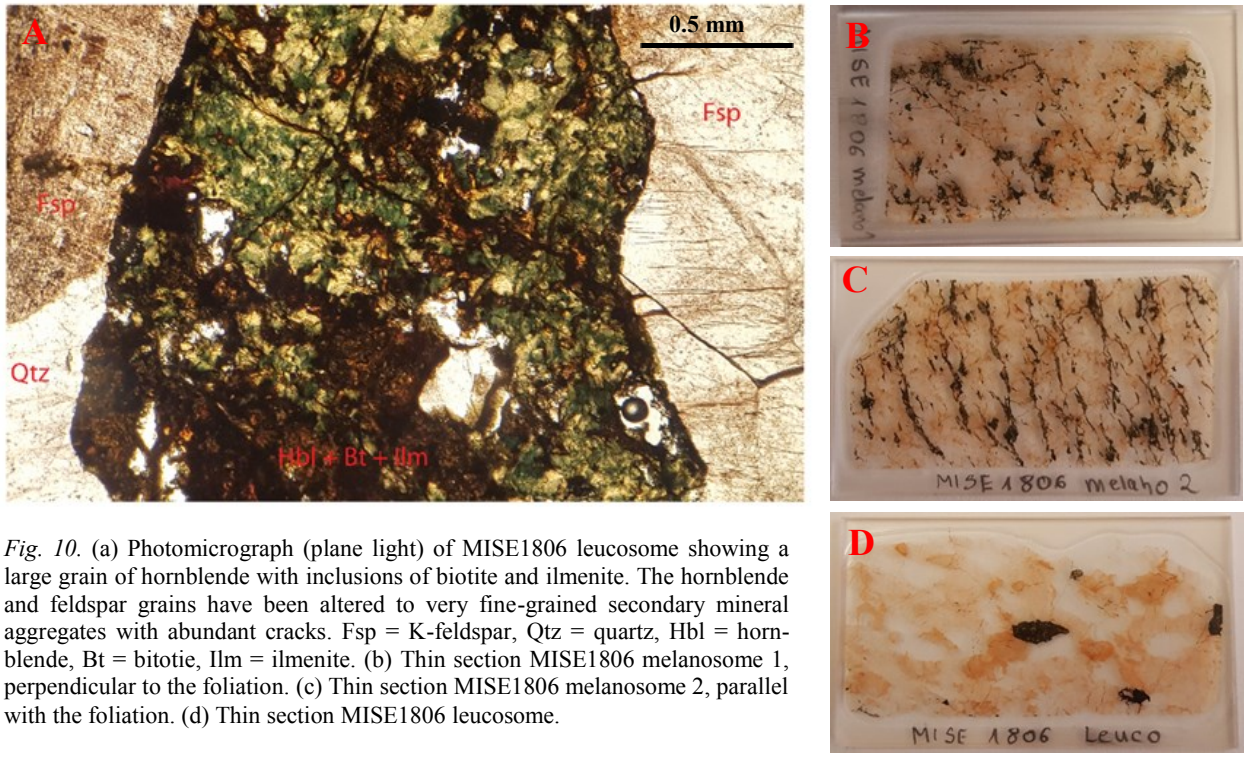

Fig. 10. (a) Photomicrograph (plane light) of MISE1806 leucosome showing a large grain of hornblende with inclusions of biotite and ilmenite. The hornblende and feldspar grains have been altered to very fine-grained secondary mineral aggregates with abundant cracks. Fsp = K-feldspar, Qtz = quartz, Hbl = hornblende, Bt = bitotie, Ilm = ilmenite. (b) Thin section MISE1806 melanosome 1, perpendicular to the foliation. (c) Thin section MISE1806 melanosome 2, parallel with the foliation. (d) Thin section MISE1806 leucosome.

some. K-feldspar crystals are dusty and show tartan twinning, perthitic and sieve texture. Hornblende crystals have been altered to a very fine-grained aggregate of hornblende, biotite and ilmenite. The biotizated hornblende crystals are no longer pleochroic and cleavage cannot be seen. Ilmenite have partly formed pseudomorphs after titanite and often lies adjacent to and within biotite and hornblende. The mafic minerals define a pronounced foliation.

4.3 Median Segment (Samples MISE1814 and MISE1816)

4.3.1 MISE1814

Sample MISE1814, near Hälltorp is a garnet-bearing migmatitic gneiss that was sampled at locality 9.1 east of the Göta Älv Shear Zone in the Median Segment (Fig. 3c and Fig. 11). The sample consists of three subsamples, MISE1814a, MISE1814b and MISE1814c. Subsample MISE1814a, which was dated was taken from a 3 cm thick leucosome vein along the fold-axial plane of a tight fold (Fig. 11a,b). There are no thin sections of this sample since the whole sample was used for zircon U-Pb dating.

4.3.2 MISE1816

Sample MISE1816 was sampled from the same garnet-bearing migmatitic gneiss as sample MISE1814 above, at locality 9.1 (Fig. 3c and Fig. 12). This rock is an example of a *fold-structured migmatite* (cp. Sawyer 2008). Abundant leucosome veins are 1-3 cm thick and have been strained and folded. Veins are common along fold-axis planes *(see section 4.3.1)*. Mafic dykes 10-30 cm in thickness are also deformed, but not as much as the gneiss. This is due to the competence contrast where mineral assemblage, texture and grain-size determines the extent of deformation. Sample MISE1816 was divided into three subsamples; MISE1816a, MISE1816b and MISE1816c, of which the latter was dated. MISE1816c consists of two pieces, one of melanosome and one of leucosome (Fig. 12b).

Hälltorp, Median Segment

Fig. 11. (a) The Hälltorp migmatite at locality 9.1 in the Median Segment, from which sample MISE1814a was taken. The sample was taken from the thick leucosome vein at the top along the fold-axial plane of the tight fold. (b) Hand-specimen representing sample MISE1814a.

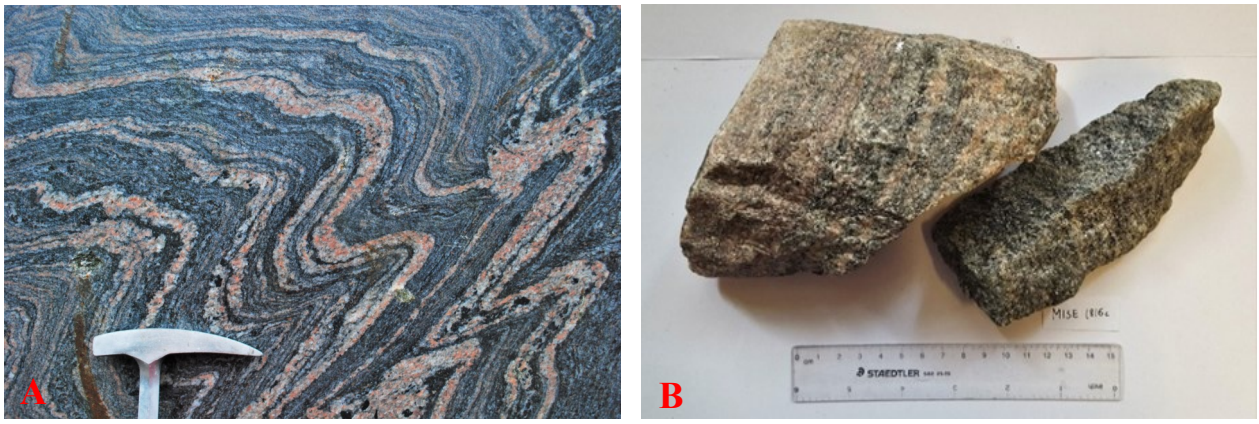

Fig. 12. (a) Close-up of the Hälltorp migmatite at locality 9.1 in the Median Segment, which sample MISE1816 belongs to. (b) The left hand-specimen represents subsample MISE1816c leucosome and the right hand-specimen represents subsample MISE1816c melanosome.

The rock is represented by four thin sections; MISE1816c leucosome, MISE1816c melanosome 1, MISE1816c melanosome 2 and MISE1816c leucosome + melanosome (Fig. 13). Quartz, K-feldspar, plagioclase, biotite, scapolite and garnet dominate the samples with minor muscovite, epidote, titanite, ilmenite, hornblende, spinel, zircon and rutile (Fig. 13e,f,g,h). The rock is inequigranular and the majority of the minerals are subhedral to anhedral except for biotite that is euhedral and defines a weak foliation. K-feldspar grains are dusty and show tartan twinning, perthitic and sieve texture. Quartz grains show signs of strain, and both granophyric and ribbon-textures occur. Hornblende was found in one thin section, MISE1816c melanosome 1. Muscovite lies adjacent to biotite and is also intergrown with biotite, scapolite and epidote. Titanite crystals are larger in the melanosome than in the leucosome. Garnet is only found in the melanosome and occur as isolated grains and as inclusions in scapolite. Alteration of scapolite in terms of oxidization and fractures is seen and the crystals are rich in inclusions. Scapolite in thin section MISE1816c leucosome + melanosome lies in two distinct bands in the foliation direction.

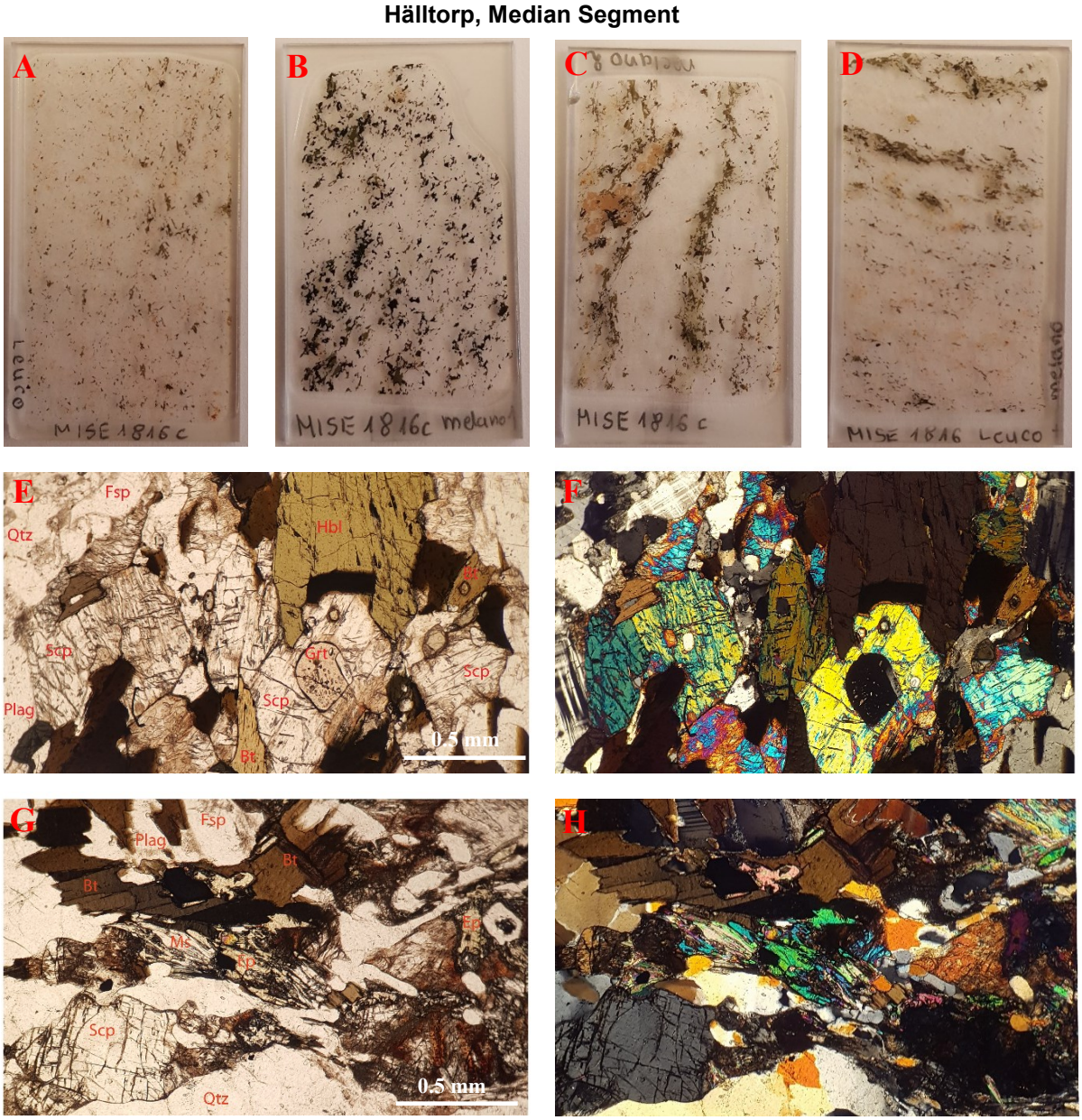

Fig. 13. (a) Thin section of MISE1816c leucosome. (b) Thin section of MISE1816c melanosome 1. (c) Thin section of MISE1816c melanosome 2. (d) Thin section of the transition between leucosome and melanosome in MISE1816c. (e) Photomicrograph (plane light) of MISE1816c melanosome 1 showing a hornblende crystal, several scapolite grains and a garnet grain enclosed in scapolite. Fsp = K-feldspar, Qtz = quartz, Bt = biotite, Hbl = hornblende, Grt = garnet, Scp = scapolite, Plag = plagioclase, Ep = epidote, Ms = muscovite. (f) Same photomicrograph as *e* but in cross-polarized light. (g) Photomicrograph (plane light) of MISE1816c melanosome 2 showing remnant of epidote, minor muscovite and a ribbon-textured quartz grain in the bottom. (h) Same photomicrograph as *g* but in cross-polarized light.

Table 1. Sample locations and sample information. Underlined samples was used for zircon U-Pb dating. Coordinates given in Decimal degrees (datum: WGS-84).

Sample-ID	Locality	Latitude	Longitude	Site information	Rock type
MISE1801	3.1	58.157841	12.060858	Western Segment, near Hasteröd	Granitic augen gneiss
MISE1802	3.2	58.132975	11.993259	Western Segment, near Arsjön	Migmatitic granodioritic gneiss
MISE1803	3.3	58.133681	11.999500	Western Segment, near Arsjön	Granodioritic gneiss
MISE1804	3.4	58.160841	12.038619	Western Segment, near Hasteröd	Muscovite-rich granitic gneiss
MISE1805	5.1	58.133368	12.084540	Western Segment, near Röstorp	Granitic gneiss
MISE1806	5.2	58.167812	12.137814	In Göta Älv Shear Zone, near Tösslanda	Migmatitic alkali granitic gneiss
MISE1807	6.2	58.163722	12.289561	Median Segment, near Upphärad church	Metabasite and granodio-ritic gneiss
MISE1808	6.3	58.152448	12.350030	Median Segment, near Bjurdammen	Garnet-rich migmatitic granitic gneiss
MISE1809	7.1	58.200764	12.208180	Median Segment, near Sörby	Recrystallized granitic pegmatite
MISE1810	7.2	58.156490	12.328507	Median Segment, near St. Boda	Garnet-rich migmatitic granitic gneiss
MISE1811	8.1	58.190145	12.331870	Median Segment, near Hälltorp	Garnet-rich migmatitic granitic gneiss and garnet amphibolite
MISE1812	8.2	58.190171	12.332324	Median Segment, near Hälltorp	Garnet-rich migmatitic granitic gneiss and garnet amphibolite
MISE1813	8.3	58.189672	12.336314	Median Segment, near Hälltorp	Migmatitic granitic gneiss
MISE1814	9.1	58.182703	12.327849	Median Segment, near Hälltorp	Garnet-rich migmatitic granitic gneiss
MISE1815	11.1	58.169287	11.992733	Western Segment, in quarry near Backamo	Augen gneiss and gran-odioritic gneiss
MISE1816	9.1	58.182345	12.329005	Median Segment, near Hälltorp	Garnet-rich migmatitic granitic gneiss

5 Results

U-Th-Pb isotopes was determined in 599 spots in 411 zircon grains from seven subsamples. The eighth subsample MISE1802b from MISE1802 was excluded due to unstable $^{207}Pb/^{206}Pb$ ratios during the analytical session. Data that were >5% discordant, had quantifiable common Pb or poor precision were rejected from age calculation. A 10% discordance criterion was used for the younger population of subsample MISE1806 melanosome and MISE1802a leucosome due to few analyses. A total of 235 spot analyses were discarded using these criteria, leaving 364 analyses for which the $^{207}Pb/^{206}Pb$ dates are summarized in a histogram in Fig. 14, showing peaks at ~1050 Ma, ~1350 Ma, ~1550 Ma, ~1580 Ma and ~1600 Ma. Spot positions in zircon crystals that yielded concordant data are shown in Appendix III, note that only a selection of zircons are represented. Analytical data for all spots are listed in Appendix IV. Tera-Wasserburg concordia diagrams for all data in all samples are shown in Appendix V and Th/U plots for all samples are shown in Appendix VI. All errors are reported as 2 standard errors. The data were not equivalent enough to calculate concordia ages for all samples, and weighted average $^{207}Pb/^{206}Pb$ ratios were used instead. This also avoids problems with minor amounts of recent Pb-loss or U-Pb calibration errors. Results are presented for each subsample as well as combined into geochronological results from the Western Segment (MISE1802), Median Segment (MISE1814 and MISE1816) and from the Göta Älv Shear Zone (MISE1806), because the subsamples were of the same age and presumably from the same origin. Zircon descriptions for each sample are also presented.

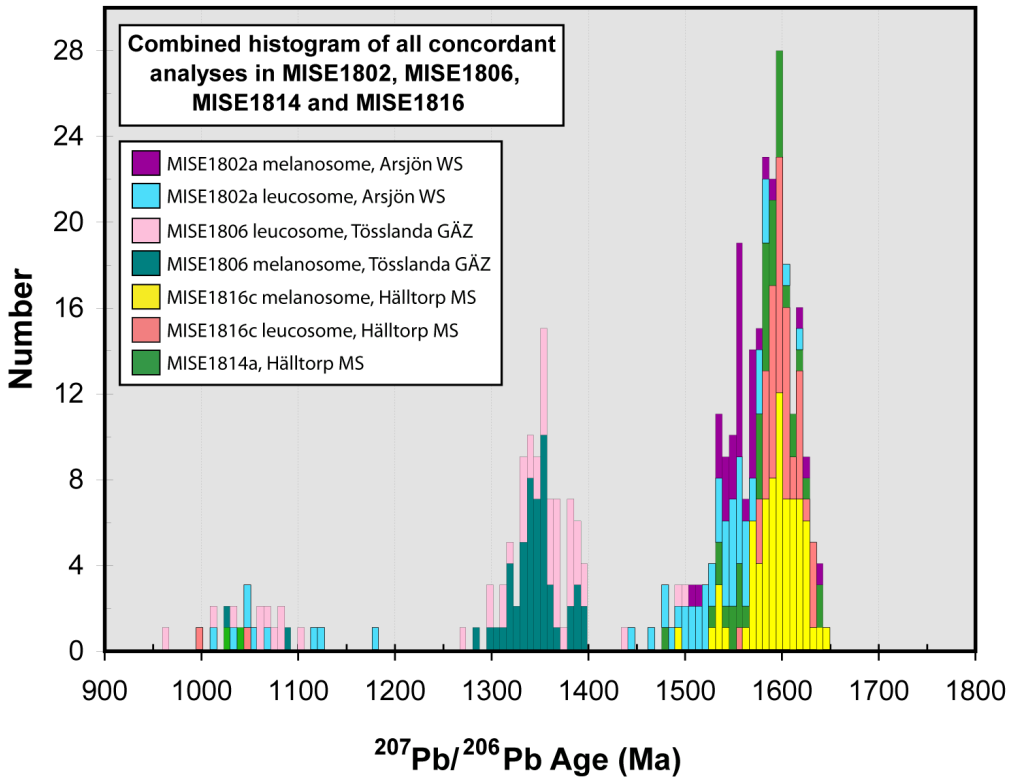

Fig. 14. Histogram of all 364 concordant analyses from MISE1802, MISE1806, MISE1814 and MISE1816, showing five major populations at ~1050 Ma, ~1350 Ma, ~1550 Ma, ~1580 Ma and ~1600 Ma. The different subsamples are represented by boxes of different colour as shown in the legend. WS = Western Segment, GÄZ = Göta Älv Shear Zone and MS = Median Segment.

5.1 Western Segment (Sample MI-SE1802)

5.1.1 MISE1802a melanosome

The zircon crystals are 100 to 200 µm long and are mostly prismatic. The grains contain microfractures and have inclusions of apatite and quartz. Most cores show concentric oscillatory zoning (Appendix III zircons 24, 31 and 44 in Fig. 6), but some cores are homogeneous (Appendix III zircons 37 and 69 in Fig. 6). A few crystals have irregularly zoned cores. The zircons have CL-bright 5-15 µm thick overgrowths that cut the zoned cores (Appendix III Fig. 6).

83 spots in 68 crystals were analysed for U-Pb (Appendices IV and V). The majority of the analyses had to be discarded due to discordance, leaving 34 analyses for an age calculation (Appendix III Fig. 6). The histogram in Appendix V illustrates the spread of the analyses around a mean date of ~1560 Ma. A $^{207}Pb/^{206}Pb$ weighted average of the population yields a 1557±6 Ma (MSWD = 3.4, n = 30/34) date (Fig. 15). U concentration ranges between 57 ppm and 755 ppm with an average of 326 ppm and Th varies between 27 ppm and 730 ppm with an average of 296 ppm. Th/U vary from 0.274 to 1.830 with an average of 0.945 (Appendix VI Fig. 1b). Two analyses have distinctly lower Th/U of 0.068 and 0.093. These analyses are spot 76 in zircon 39 (U = 385 ppm and Th = 28 ppm) and spot 77 in zircon 40 (U = 673 ppm and Th = 67 ppm) (Appendix III Fig. 6 and Appendix VI Fig. 1b).

5.1.2 MISE1802 leucosome

The zircon crystals are rounded and prismatic, although some only make up a fragment of a grain. The crystals vary in size between 100 and 200 µm. The grains contain a few inclusions of apatite and quartz. The cores are mostly homogeneous or irregularly zoned (Appendix III zircons 2, 13 and 20 in Fig. 7). Some cores also display concentric oscillatory zoning (Appendix III zircons 6, 10 and 56 in Fig. 7), and one grain show sector zoning (Appendix III zircon 45 in Fig. 7). CL-bright overgrowths (<40µm thick), that cut the zoned cores, are abundant (Appendix III Fig. 7). Zircon 31 is entirely CL-bright (Appendix III Fig. 7).

112 spots in 70 grains were analysed for U-Pb (Appendices IV and V). All but 57 analyses had to be discarded due to discordance (Appendix III Fig. 7). Two main populations are seen in the histogram, one around 1550 Ma and another around 1050 Ma (Appendix V). The older population yields a $^{207}Pb/^{206}Pb$ weighted average date of 1545±9 Ma (MSWD = 7.9, n = 45/48) with U concentrations from 13 ppm to 615 ppm (average 173 ppm) and Th from 4 ppm to 753 ppm with an average of 160 ppm (Fig. 16a,b). Th/U for the older population ranges between 0.136 and 1.790 with an average of 0.8 (Appendix VI Fig. 1b).

11 spots in total belong to the younger population, due to discordance, 9 spots were used for an age calculation. Note that 3 of the analyses are up to 10% discordant. A $^{207}Pb/^{206}Pb$ weighted average of the young-

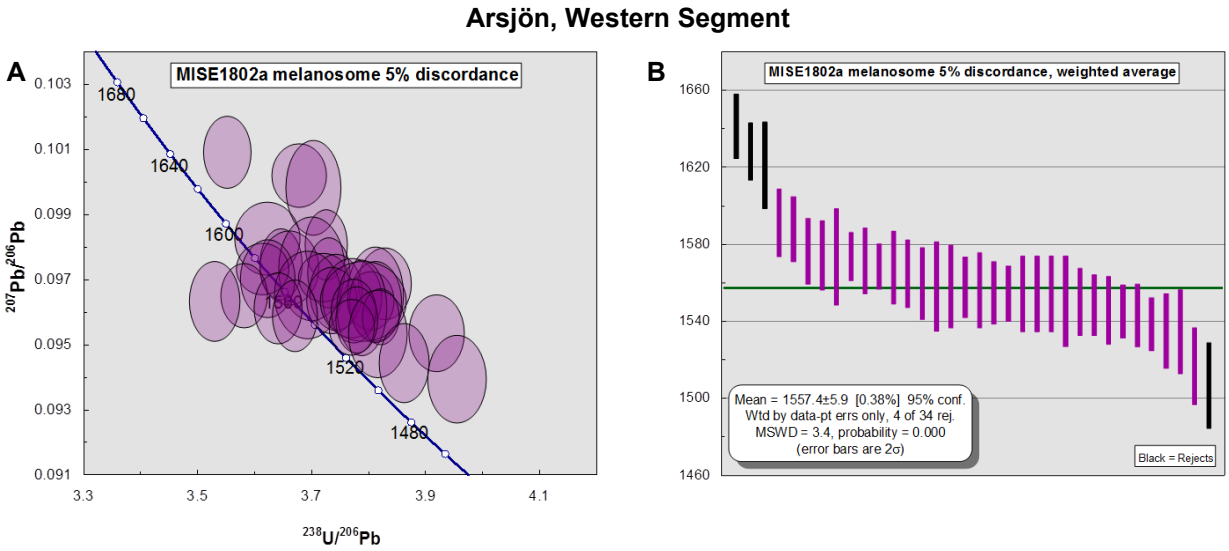

Fig. 15. Arsjön, Western Segment. (a) Tera-Wasserburg concordia diagram for sample MISE1802a melanosome. (b) $^{207}Pb/^{206}Pb$ weighted average date of sample MISE1802a melanosome. Age in million years on the y-axis. The plotted analyses are <5% discordant.

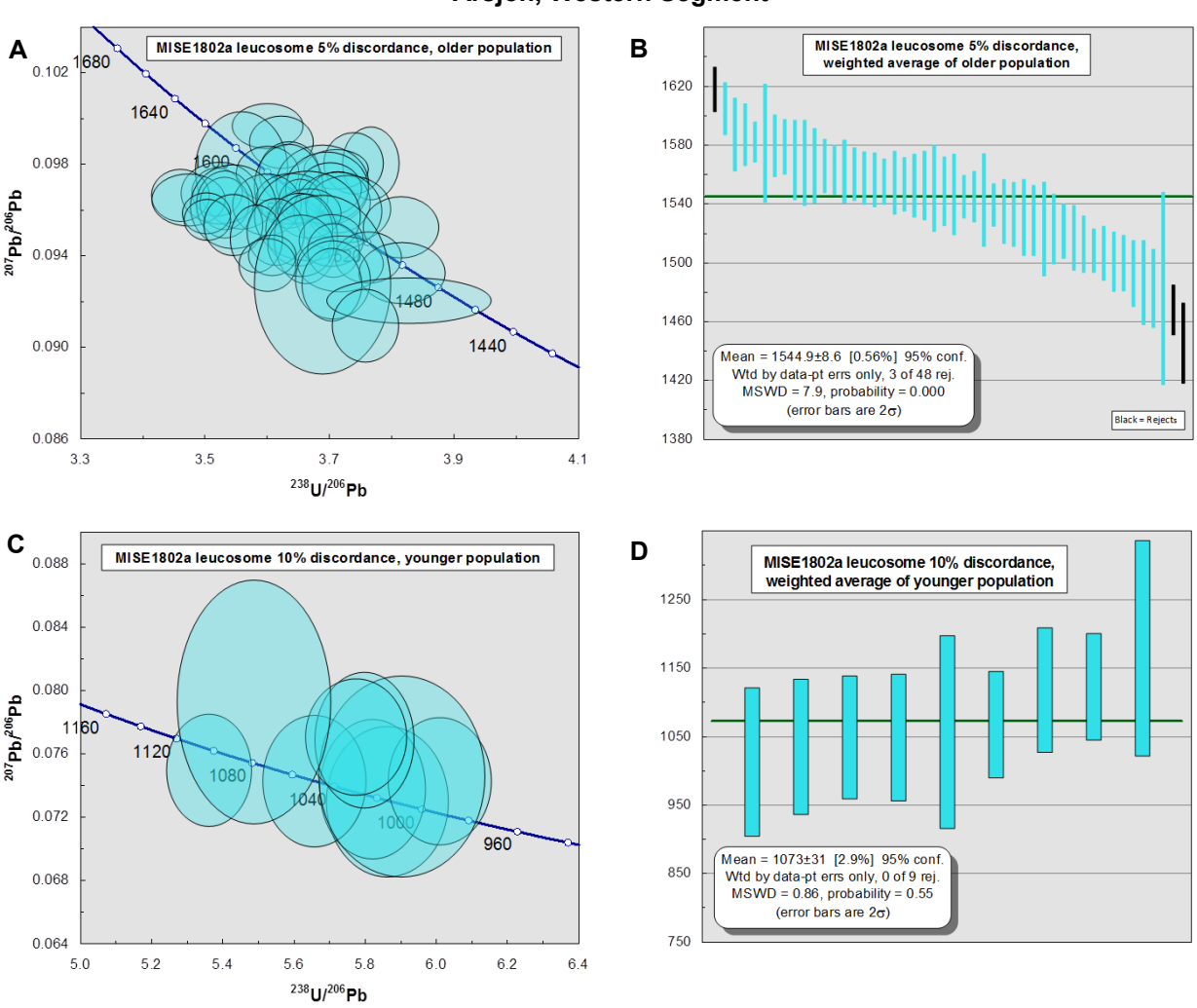

Fig. 16. Arsjön, Western Segment. (a) Tera-Wasserburg concordia diagram of the older population in sample MISE1802a leucosome. (b) $^{207}Pb/^{206}Pb$ weighted average date of the older population in sample MISE1802a leucosome. Age in million years on the y-axis. The plotted analyses are <5% discordant. (c) Tera-Wasserburg concordia diagram for the younger population in sample MISE1802a leucosome. (d) $^{207}Pb/^{206}Pb$ weighted average date of the younger population in sample MISE1802a leucosome based on zircon rims. The plotted analyses are <10% discordant.

er population yields a 1073±31 Ma (MSWD = 0.86, n = 9) date (Fig. 16c,d). The younger population has U concentrations ranging from 5 ppm to 12 ppm (average 10 ppm), Th concentrations from 0.005 ppm to 1 ppm (average 0.18 ppm) and Th/U vary between 0.002 and 0.111 with an average of 0.027 (Appendix VI Fig. 1b).

5.1.3 Combined results

Subsamples MISE1802a melanosome and MISE1802a leucosome come from the same rock piece and therefore the results from these two datasets were combined. The age calculation is based on 5% discordance for the older population but 10% discordance for the younger population. Both subsamples contain data representing the older population, but dates belonging to the younger population was only found in MISE1802a leucosome. The MISE1802a leucosome 1545±9 Ma date for its older population is slightly, but not significantly younger than that of the MISE1802a melanosome that yielded a 1557±6 Ma date. The combined $^{207}Pb/^{206}Pb$ weighted average of the older populations of the two subsamples is 1551±6 Ma (MSWD = 6.6, n = 76/82) (Fig. 17a,b).

As for the younger population the combined results are the same as for the dataset of subsample MISE1802a leucosome, namely a 1073±31 Ma (MSWD = 0.86, n = 9) date (Fig. 17c,d).

5.2 Göta Älv Shear Zone (Sample MISE1806)

5.2.1 MISE1806 melanosome

The zircon crystals are 75 to 275 µm along the c-axis, with both prismatic and rounded shapes. A few grains are broken. Inclusions of apatite, quartz and K-feldspar

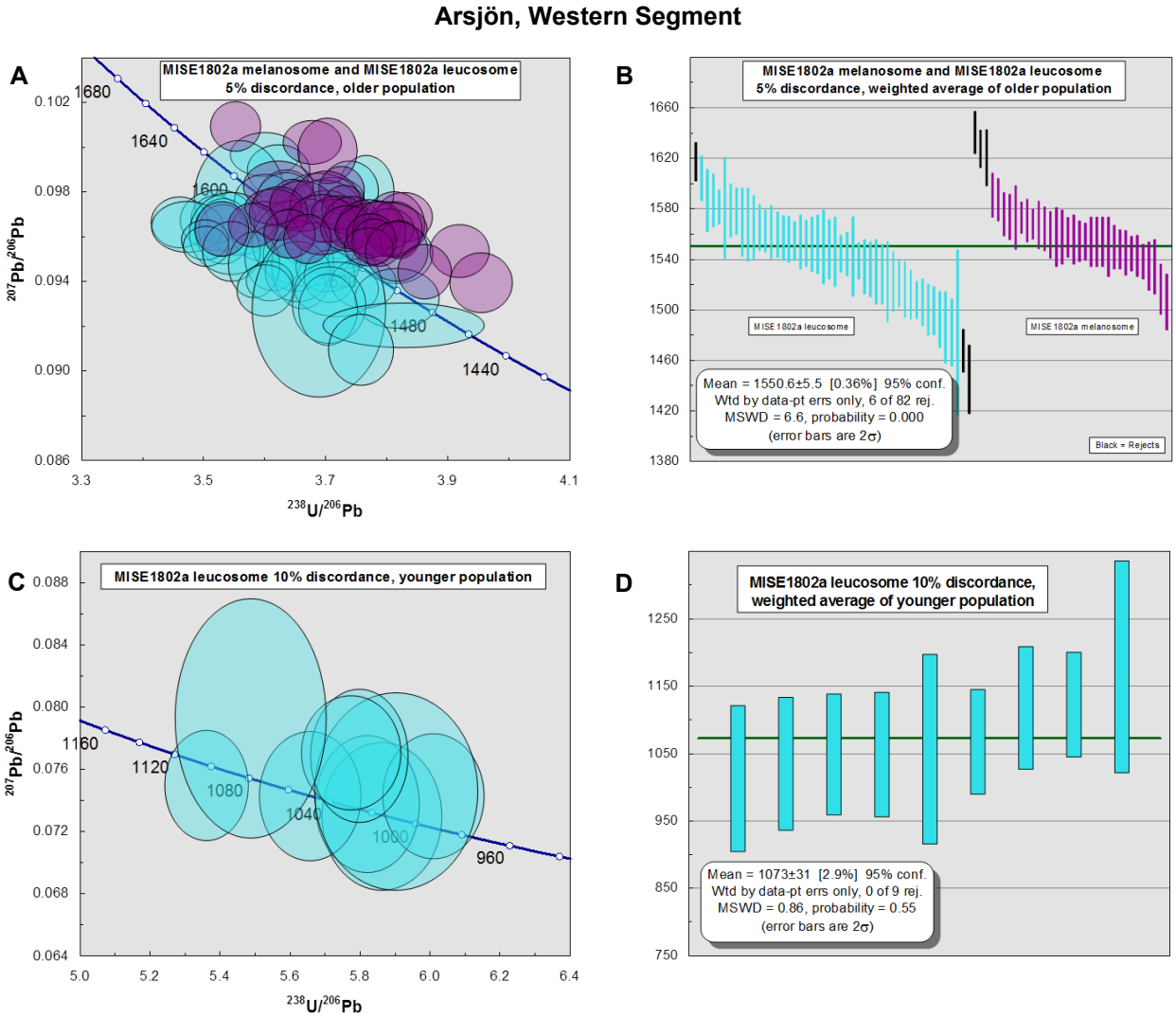

Fig. 17. Arsjön, Western Segment. (a) Combined Tera-Wasserburg concordia diagram of the older population for samples MISE1802a leucosome and MISE1802a melanosome. (b) Combined $^{207}Pb/^{206}Pb$ weighted average date of the older population for samples MISE1802a leucosome and MISE1802a melanosome. Age million years on the y-axis. The plotted analyses are <5% discordant. (c) Combined Tera-Wasserburg concordia diagram for the younger population for sample MISE1802a leucosome. No younger ages were found in MISE1802a melanosome. (d) Combined $^{207}Pb/^{206}Pb$ weighted average date of the younger population for sample MISE1802a leucosome, based on zircon rims. The plotted analyses are <10% discordant. Ellipses correspond to 2 standard errors.

are abundant. The crystals are CL-dark with irregularly zoned or homogeneous cores. Overgrowths are difficult to see since they are CL-dark, but a few can be distinguished (Appendix III zircons 9 and 31 in Fig. 2).

78 spots in 59 grains were analysed for U-Pb (Appendices IV and V) out of which 53 analyses were used for age calculations (Appendix III Fig. 2). The remaining 25 analyses were discarded due to discordance. Histograms with peaks at ~1350 Ma and ~1050 Ma are shown in Appendix V. A $^{207}Pb/^{206}Pb$ weighted average of the older population yields a 1347±6 Ma (MSWD = 4.6; n = 48/51) date (Fig. 18a,b). U concentrations for the older population range from 287 ppm to 2004 ppm (average 710 ppm) and Th from 154 ppm to 1796 ppm (average 563 ppm). Th/U vary from 0.248 to 2.066 with an average of 0.785 (Appendix VI Fig. 1a).

The two remaining analyses belongs to the younger population and a $^{207}Pb/^{206}Pb$ weighted average yields the date: 1081±270 Ma (MSWD = 3.1; n = 2) (Fig. 18c,d). The younger population consist of spot 57 in zircon 31 (U = 870 ppm, Th = 342 ppm and Th/U = 0.373) and spot 99b in zircon 83 (U = 254 ppm, Th = 13 ppm and Th/U = 0.047) (Appendix III Fig. 2 and Appendix VI Fig. 1a). Due to few young dates, the age calculation of the young population is based on 10% discordance.

5.2.2 MISE1806 leucosome

The zircon crystals are prismatic and rounded and vary in size from 75 to 275 µm. A third of the crystals only make up a fragment of a grain. Apatite-, quartz- and K-feldspar inclusions are common. The crystals are CL-dark with irregularly zoned or homogeneous cores.

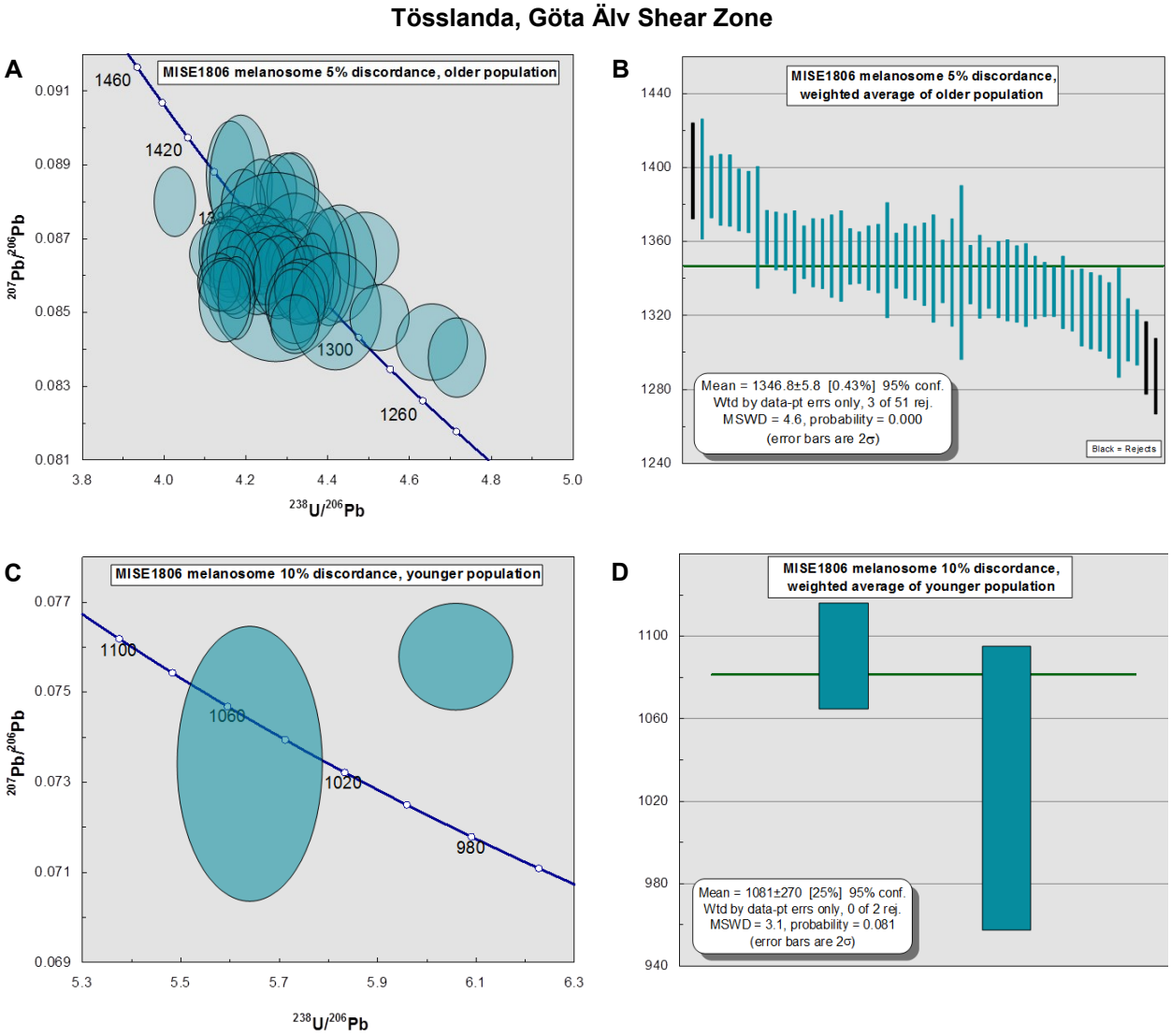

Fig. 18. Tösslanda, Göta Älv Shear Zone. (a) Tera-Wasserburg concordia diagram for the older population in sample MISE1806 melanosome. (b) $^{207}Pb/^{206}Pb$ weighted average date of the older population in sample MISE1806 melanosome. Age in million years on the y-axis. The plotted analyses are <5% discordant. (c) Tera-Wasserburg concordia diagram for the younger population in sample MISE1806 melanosome. (d) $^{207}Pb/^{206}Pb$ weighted average date of the younger population in sample MISE1806 melanosome based on zircon rims. The plotted analyses are <10% discordant.

Due to whole grains being CL-dark the overgrowths are hard to distinguish, but a few can be observed (Appendix III zircon 63 in Fig. 3).

93 spots in 56 zircons were analysed for U-Pb (Appendices IV and V). 40 spot analyses were rejected due to discordance. The remaining 53 spot analyses (Appendix III Fig. 3) generate two main populations, one at ~1350 Ma and one at ~1050 Ma which be seen in a histogram in Appendix V. A $^{207}Pb/^{206}Pb$ weighted average of the older population yields a 1355±8 Ma (MSWD = 4.4; n = 39/43) date (Fig. 19a,b) with U from 148 ppm to 1119 ppm (average 541 ppm) and Th from 66 ppm to 2083 ppm (average 586 ppm). Th/U range from 0.412 to 3.500 with an average of 1.020 (Appendix VI Fig. 1a).

A $^{207}Pb/^{206}Pb$ weighted average of the younger population yields a 1046±22 Ma (MSWD = 4.6; n = 9/10) date (Fig. 19c,d). The younger population has U concentrations between 728 ppm and 3680 ppm with an average of 1708 ppm and Th concentrations from 12 ppm to 833 ppm with an average of 130 ppm. Th/U vary between 0.005 and 0.716 with an average of 0.035 (Appendix VI Fig. 1a).

5.2.3 Combined results

Subsamples MISE1806 leucosome and MISE1806 melanosome come from the same rock piece and thus the two datasets were combined. A 5% discordance criterion was applied for the combined results. Both subsamples yield dates from an older and a younger population. The 1347±6 Ma MISE1806 melanosome yields a younger date for the older population than the 1355±8 Ma MISE1806 leucosome but the dates overlap within error. The combined weighted average for the older populations of the two subsamples is 1349±5 Ma (MSWD = 5.0, n = 89/ 94) (Fig. 20a,b).

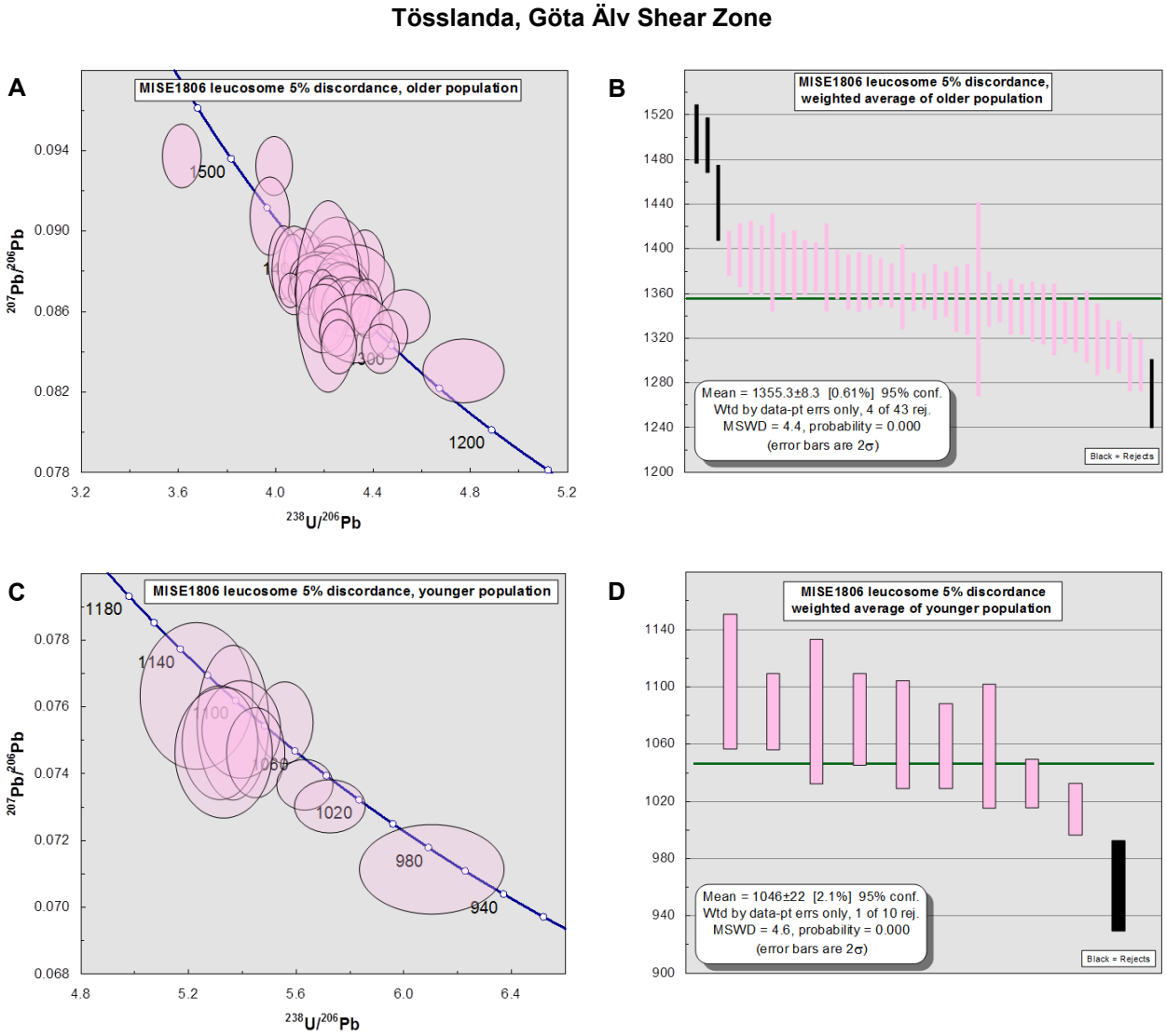

Fig. 19. Tösslanda, Göta Älv Shear Zone. (a) Tera-Wasserburg concordia diagram for the older population in sample MISE1806 leucosome. (b) $^{207}Pb/^{206}Pb$ weighted average date of the older population in sample MISE1806 leucosome. Age in million years on the y-axis. The plotted analyses are <5% discordant. (c) Tera-Wasserburg concordia diagram for the younger population in sample MISE1806 leucosome. (d) $^{207}Pb/^{206}Pb$ weighted average date of the younger population in sample MISE1806 leucosome based on zircon rims. The plotted analyses are <5% discordant.

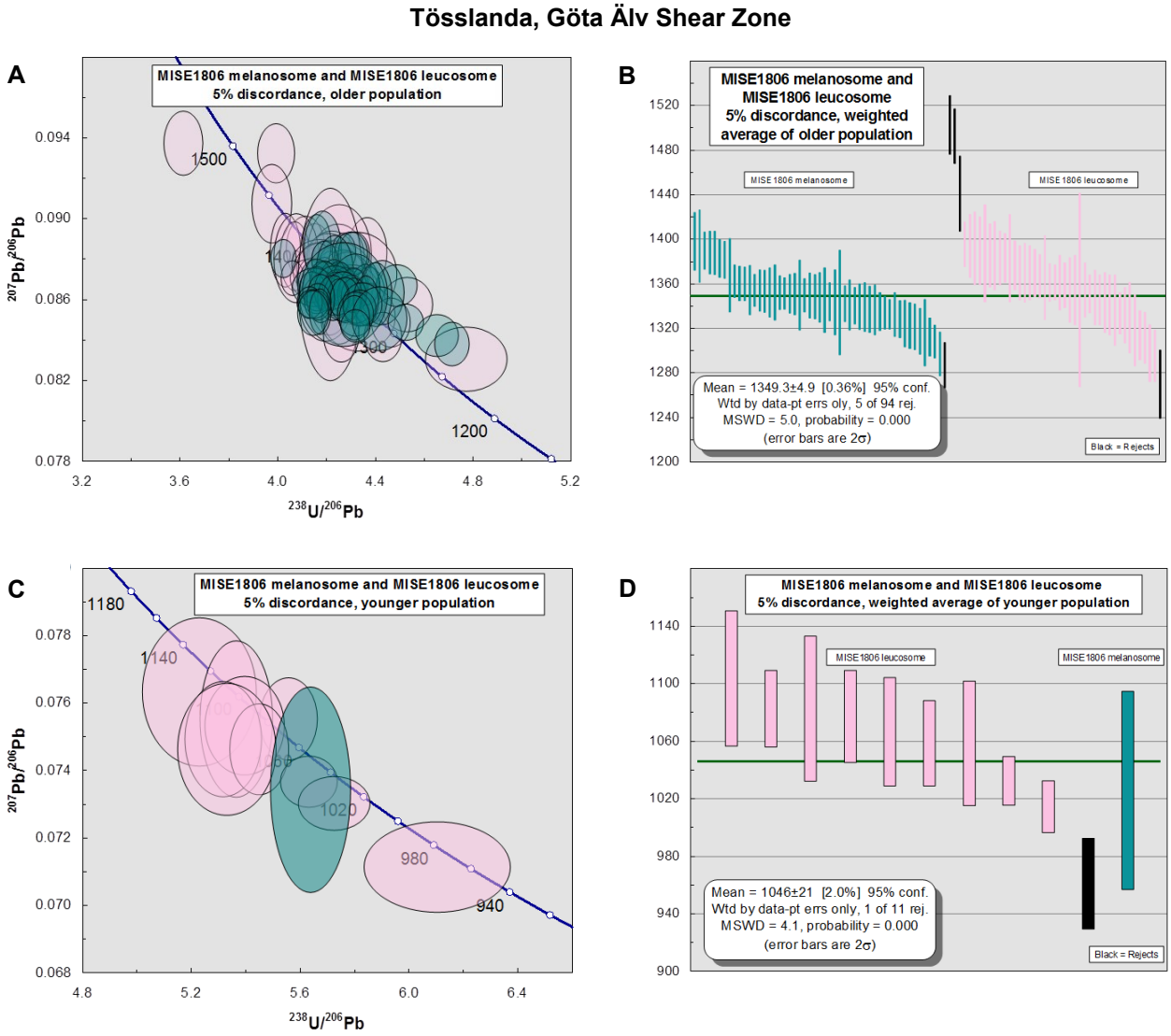

Fig. 20. Tösslanda, Göta Älv Shear Zone. (a) Combined Tera-Wasserburg concordia diagram of the older population for samples MISE1806 leucosome and MISE1806 melanosome. (b) Combined $^{207}Pb/^{206}Pb$ weighted average date of the older population for samples MISE1806 leucosome and MISE1806 melanosome. Age in million years on the y-axis. The plotted analyses are <5% discordant. (c) Combined Tera-Wasserburg concordia diagram for the younger population for sample MISE1806 leucosome and MISE1806 melanosome. (d) Combined $^{207}Pb/^{206}Pb$ weighted average date of the younger population for sample MISE1806 leucosome and MISE1806 melanosome, based on zircon rims. The plotted analyses are <5% discordant.

For the younger population the average dates overlap between the two subsamples, in large part due to the poor precision of the 1081±270 Ma MISE1806 melanosome compared to the 1046±22 Ma MISE1806 leucosome. A 5% discordance criterion was used for the combined age calculation for the young population. The combined weighted average of the younger populations of the two subsamples is 1046±21 Ma (MSWD = 4.1, n = 10/11) (Fig. 20c,d).

5.3 Median Segment (Samples MISE1814 and MISE1816)

5.3.1 MISE1814a

The zircon crystals are 50 to 200 µm in size and are both prismatic and rounded. A few apatite inclusions are present in some grains. The majority of the cores are CL-dark and complex with irregular zoning. A few zircons have CL-dark cores with distinct concentric oscillatory zoning (Appendix III zircons 53 and 56 in Fig. 1) and two zircons show sector zoning. Several crystals have two or more generations of 5-15 µm thick overgrowths; an inner CL-bright rim and a CL-dark outer rim (Appendix III zircons 65 and 78 in Fig. 1). The inner rims often cut the zoned cores and the outer rims cut the inner rims (Appendix III zircon 74 in Fig. 1).

85 spots in 55 crystals were analysed for U-Pb (Appendices IV and V). 39 out of the 85 analyses were used for age calculations (Appendix III Fig. 1). The remaining analyses were omitted due to discordance and lack of precision. A histogram of all analyses yields two major peaks, one larger at ~1580 Ma and

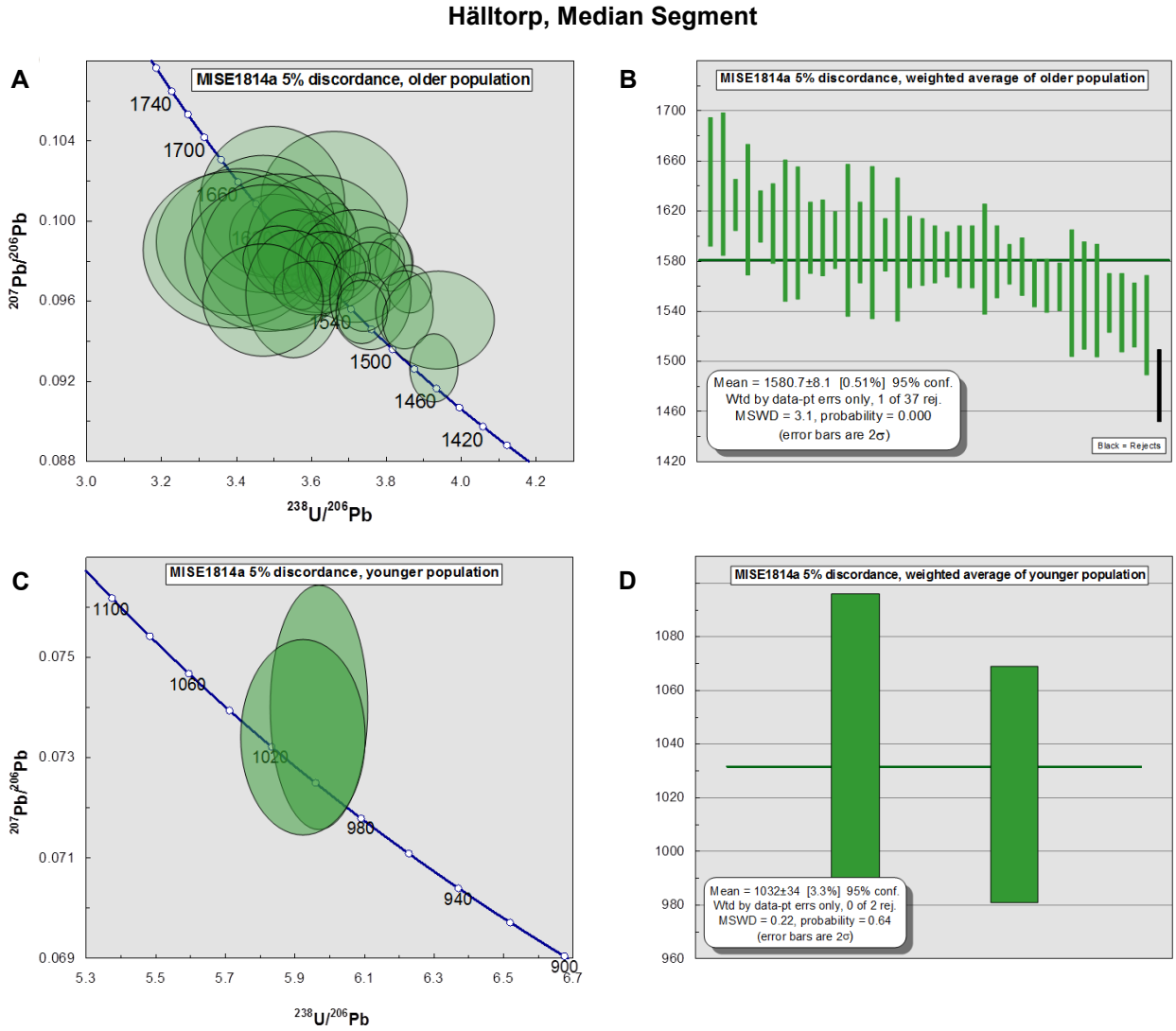

Fig. 21. Hälltorp, Median Segment. (a) Tera-Wasserburg concordia diagram for the older population in sample MISE1814a. (b) $^{207}Pb/^{206}Pb$ weighted average date of the older population in sample MISE1814a. Age in million years on the y-axis. The plotted analyses are <5 % discordant. (c) Tera-Wasserburg concordia diagram for the younger population in sample MISE1814a. (d) $^{207}Pb/^{206}Pb$ weighted average date of the younger population in sample MISE1814a based on zircon rims. The plotted analyses are <5% discordant.

one smaller at ~1030 Ma (Appendix V). A $^{207}Pb/^{206}Pb$ weighted average for the older population yields a 1581±8 Ma (MSWD = 3.1; n = 36/37) date (Fig. 21a,b). For these 37 analyses U concentrations range from 65 ppm to 701 ppm with an average of 262 ppm. Th concentrations range from 10 ppm to 904 ppm with an average of 256 ppm. Th/U vary from 0.162 to 1.495, with an average of 0.912 (Appendix VI Fig. 1b). Spot 81 of zircon 78 sticks out in having a distinctly lower Th/U value of 0.071 (U = 103 ppm, Th = 9.8 ppm) (Appendix III Fig. 1).

A weighted average for the younger population yields a 1032±34 Ma (MSWD = 0.22; n = 2) date (Fig. 21c,d). Spot 32 in zircon 22 (U = 214 ppm, Th = 1.0 ppm) and spot 75 in zircon 68 (U = 57 ppm, Th = 0.2 ppm) belongs to the younger population (Appendix III Fig. 1). These spots yield Th/U of 0.004 and 0.002 respectively (Appendix VI Fig. 1b).

5.3.2 MISE1816c melanosome

The zircon crystals are between 100 and 300 µm along the c-axis, with prismatic and rounded shapes. The grains are heterogeneous and fractured. The crystals contain a few inclusions of apatite, K-feldspar and quartz. The cores are both CL-dark and CL-bright and some show concentric oscillatory zoning (Appendix III zircons 53, 73 and 79 in Fig. 4) and a few cores show sector zoning (Appendix III zircons 4, 49 and 75 in Fig. 4). The zircon crystals have 10-15 µm thick CL -bright overgrowths (Appendix III Fig. 4).

86 spots in 56 grains were analysed for U-Pb (Appendices IV and V). 74 of these 86 analyses were used for age calculations and the rest were discarded (Appendix III Fig. 4). A histogram of all analyses reveals one peak at about 1600 Ma (Appendix V). A $^{207}Pb/^{206}Pb$ weighted average of the population yields a 1601±4 Ma (MSWD = 2.3; n = 68/74) date (Fig. 22).

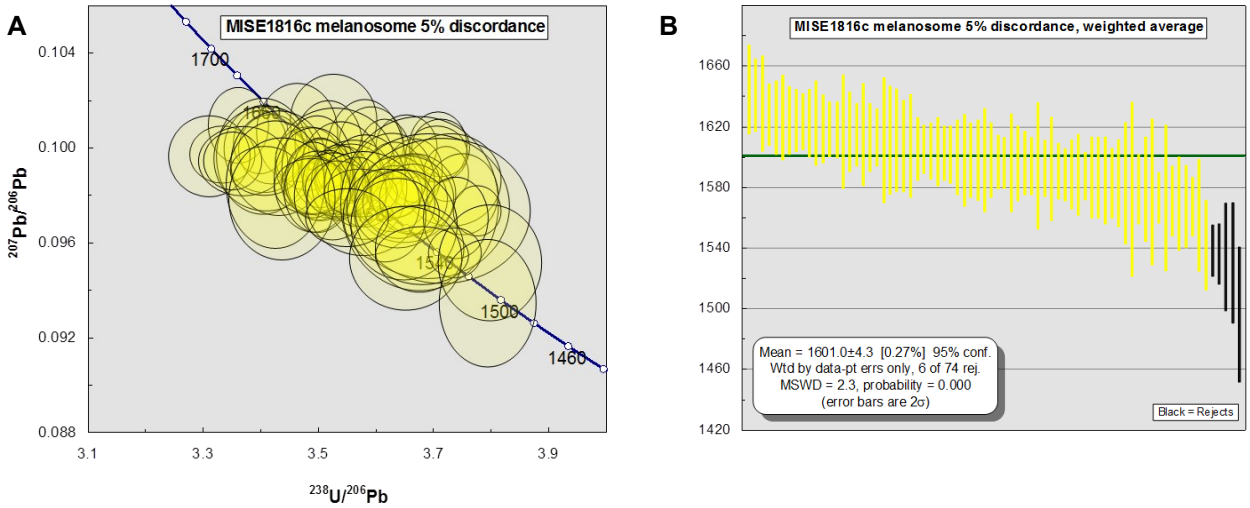

Fig. 22. Hälltorp, Median Segment. (a) Tera-Wasserburg concordia diagram for sample MISE1816c melanosome. (b) $^{207}Pb/^{206}Pb$ weighted average date of sample MISE1816c melanosome. Age in million years on the y-axis. The plotted analyses are <5% discordant and ellipses correspond to 2 standard errors.

U concentrations vary from 55 ppm to 875 ppm (average 273 ppm), Th varies from 43 ppm to 664 ppm (average 208 ppm) and Th/U range between 0.209 and 1.330 with an average of 0.766 (Appendix VI Fig. 1b). One analysis, spot 55 in zircon 28, has a higher U concconcentration of 1153 ppm (Th = 465 ppm, Th/U = 0.398) (Appendix III Fig. 4).

5.3.3 MISE1816c leucosome

The zircon crystals are prismatic and rounded and vary in size from 100 to 300 µm. A few inclusions of apatite, K-feldspar and quartz are present. The crystals are fractured, show no zonation and are CL-dark. Most of the grains are completely homogeneous but in a few grains several generations of overgrowths can be seen. Zircons 11, 12 and 32 show CL-bright (5-10 µm thin) inner rims with CL-dark outer rims (Appendix III Fig. 5). Zircons 2 and 36 only have a CL-bright (5-10 µm thin) outer rim (Appendix III Fig. 5).

62 spots in 47 crystals were analysed for U-Pb (Appendices IV and V). 54 out of the 62 analyses were included in the age calculations, the remaining analyses were omitted due to discordance (Appendix III Fig. 5). The sample generates two population peaks, one at ~1600 Ma and one at ~1000 Ma which can be seen in the histogram in Appendix V. The older population yields a $^{207}Pb/^{206}Pb$ weighted average date of 1600±4 Ma (MSWD = 2.5; n = 49/52), with U from 412 ppm to 3980 ppm (average 1311 ppm) and Th from 168 ppm to 1960 ppm (average 665 ppm) (Fig. 23a,b). Th/U range from 0.107 to 1.088 with an average of 0.549 (Appendix VI Fig. 1b). One analysis (spot 92 in zircon 70) deviates from the rest in having high concentrations of U (12 000 ppm), Th (11 030 ppm) and higher Th/U (1.088) (Appendix III Fig. 5).

The younger population consists of spot 61 in zircon 32 (U = 1385 ppm, Th = 64 ppm, Th/U = 0.046) and spot 77 in zircon 48 (U = 841 ppm, Th = 9 ppm, Th/U = 0.010) (Appendix III Fig. 5 and Appendix VI Fig. 1b). A $^{207}Pb/^{206}Pb$ weighted average of the younger population yields a 1037±200 Ma (MSWD = 3.6, n = 2) date (Fig. 23c,d).

5.3.4 Combined results

Subsamples MISE1816c leucosome and MISE1816c melanosome come from the same rock in the Median Segment and thus the results from these two datasets were combined. Sample MISE1814 yielded a significantly younger date (1581±8 Ma) for the older population than subsamples MISE1816c melanosome (1601±4 Ma) and MISE1816c leucosome (1600±4 Ma). The MISE1814 date for the older population was therefore not combined with the MISE1816 older population date, even though the rocks were indistinguishable in the field. The date for the younger population on the other hand was similar for MISE1814 and MISE1816c leucosome and these results were combined to enhance the precision of the age calculation. A 5% discordance criterion was used for the combined results.

A combined $^{207}Pb/^{206}Pb$ weighted average of the older populations in the MISE1816 subsamples yield a 1601±3 Ma (MSWD = 2.5, n = 118/126) date (Fig. 24a,b).

Spot 77 in zircon 48 in subsample MISE1816c leucosome (Fig. 23c left ellipse) was not included in the combined age calculation of the young population for MISE1814 and MISE1816c leucosome. The reason is that the zircon does not have a clear boundary between the core and the rim and that the core has high U concentrations (3420 ppm) and high Pb concentrations (2830 ppm), while the rim has relatively low

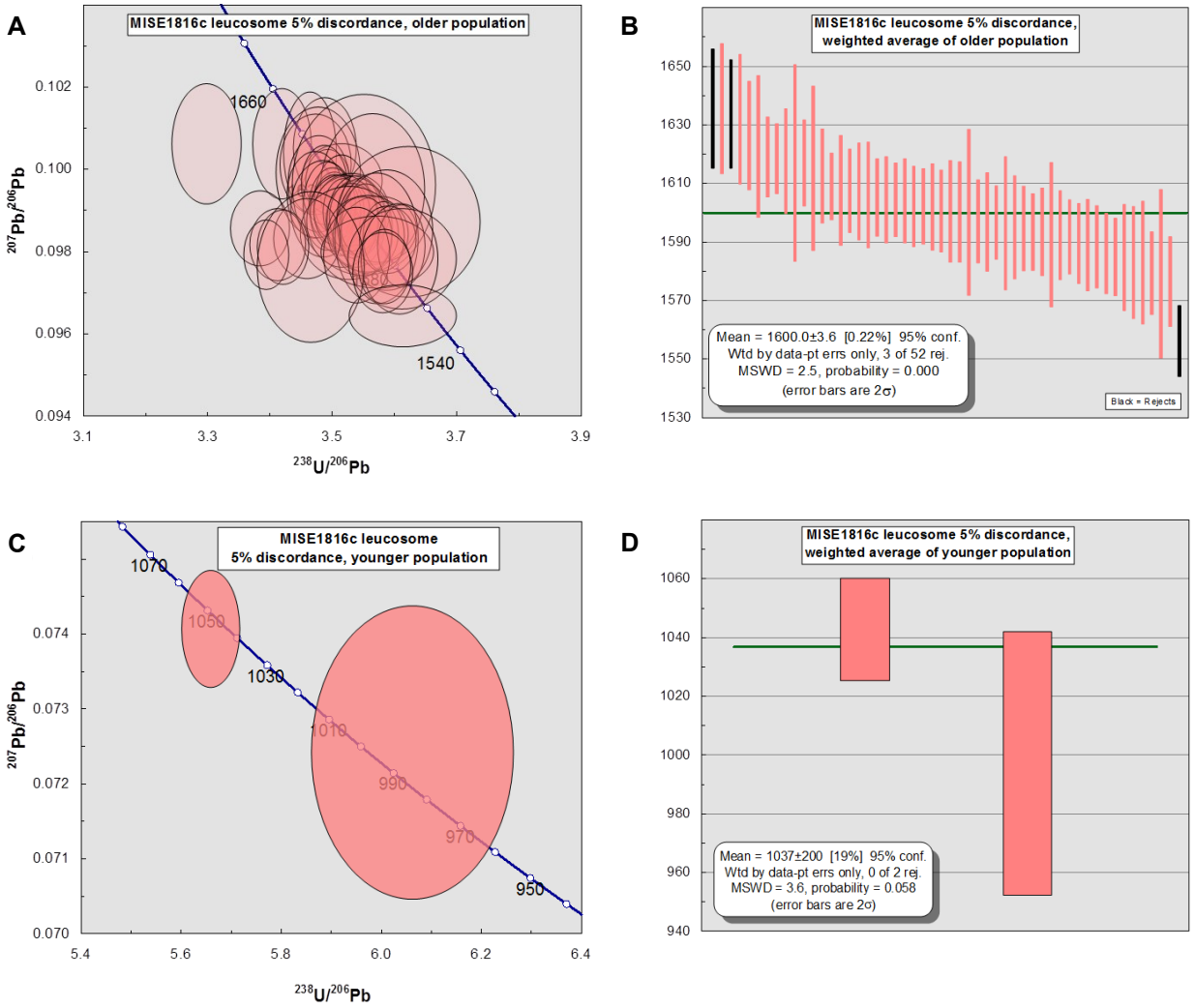

Fig. 23. Hälltorp, Median Segment. (a) Tera-Wasserburg concordia diagram for the older population in sample MISE1816c leucosome. (b) $^{207}Pb/^{206}Pb$ weighted average date of the older population in sample MISE1816c leucosome. Age in million years on the y-axis. The plotted analyses are <5% discordant. (c) Tera-Wasserburg concordia diagram for the younger population in sample MISE1816c leucosome. (d) $^{207}Pb/^{206}Pb$ weighted average date of the younger population in sample MISE1816c leucosome based on zircon rims. The plotted analyses are <5% discordant and ellipses correspond to 2 standard errors.

concentrations of both U and Pb (841 ppm and 58 ppm respectively). This means that there is risk for domain mixing between the rim and the core. A combined $^{207}Pb/^{206}Pb$ weighted average of the young population in the two subsamples yields the date: 1019±27 Ma (MSWD = 0.85, n = 3) (Fig. 24c,d).

6 Discussion

6.1 Limitations of the method

Several zircons in all samples have rims that yield dates belonging to an older population, despite that, given the textural context, a younger metamorphic date was expected. A possible explanation is that the laser beam ablates into the zircon core even if it looks like a thick metamorphic rim on the surface (Fig. 25). If the zircon is insufficiently polished, meaning if a cross section through the grain has not been achieved, then the surface image can give a false appearance of the subsurface of the zircon. An image of a thicker rim on the surface can in fact just be a thin rim at depth. Dating that rim can thus give a ‘‘false’’ age, dating the igneous core instead of the metamorphic rim.

Another possibility is that these are indeed correct dates of an old magmatic or metamorphic event. In some cases a younger metamorphic signature was detected in the first few pulses of ablation, followed by an older magmatic signature. In a few analyses the spectra could be split in two, thus yielding both a younger and an older date. Spot 99b in MISE1806 melanosome is a split analysis (Appendix III Fig. 2). Spots 4b, 18a, 61a and 69a in MISE1806 leucosome are also split analyses (Appendix III Fig. 3). Spots 43, 132 and 137 in MISE1802a leucosome and spot 108 in MISE1802a melanosome are all CL-bright rims that yielded dates belonging to an older population when a

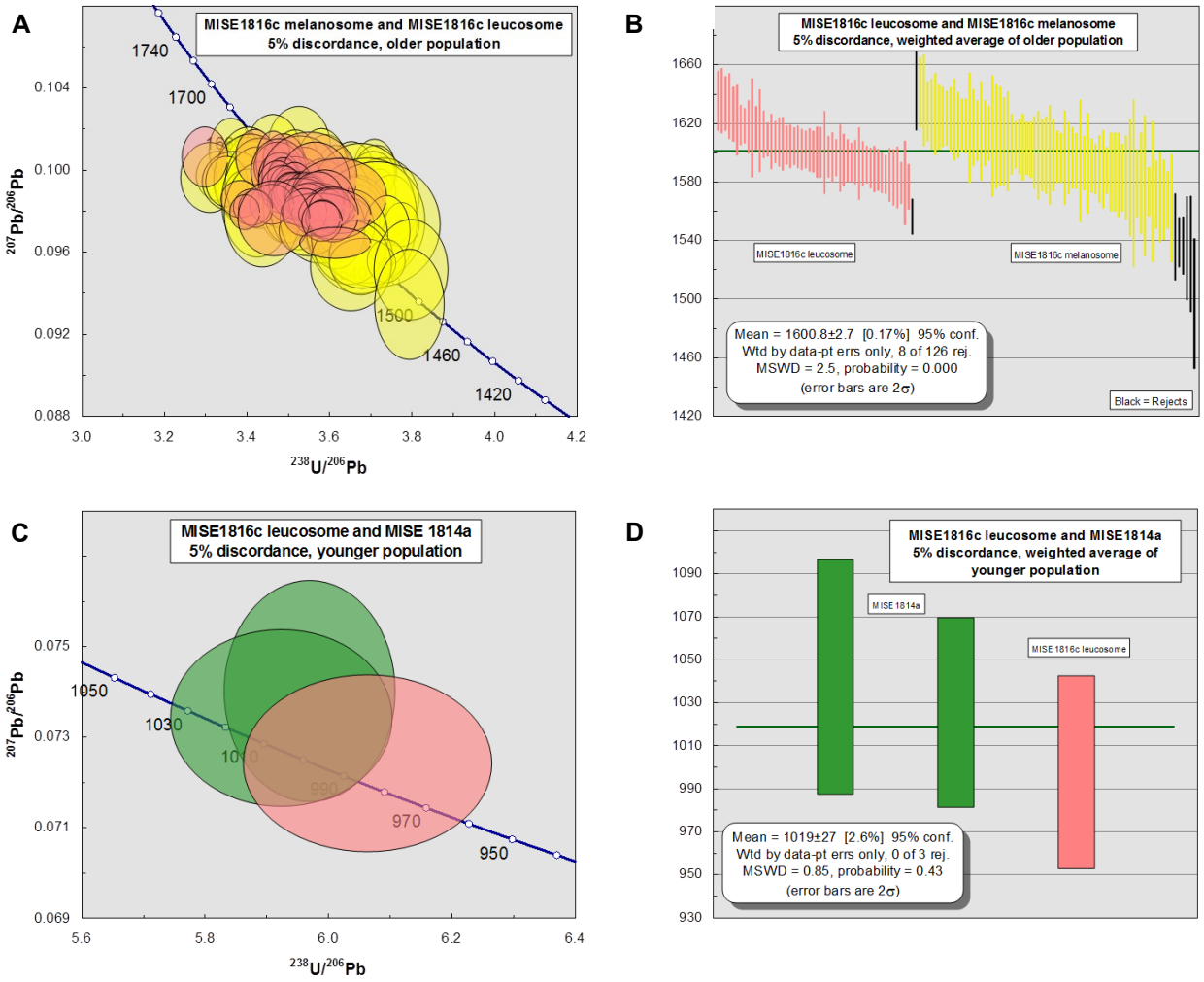

Fig. 24. Hälltorp, Median Segment. (a) Combined Tera-Wasserburg concordia diagram of the older population for subsamples MISE1816c melanosome and MISE1816c leucosome. (b) Combined $^{207}Pb/^{206}Pb$ weighted average date of the older population for subsamples MISE1816c melanosome and MISE1816c leucosome. Age in million years on the y-axis. The plotted analyses are <5% discordant. (c) Combined Tera-Wasserburg concordia diagram of the younger population for sample MISE1814 and subsample MISE1816c leucosome. (d) Combined $^{207}Pb/^{206}Pb$ weighted average date of the younger population for sample MISE 1814 and subsample MISE1816c leucosome, based on zircon rims. The plotted analyses are <5% discordant.

metamorphic date was expected (Appendix III Figs. 6 and 7). Spots 47 and 90 in MISE1806 melanosome and spots 13, 41, and 46 in MISE1806 leucosome could also be rims that are actually metamorphic (Appendix III Figs. 2 and 3). Sample MISE1814a has several zircons with thick CL-bright rims that did not yield younger metamorphic dates (Appendix III Fig. 1) and in MISE1816c leucosome thicker CL-bright zircon rims was expected but was not seen due to insufficient polishing of the zircons.

6.2 A comparison of the structural and textural relationships between the Western and the Median Segments

In the Western Segment, the bedrock is dominated by homogeneous granodioritic gneisses and augen gneisses, with discordant intrusions of pegmatites that rarely show any signs of deformation. Migmatite was only observed in one rock which is folded along gentle to open folds. In the thin sections, quartz, K-feldspar, plagioclase, biotite and epidote dominate the mineral assemblage. Most grains are euhedral to subhedral. Accessory muscovite is also found in the thin sections. Garnet and hornblende have not been observed in the field or in the thin sections in any of the sampled rocks from the Western Segment.

In the Median Segment, the heterogeneous bedrock is made up of granitic to granodioritic gneisses, amphibolites and ultramafics. The rocks often contain garnet and occasionally hornblende and muscovite. Pegmatites that intruded the gneisses are strongly deformed. Stromatic and fold-structured migmatites are common. Folding of the bedrock is common in the whole field area with tight to isoclinal folds. Quartz, K

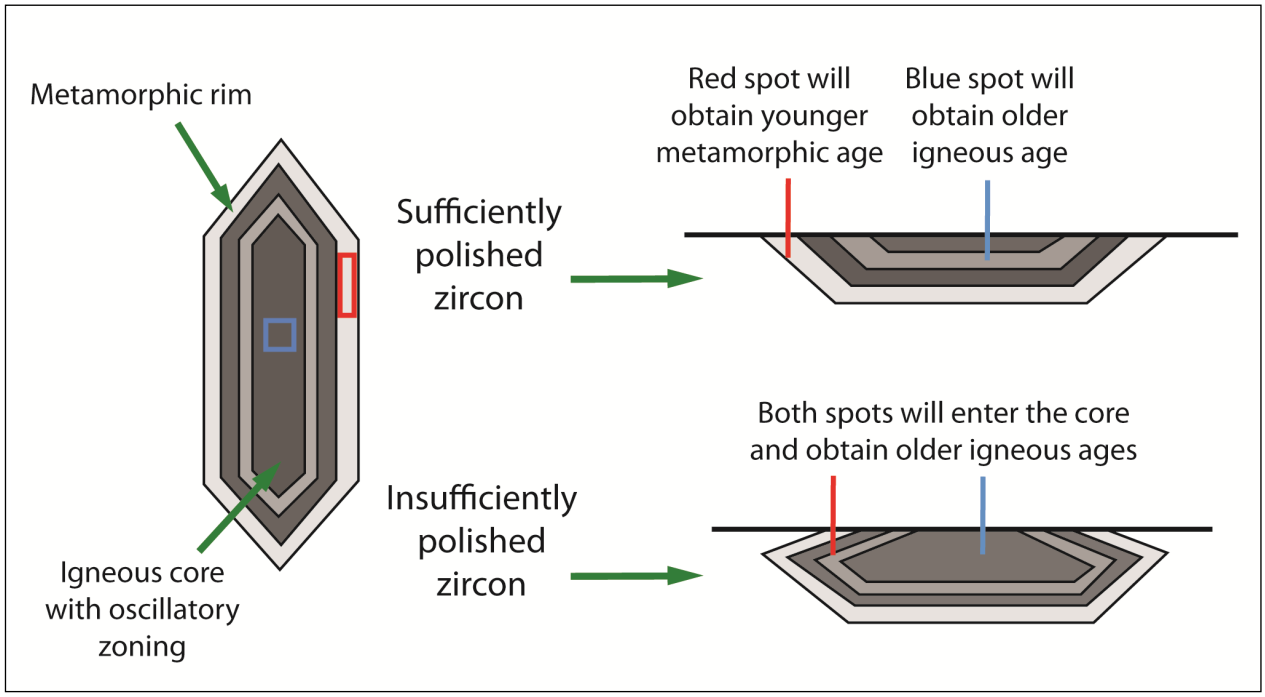

Fig. 25. Illustration showing the issues with polishing zircons insufficiently. The left drawing represents a cathodoluminescence image of a zircon as seen from above when polished. A core with oscillatory zoning and a metamorphic rim can be distinguished and ablation spots are put in the core and in the rim. The right drawings illustrate the zircon as seen in cross section. The top scenario represents a sufficiently polished zircon in which the blue spot will obtain the igneous age and the red will obtain the metamorphic age as expected. In the bottom scenario the zircon is insufficiently polished which will cause the laser beam to ablate into the core. As a result, the igneous age is obtained instead of the metamorphic age.

-feldspar, plagioclase, biotite, scapolite and garnet dominate the thin sections. There is also minor hornblende, traces of anhedral epidote grains and some minor muscovite. Quartz grains are elongate, some ribbon-textured, indicating high strain in the rock. Mineral grains are subhedral to anhedral.

Within the Göta Älv Shear Zone the bedrock is dominated by granitic to granodioritic gneisses with layers of mafic rocks and intrusions of pegmatite veins. Migmatites with gentle folds have been observed but no fold-structures were seen at the sampled locality. The thin sections are dominated by quartz, K-feldspar, plagioclase, biotite, hornblende and opaque minerals, which have been oxidized. Biotization of hornblende is also common. Interstitial fine-grained quartz with sutured boundaries is abundant. In the Göta Älv Shear Zone both ductile and brittle deformation have taken place, the latter evident from the faults cutting the foliation. The brittle deformation can also be seen in micro-scale in the thin sections where fractures are abundant. The migmatization of the rock took place in a ductile environment and the alteration and the fracturing of the rock occurred after the migmatization in a cooler environment. Since the rock is found in a zone of weakness it is highly plausible that the zone has been reactivated several times throughout the Sveconorwegian orogeny (and after). Therefore, the rock could have gone through metamorphism more than once during this period.

Overall, there is striking contrast between the Western and Median Segments, with strain, migmatite abundance and mineral parageneses. The migmatization of the rocks in the Western and Median Segments, and within the Göta Älv Shear Zone must have occurred during upper amphibolite facies conditions since the rocks must reach above 650°C to start melting. Signs of prograde metamorphism in upper amphibolite-facies is not preserved in the mineral assemblage of the Arsjön migmatite in the Western Segment nor in the Tösslanda migmatite within the Göta Älv Shear Zone. Instead mineral assemblages typical for greenschist-facies to lower amphibolite-facies conditions are present, that possibly formed through mineral re-equilibration during decompression and overprinted earlier upper amphibolite-facies minerals. In the Hälltorp migmatites in the Median Segment the preserved amphibolite-facies mineral assemblages suggest less retrograde metamorphic overprint, although traces of epidote grains have been found. This difference in preserved metamorphic grade on either side of the Göta Älv Shear Zone was also described by Austin Hegardt (2010). Furthermore, strain is greater in the Median Segment of the study area and tight to isoclinal folds are abundant in contrast to the Western Segment. The causes for the contrast in deformation between the two segments remain unclear and further work is required to investigate this. Perhaps the Median Segment has been buried to a greater depth than the Western Segment during the Sveconorwegian orogeny, which generated higher strain and formed more migmatites in the Median Segment.

6.3 Geochronology

The samples analysed in this study yield three generations of zircon, two older populations (Fig. 26a) and one younger population (Fig. 26b). The combined data for MISE1802 (Western Segment), MISE1806 (Göta Älv Shear Zone), MISE1814 and MISE1816 (Median Segment) will be used when discussing the data and its implications. First, the older populations will be discussed followed by the younger population. Lastly implications for the younger population for all samples combined will be reviewed.

6.3.1 Protolith ages

The combined weighted average of 1551±6 Ma (MSWD = 6.6, n = 76/82 for sample MISE1802 (the Arsjön migmatite) in the Western Segment is interpreted to be the magmatic crystallization age of the rock and corresponds to the 1.58-1.52 Ga Hisingen Suite (Åhäll & Connelly 2008). The majority of the zircons in the melanosome exhibit concentric oscillatory zoning, which is a common feature in igneous zircon (Hoskin & Black 2000; Hoskin & Schaltegger 2003; Corfu et al. 2003). The igneous origin is further supported by high Th/U values with a mean of ~0.8, values >0.2 is typical for igneous zircon (Williams & Claesson 1987; Yakymchuk et al. 2018 and references therein). Due to unstable $^{207}Pb/^{206}Pb$ several analyses were rejected from age calculations.

The combined weighted average for sample MISE1806 (the Tösslanda migmatite) in the Göta Älv Shear Zone yields a date of; 1349±5 Ma (MSWD = 5.0, n = 89/94), which is interpreted to be the magmatic crystallization age of the rock. Th/U around ~0.9 support the magmatic origin of the zircons (Yakymchuk et al. 2018 and references therein). This rock most likely belongs the Kungsbacka Bimodal Suite even though it is slightly older than the 1.34-1.30 Ga ages hitherto obtained from this suite along the Göta Älv Shear Zone (Austin Hegardt et al. 2007). Although this age is the oldest reported from the Kungsbacka Bimodal Suite, it is still significantly younger than the petrographically similar 1368±4 Ma Tjärnesjö (Andersson et al. 1999) and the 1380±6 Ma Torpa (Åhäll et al. 1997) granites in the Eastern Segment, confirming the lack of temporal and petrogenetic correlation of these rocks across the Mylonite Zone (Austin Hegardt et al. 2007).

The combined weighted average of 1601±3 Ma (MSWD = 2.5, n = 118/126) for sample MISE1816 and the weighted average of 1581±8 Ma (MSWD = 3.1, n = 36/37) for sample MISE1814a both belonging to the Hälltorp migmatite in the Median Segment, are interpreted to be magmatic crystallization ages. The 1601±3 Ma MISE1816 age correlates well with the rocks belonging to the 1.63-1.59 Ga Göteborg-Åmål Suite (Åhäll & Connelly 2008). The 1581±8 Ma MISE1814 on the other hand is thought to belong to a local pluton of the Hisingen Suite (1.58-1.52 Ga) which have intruded the Göteborg-Åmål belt. Although the two samples were taken from identical looking rocks a few metres apart, it cannot be ruled out that MISE1816 and MISE1814 originally were two different rocks. The U and Th concentrations are significantly different and so are the protolith ages. This serves to illustrate the challenge with high-strained migmatite gneisses (see cover picture). The magmatic source for both samples is supported by Th/U values around ~0.7, characteristic for igneous zircon (Williams & Claesson 1987; Yakymchuk et al. 2018 and references therein).

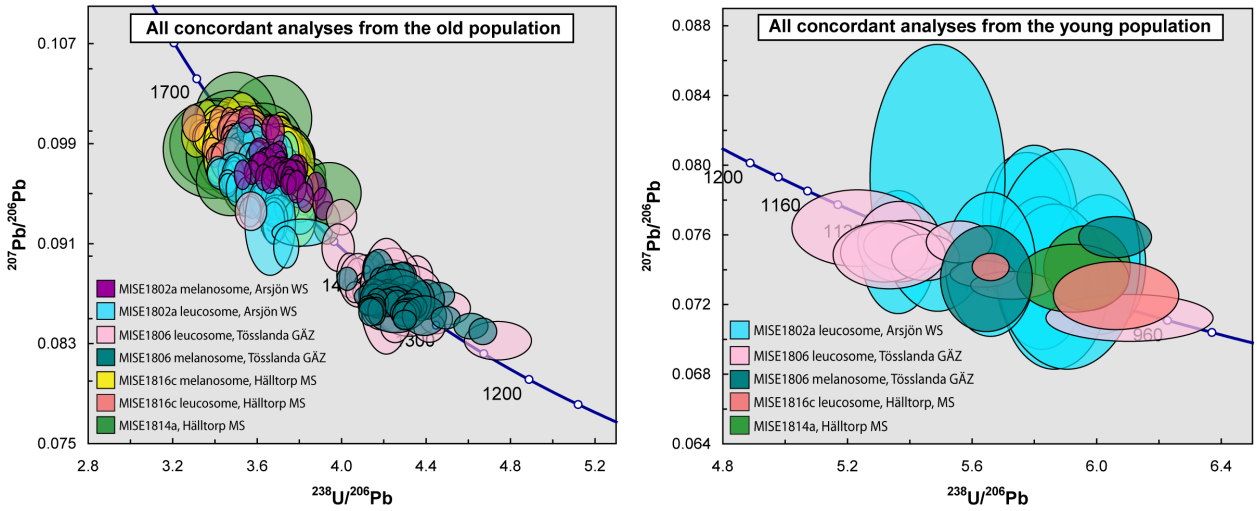

Fig. 26. (a) Combined Tera-Wasserburg concordia diagram of the concordant protolith ages of all samples. The plotted analyses are <5% discordant. The different samples are represented by ellipses of different colour as shown in the legend. WS = Western Segment, GÄZ = Göta Älv Shear Zone and MS = Median Segment. (b) Combined Tera-Wasserburg concordia diagram of the concordant Sveconorwegian metamorphic ages of all samples. The plotted analyses are <10% discordant. The different samples are represented by ellipses of different colour as shown in the legend. All ellipses correspond to 2 standard errors.

MISE1814a and MISE1816c melanosome got zircons cores with irregular zoning and a few cores with magmatic oscillatory zoning still preserved, further reinforcing the igneous origin of the zircons. Zircon in MISE1816c leucosome on the other hand are completely homogeneous. This homogeneity is probably caused by overprinting of an igneous zonation during metamorphism, since zonation is still preserved in the melanosome of the sample.

6.3.2 Sveconorwegian ages

The timespan from partial melting of a rock to metamorphic crystallization of the partial melt is relatively short (Sawyer 2008), and most likely lies within the error of the metamorphic dates yielded in this study. Therefore, the migmatite formation is considered to be the process of metamorphic crystallization of partial melts in this study. Zircon rims from the Arsjön migmatite (MISE1802) in the Western Segment yielded a weighted average date of 1073±31 Ma (MSWD = 0.86, n = 9) based solely on rims from the leucosome since no rims with younger dates were found in the melanosome. This date is interpreted to be the age of metamorphism and associated migmatite formation and coincides with Sveconorwegian metamorphism (1.14-0.90 Ga) in southwestern Fennoscandia (Bingen et al. 2005; Bingen et al. 2008b). The analyses have low concentrations of U (5-12 ppm) with a mean of 10 ppm and low Th concentrations (0.005-1 ppm) with an average of 0.18 ppm. Low Th/U values (0.002-0.111) with an average of 0.027 also define the population. Low Th concentrations and low Th/U values are both characteristic for metamorphic zircon (Yakymchuk et al. 2018 and references therein). The zircon rims that yielded the metamorphic signature are all CL-bright and both the cores and the rims are homogeneous, also typical for metamorphic zircon (Corfu et al. 2003). Zircon 31 is CL-bright throughout the grain with the same brightness as in metamorphic rims. The Th/U in conjunction with the Sveconorwegian date indicate that this crystal either formed after complete dissolution reprecipitation processes during metamorphism, or that it crystallized as a discrete grain during migmatization (Appendix III Fig. 7).

Inside the Göta Älv Shear Zone a weighted average of zircon rims from sample MISE1806 (the Tösslanda migmatite) yielded a date of 1046±21 Ma (MSWD = 4.1, n = 10/11), interpreted to be the age of metamorphism and migmatite formation. The age is coeval with the Sveconorwegian metamorphic event at 1.14-0.90 Ga (Bingen et al. 2005; Bingen et al. 2008b). The metamorphic signature is supported by high U concentrations (254-3680 ppm, average ~1700 ppm) and relatively low Th concentrations (12-830 ppm, average ~130 ppm) as well as low Th/U values (0.004-0.300, average ~0.03), typical for metamorphic zircon according to Yakymchuk et al. (2018 and references therein). The metamorphic homogeneous overgrowths are hard to see since the zircons are CL-dark and unzoned. MISE1806 is the only sample in which the melanosome also yielded metamorphic dates, this is probably due to the leucosome-looking veins present in the melanosome parts of the rock. Two analyses in MISE1806 leucosome, spot 38 in zircon 36 and spot 77 in zircon 84 yielded significantly younger dates of 945±19 Ma and 960±32 Ma respectively, interpreted to be metamorphic ages (Appendix IV). Spot 77 is included in the age calculation of the younger population since it is within 5% discordant. Spot 38 is within 10% discordant and was not included in the age calculation. These two analyses could indicate a later stage of Sveconorwegian metamorphism, at least in the Göta Älv Shear Zone, but the small data set makes any conclusions speculative at best and more work is required to confirm the existence of a younger phase of zircon growth within the Göta Älv Shear Zone.

In the Median Segment zircon rims from samples MISE1814a and MISE1816c leucosome (the Hälltorp migmatites) gave a weighted average date of 1019±27 Ma (MSWD = 0.85, n = 3). The date is interpreted to be the age of metamorphism and migmatite formation, and it coincides with Sveconorwegian metamorphism at 1.14-0.90 Ga (Bingen et al. 2005; Bingen et al. 2008b). The two subsamples most likely belong to different protoliths since the protolith dates and the U and Th concentrations are distinct between the two. The metamorphic overprint and associated migmatite formation is although thought to be coeval between the subsamples. The reason is that the two rocks look identical in the field and that they yielded similar metamorphic dates. The metamorphic signature is supported by low Th/U values between 0.003 and 0.04 with an average of 0.018. The analyses have high U concentrations (57-1385 ppm) with an average of 552 ppm and low Th concentrations (0.2-64 ppm) with an average of 21 ppm, also indicative for metamorphic zircon (Yakymchuk et al. 2018 and references therein). The two metamorphic zircon rims in MISE1814a are both CL-bright and homogeneous, and the cores are irregularly zoned or unzoned. The zircon rim in MISE1816c leucosome is CL-dark with an unzoned core. Several CL-bright zircon rims yielded discordant protolith ages but had metamorphic Th/U signatures of ~0.05. An example is spot 4 in zircon 2 (Appendix III Fig. 1). This could indicate the presence of Gothian migmatization, though highly speculative, or that analyses yielded a mixed date with signatures from both an igneous core and a metamorphic rim. Zircons in MISE1816c leucosome are all homogeneous, while zircons in the melanosome are more diverse.

6.3.3 Implications for the Sveconorwegian ages

The three Sveconorwegian ages from the study area differ in age, from older in the west to younger in the east. This coincides well with the overall Sveconorwegian age decrease from west to east recorded in the Sveconorwegian orogenic belt from 1.14 Ga in the Bamble terrane to 0.98 Ga in the Eastern Segment (Bingen et al. 2008b; Austin Hegardt 2010; Möller et

al. 2015). The main Sveconorwegian metamorphic ages recorded in the Idefjorden terrane are constrained to the Agder phase, between 1.05-0.98 Ga (Bingen et al. 2008b). All the dates of migmatite formation in the 1073±31 Ma Arsjön migmatite (MISE1802), the 1046±21 Ma Tösslanda migmatite (MISE1806) and the 1019±27 Ma Hälltorp migmatites (MISE1814 and MISE1816) overlap with the timespan of the Agder phase. The oldest metamorphic record from the Begna sector, (the Norwegian part of the Idefjorden terrane west of the Oslo rift) is dated at 1.09 Ga (Bingen et al. 2008b,c), so a date of 1073±31 Ma in the Western Segment might be reasonable even if better precision of the date is obtained.

Sveconorwegian metamorphic ages in the Western Segment are scarce but a few have been recorded centred around 1.04-1.03 Ga (Austin Hegardt 2010), although no Sveconorwegian ages of migmatite formation have been found. Austin Hegardt et al. (2007) analysed metamorphic overgrowths on zircons from the Kärra pegmatite that yielded a U-Pb upper intercept age of 1043±11 Ma, coeval within error with the Arsjön migmatite (1073±31 Ma) from this study. A Sm-Nd garnet isochron from an amphibolite in Nordön gave a date of 1029±6 Ma and Ar-Ar muscovite analyses on a metagraywacke yielded a cooling age of 981±4 Ma (Austin Hegardt 2010). Three rare-mineral pegmatites near the coast in the Western Segment yielded magmatic U-Pb columbite ages of 1041±2 Ma (Skantorp), 1039±3 Ma (Timmerhult) and 1030±1 Ma (Högsbo; Romer & Smeds 1996). These pegmatites, which intruded into brittle crust are discordant to the gneissosity and thereby constrain minimum ages for ductile deformation and migmatite formation in the Western Segment. This means that the 1073±31 Ma Arsjön migmatite must have formed before the pegmatites intruded.

There are a greater number of age records of Sveconorwegian metamorphism and migmatite formation in the Median Segment. Söderlund et al. (2008) analysed the Haregården and the Lunden metadolerite dykes, near Trollhättan, which yielded a 1026±5 Ma and 1046±6 Ma date respectively. These two metadolerite dykes are the only record of high-grade metamorphism in high-pressure granulite-facies found in the Idefjorden terrane (Söderlund et al. 2008). Migmatitic gneisses further south, near Mölnlycke, have been dated to 974±22 Ma by Ahlin et al. (2006) and to 1017±17 Ma (Austin Hegardt 2010). Another migmatitic gneiss, near the Lake Stora Delsjön, was dated to 1002±9 Ma by Ingered (2017) and the Lake Horsika migmatite in the same area yielded a date of 1060±77 Ma (Haeggman 2015). The Hälltorp migmatites (1019±27 Ma) in the Median Segment all overlap with the Sveconorwegian dates mentioned above.

It is notable that all protolith ages are older than the beginning of the Sveconorwegian orogeny and that all the investigated rocks were affected by the orogenesis. Yet, there are striking contrasts in strain, migmatite abundance and preserved mineral assemblages between the different rocks. Although, the composition of the investigated rocks is not different enough to explain the varying response to the Sveconorwegian metamorphism and further studies are therefore required. The Tösslanda migmatite (1046±21 Ma) in the transitional Kungsbacka Bimodal Suite, located within the Göta Älv Shear Zone, serves as an important marker horizon as it post-dates any possible Gothian metamorphic overprint and that it provides strong support for substantial Sveconorwegian migmatite formation. It might thus be inferred that the metamorphism of both the Western and Median Segments are also the result of Sveconorwegian orogeny.

Given the dates recorded in the Idefjorden terrane and especially due to the dates in this study Sveconorwegian metamorphism and associated migmatite formation is not coeval between the Western and Median Segments. It is possible that metamorphism started in the Idefjorden terrane already at 1.07 Ga and that the Agder phase therefore started earlier than 1.05 Ga, although restricted to the Western Segment, The period between the Arendal phase (1.14-1.08 Ga) and the Agder phase (1.05-0.98 Ga) was thought to be characterized by tectonic quiescence (Bingen et al. 2008b). This might not be the case, at least not locally. If Sveconorwegian metamorphism and associated migmatite formation started in the Western Segment around 1080-1040 Ma, this supports the interpretation that the 1.04-1.03 Ga pegmatites dated by Romer and Smeds (1996) constrain a minimum age for ductile deformation and migmatite formation in the Western Segment. Furthermore, the emplacement of the pegmatites in the Western Segment pre-dates the migmatite formation in the Median Segment. Metamorphism of the Idefjorden terrane during the Agder phase should be revised to include the period between ca. 1.08 Ga and 1.05 Ga. The Agder phase is better described as a phase of metamorphism in the Idefjorden terrane between 1.08-0.98 Ga.

7 Conclusions

Migmatites have been found in both the Western and Median Segments, and within the Göta Älv Shear Zone, but they are different in extent and style. In the Median Segment migmatites are more abundant, higher-strained and preserved a higher-grade mineral assemblage. In the Western Segment and within the Göta Älv Shear Zone migmatites are rare, and the lower-grade mineral assemblages are most likely the result of mineral re-equilibration through decompression.

- The protolith age for the migmatite in the Western Segment is 1551±6 Ma which belongs to the Hisingen Suite.
- The migmatite within the Göta Älv Shear Zone yields a protolith age of 1349±5 Ma corresponding to the Kungsbacka Bimodal Suite.
- The migmatites in the Median Segment yield two protolith ages, one at 1601±3 Ma belonging to the Göteborg-Åmål belt, and one at

1581±8 Ma which is interpreted as a local pluton of the Hisingen Suite. The two migmatites were initially thought to be of the same origin, but since the protolith ages reveal this not to be the case, it demonstrates the complexity with high-strained migmatite gneisses.

- Ages of metamorphism and migmatite formation are 1073±31 Ma in the Western Segment, 1046±21 Ma within the Göta Älv Shear Zone and 1019±27 Ma in the Median Segment. Since the migmatite within the Göta Älv Shear Zone post-dates any Gothian (ca. 1.6 Ga) metamorphic overprint, it demonstrates that migmatite formation during the Sveconorwegian orogeny was significant. So far, evidence for older migmatite events is lacking in the studied area.
- The results here in combination with literature data on pegmatites in the Western Segment (Romer & Smeds 1996) and on migmatite formation in the Median Segment (Ingered 2017), indicate that migmatite formation occurred earlier in the Western Segment, before ca. 1040 Ma and later in the Median Segment after ca. 1020 Ma.

8 Suggestions for further research

- Since Sveconorwegian migmatite formation in the Western Segment is poorly recorded more migmatites need to be dated in this area.
- To better understand the cause for the different response to Sveconorwegian metamorphism and deformation in the Idefjorden terrane, further studies are required. A comparison of P-T-t paths for migmatites in the Western and Median Segments could give insight to this problem.

9 Acknowledgements

I would like to thank my supervisor, Anders Scherstén for his support and enthusiasm for this project. I would also like to thank Lena Lundqvist from SGU in Gothenburg for helping me with the field work and Tomas Næraa for helping me run LA-ICP-MS analyses and the subsequent data reduction. My most humble thanks to Anna Sartell, with whom I did the field work. Last but not least, I would like to thank my fellow students, especially Hanna, for these past 5 years. It has truly been an adventure!

10 References

Åhäll, K.I. & Connelly, J.N., 2008: Long-term convergence along SW Fennoscandia: 330 m.y. of Proterozoic crustal growth. *Precambrian Research 163,* 402-421.

Åhäll, K.I., Samuelsson, L. & Persson, P.-O., 1997: Geochronology and structural setting of the 1.38 Ga Torpa granite; implications for the charnockite formation in SW Sweden. *GFF 119,* 37-43.

Ahlin, S., Austin Hegardt, E. & Cornell, D., 2006: Nature and stratigraphic position of the 1614 Ma Delsjön augen granite-gneiss in the Median Segment of southwest Sweden. *GFF 128,* 21-32.

Austin Hegardt, E., Cornell, D., Claesson, L., Simakov, S., Stein, H. & Hannah, J., 2005: Eclogites in the central part of the Sveconorwegian Eastern Segment of the Baltic Shield: Support for an extensive eclogite terrane. *GFF 127,* 221-232.

Austin Hegardt, E., Cornell, D.H., Hellström, F.A. & Lundqvist, I., 2007: Emplacement ages of the mid-Proterozoic Kungsbacka Bimodal Suite, SW Sweden. *GFF 129,* 227-234.

Austin Hegardt, E., 2010: Pressure, temperature and time constraints on tectonic models for southwestern Sweden. *Department of Earth Sciences, University of Gothenburg. A134*, 1-26.

Andersson, J., Söderlund, U., Cornell, D., Johansson, L. & Möller, C., 1999: Sveconorwegian (-Grenvillian) deformation, metamorphism and leucosome formation in SW Sweden, SW Baltic Shield: Constraints from a Mesoproterozoic granite intrusion. *Precambrian Research 98,* 151-171.

Andersson, J., Möller, C. & Johansson, L., 2002: Zircon geochronology of migmatite gneisses along the Mylonite Zone (S Sweden): A major Sveconorwegian terrane boundary in the Baltic Shield. *Precambrian Research 114,* 121-147.

Berthelsen, A., 1980: Towards a palinspastic tectonic analysis of the Baltic Shield. *In J.* Cogne & M. Slansky (eds.): Geology of Europe, from Precambrian to the post-Hercynian sedimentary basins, 5 -21. *International Geological Congress Colloque C6.*

Bingen, B., Skår, Ø., Marker, M., Sigmond, E.M.O., Nordgulen, Ø., Ragnhildstveit, J., Mansfeld, J., Tucker, R.D. & Liégeois, J.P., 2005: Timing of continental building in the Sveconorwegian orogen, SW Scandinavia. *Norwegian Journal of Geology 85,* 87-116.

Bingen, B., Andersson, J., Söderlund, U. & Möller, C., 2008a: The Mesoproterozoic in the Nordic countries. *Episodes 31*, 29-34.

Bingen, B., Nordgulen, Ø. & Viola, G., 2008b: A four-phase model of the Sveconorwegian orogeny, SW Scandinavia. *Norwegian Journal of Geology 88,* 43-72.

Bingen, B., Davis, W.J., Hamilton, M.A., Engvik, A.K., Stein, H.J., Skår, Ø. & Nordgulen, Ø., 2008c: Geochronology of high-grade metamorphism in the Sveconorwegian belt, S. Norway: U-Pb, Th-Pb and Re-Os data. *Norwegian Journal of Geology 88,* 13-42.

Bogdanova, S., Bingen, B., Gorbatschev, R., Kheraskova, T., Kozlov, V., Puchkov, V. & Volozh, Y., 2008: The east European craton (Baltica) before and during the assembly of Rodinia. *Precambrian Research 160,* 23-45.

Brewer, T.S., Åhäll, K.I., Darbyshire, D.P.F. & Menuge, J.F., 2002: Geochemistry of late Mesopro-

terozoic volcanism in southwestern Scandinavia: implications for Sveconorwegian / Grenvillian plate tectonic models. *Journal of the Geological Society, London 159*, 129-144.

Corfu, F., Hanchar, J.M., Hoskin, P.W.O. & Kinny, P., 2003: Atlas of Zircon Textures. *In* J.M Hanckar & P.W.O. Hoskin (eds.): Zircon, 469-500. *Reviews in Mineralogy and Geochemistry 53*. Egerton, R.F., 2016: *Physical Principles of Electron Microscopy: an introduction to TEM, SEM and AEM.* 2nd edition. Springer International Publishing, Cham. 196 pp.

Eliasson, T. & Schöberg, H., 1991: U-Pb dating of the post-kinematic Sveconorwegian (Grenvillian) Bohus granite, SW Sweden: evidence of restitic zircon. *Precambrian Research 51,* 337-350.

Engvik, A.K., Bingen, B. & Solli, A., 2016: Localized occurrences of granulite: P-T modeling, U-Pb geochronology and distribution of early-Sveconorwegian high-grade metamorphism in Bamble, South Norway. *Lithos 240-243, 84-103*.

Faure, G. & Mensing, T.M., 2005: *Isotopes: principles and applications*. 3rd edition. John Wiley & Sons, Hoboken. 897 pp.

Faure, G., 2001: *Origin of igneous rocks: the isotopic evidence*. Springer, Berlin. 496 pp.

Frei, D. & Gerdes, A., 2009: Precise and accurate in situ U-Pb dating of zircon with high sample throughput by automated LA-SF-ICP-MS. *Chemical Geology 261,* 261-270.

Gehrels, G., 2014: Detrital zircon U-Pb geochronology applied to tectonics. *Annual Review of Earth and Planetary Sciences 42,* 127-149.

Goldstein, J.I., Newbury, D.E., Michael, J.R., Ritchie, N.W.M., Scott, J.H.J. & Joy, D.C., 2018: *Scanning Electron Microscopy and X-Ray Microanalysis*, 4th edition. Springer, New York. 550 pp.

Gorbatschev, R. Bogdanova, S., 1993: Frontiers in the Baltic Shield. *Precambrian Research 64,* 3-21.

Haeggman, R., 2015: Zircon dating of the Lake Horsika migmatite. *Department of Earth Sciences, University of Gothenburg. B875,* 1-17.

Hanchar, J.M. & Miller, C.F., 1993: Zircon zonation patterns as revealed by cathodoluminescence and backscattered electron images: implications for interpretation of complex crustal histories. *Chemical Geology 110,* 1-13.

Hoskin, P.W.O. & Black, L.P., 2000: Metamorphic zircon formation by solid-state recrystallization of protolith igneous zircon. *Journal of Metamorphic Geology 18,* 423-439.

Hoskin, P.W.O. & Schaltegger, U., 2003: The composition of zircon and igneous and metamorphic petrogenesis. *In* J.M Hanckar & P.W.O. Hoskin (eds.): Zircon, 27-62. *Reviews in Mineralogy and Geochemistry 53*.

Ingered, M., 2017: U-Pb datering av zirkon från migmatitisk gnejs i Delsjöområdet, Idefjordenterrängen. *Dissertations in Geology at Lund University, Bachelor's thesis 512,* 1-23.

Jackson, S., Pearson, N.J., Griffin, W.L. & Belousova, E.A., 2004. The application of laser ablation - inductively coupled plasma - mass spectrometry to in situ U-Pb zircon geochronology. *Chemical Geology 211*, 47-69.

Johansson, L., Lindh, A. & Möller, C., 1999: Late Sveconorwegian (Grenville) high-pressure granulite facies metamorphism in southwest Sweden. *Journal of Metamorphic Geology 9,* 283-292.

Linders, W., 2016: U-Pb geochronology and geochemistry of host rocks to the Bastnäs-type REE mineralization in the Riddarhyttan area, west central Bergslagen, Sweden. *Dissertations in Geology at Lund University, Master´s Thesis 466*, 1-60.

Ludwig, K.R., 2012: User's manual for Isoplot 3.75. A geochronological toolkit for Microsoft Excel. *Berkeley Geochronology Center Special Publications 5,* 1-75.

Möller, C., 1998: Decompressed eclogites in the Sveconorwegian (-Grenvillian) orogen of SW Sweden: petrology and tectonic implications. *Journal of Metamorphic Geology 16,* 641-656.

Möller, C. & Andersson, J., 2018: Metamorphic zoning and behaviour of an underthrusting continental plate. *Journal of Metamorphic Geology 36,* 567 -589.

Möller, C., Andersson, J., Dyck, B. & Antal Lundin, I., 2015: Exhumation of an eclogite terrane as a hot migmatitic nappe, Sveconorwegian orogen. *Lithos 226,* 147-168.

Möller, C., Andersson, J., Lundqvist, I. & Hellström, F., 2007: Linking deformation, migmatite formation and zircon U-Pb geochronology in polymetamorphic orthogneisses, Sveconorwegian Province, Sweden. *Journal of Metamorphic Geology 25,* 727-750.

Park, R.G., Åhäll, K.I. & Boland, M.P., 1991: The Sveconorwegian shear-zone network of SW Sweden in relation to mid-Proterozoic plate movements. *Precambrian Research 49,* 245-260.

Paton, C., Hellstrom, J., Paul, B., Woodhead, J. & Hergt, J., 2011: Iolite: Freeware for the visualisation and processing of mass spectrometric data. *Journal of Analytical and Atomic Spectrometry 26,* 2508-2518.

Petersson, A., Scherstén, A., Bingen, B., Gerdes, A. & Whitehouse, M.J., 2015: Mesoproterozoic continental growth: U-Pb-Hf-O zircon record in the Idefjorden Terrane, Sveconorwegian Orogen. *Precambrian Research 261,* 75-95.

Roberts, N.M.W. & Slagstad, T., 2014: Continental growth and reworking on the edge of the Columbia and Rodinia supercontinents; 1.86-0.9 Ga accretionary orogeny in southwest Fennoscandia. *International Geology Review 57,* 1-25.

Romer, R. & Smeds, S.-A., 1996: U-Pb columbite ages of pegmatites from Sveconorwegian terranes in Southwestern Sweden. *Precambrian Research* 76, 15-30.

Samuelsson, L. & Lundqvist, I., 1988: Bedrock map

8B Vänersborg SO. Scale 1:50 000. *Swedish Geological Survey, Af 160.*

Sawyer, E.W., 2008: *Atlas of Migmatites.* NRC Research Press, Ottawa. 371 pp.

Schoene, B., 2014: U-Th-Pb Geochronology, *In* H.D. Holland & K.K. Turekian (eds.): *Treatise on Geochemistry vol. 4*, 341-378. Elsevier, Oxford.

Slagstad, T., Roberts, N.M.W., Marker, M., Røhr, T.S. & Schiellerup, H., 2013: A non-collisional, accretionary Sveconorwegian orogen. *Terra Nova 25,* 30-37.

Sylvester, P., 2001: Laser-Ablation-ICPMS in the Earth Sciences: principles and applications. *Short course series / Mineralogical Association of Canada 29,* 1-243.

Söderlund, U., Persson, P.-O., Jarl., L.G., Stephens, M.B. & Wahlgren, C.H., 1999: Protolith ages and timing of deformation in the eastern marginal part of the Sveconorwegian orogen, southwestern Sweden. *Precambrian Research 94,* 29-48.

Söderlund, U., Möller, C., Andersson, J., Johansson, L. & Whitehouse, M.J., 2002: Zircon geochronology in polymetamorphic gneisses in the Sveconorwegian orogen, SW Sweden: ion microprobe evidence for 1.46-1.42 Ga and 0.98-0.96 Ga reworking. *Precambrian Research 113*, 193-225.

Söderlund, U., Hellström, F.A. & Kamo, S.L, 2008: Geochronology of high-pressure mafic granulite dykes in SW Sweden: tracking the P-T-t path of metamorphism using Hf isotopes in zircon and baddeleyite. *Journal of Metamorphic Geology 26,* 539-560.

Tera, F. & Wasserburg, G.J., 1972a: U-Th-Pb systematics in lunar highland samples from the Luna 20 and Apollo 16 missions. *Earth and Planetary Science Letters 17,* 36-51.

Tera, F. & Wasserburg, G.J., 1972b: U-Th-Pb systematics in three Apollo 14 basalts and the problem of initial Pb in lunar rocks. *Earth and Planetary Science Letters 14,* 281-304.

Tual, L., Pitra, P. & Möller, C., 2017: P-T evolution of Precambrian eclogite in the Sveconorwegian orogen, SW Sweden. *Journal of Metamorphic Geology 35,* 493-515.

Ulmius, J., Andersson, J. & Möller, C., 2015: Hallandian 1.45 Ga high-temperature metamorphism in Baltica: P-T evolution and SIMS U-Pb zircon ages of aluminous gneisses, SW Sweden. *Precambrian Research 265,* 10-39 .

Wahlgren, C.-H., Cruden, A.R. & Stephens, M.B., 1994: Kinematics of a major fan-like structure in the eastern part of the Sveconorwegian orogen, Baltic Shield, south-central Sweden. *Precambrian Research 70,* 67-91.

Wendt, I. & Carl, C., 1991: The statistical distribution of the mean squared weighted deviation. *Chemical Geology 86,* 275-285.

Wetherill, G.W., 1956: Discordant uranium-lead ages. *Transactions of the American Geophysical Union 37*, 320-326.

Wiedenbeck, M., Allé, P., Corfu, F., Griffin, W.L., Meier, M., Oberli, F., von Quadt, A., Roddick, J.C. & Spiegel, W., 1995: Three natural zircon standards for U–Th–Pb, Lu–Hf, trace element and REE analyses. *Geostandards Newsletters 19*, 1-23.

Williams, I.S. & Claesson, S., 1987: Isotopic evidence for the Precambrian provenance and Caledonian metamorphism of high-grade paragneisses from the Seve Nappes, Scandinavian Caledonides. *Contributions to Mineralogy and Petrology 97,* 205-217.

Yakymchuk, C., Kirkland, C.L. & Clark, C., 2018: Th/U ratios in metamorphic zircon. *Journal of Metamorphic Geology 36,* 715-737.

Appendix I - Bedrock map of the study area

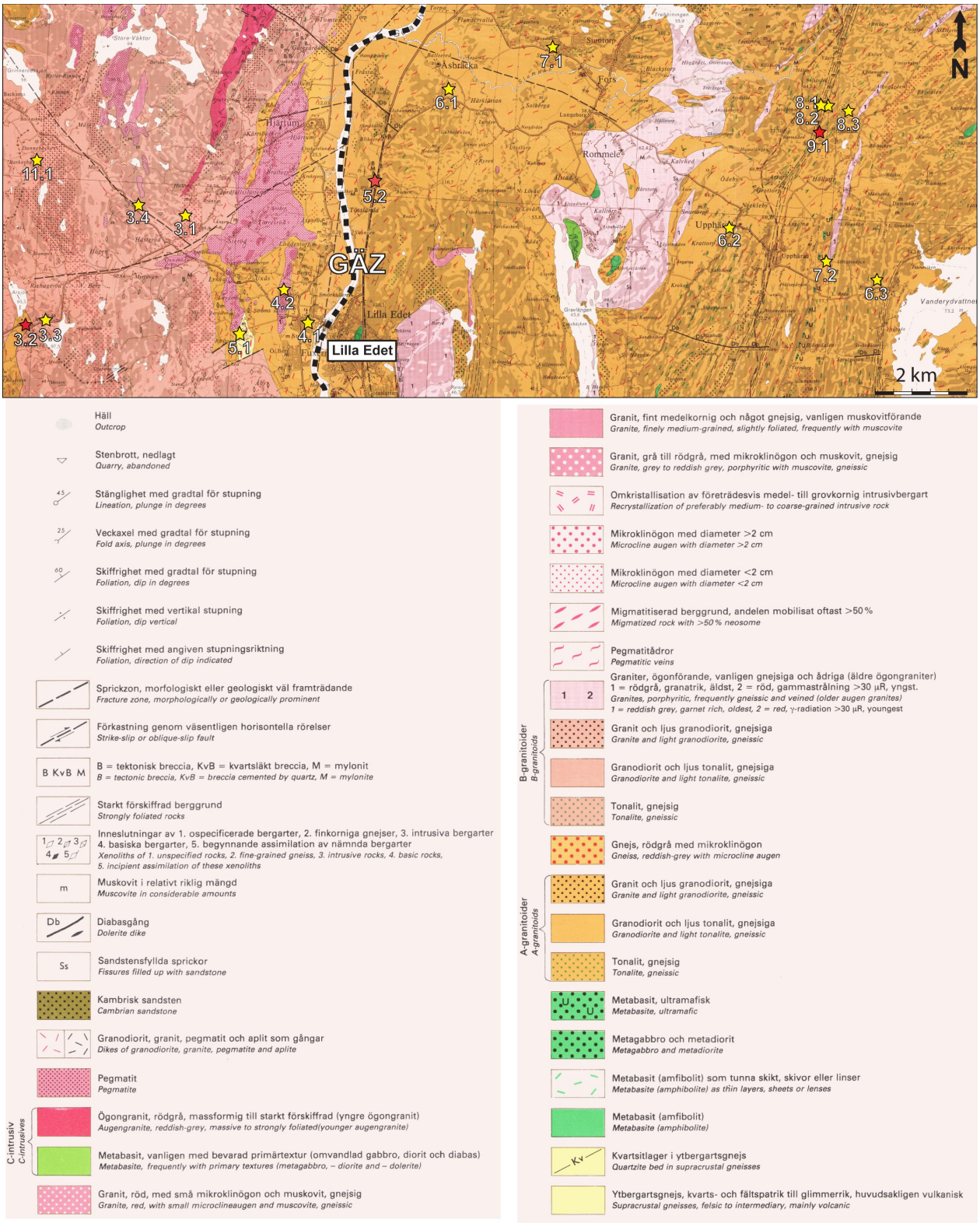

Fig. 1. Bedrock map of the study area (same as in Fig. 3c) with legend, from the Swedish Geological Survey. GÄZ = the Göta Älv Shear Zone. Sample locations are marked with stars and numbers (see Table 1 for further information). Red stars refer to the analysed samples. Modified after Samuelsson & Lundqvist (1988).

Appendix II - LA-ICP-MS Methodology

Table 1. LA-ICP-MS U-Th-Pb dating methodology, Department of Geology, Lund University.

Laboratory & Sample Preparation	
Laboratory name	LA-ICP-MS lab at Lund University
Sample type / mineral	Zircon
Sample preparation	Conventional mineral separation, 1 inch resin mount, 0,25 µm polish to finish
Imaging	SE-imaging, CL-imaging, Tescan Mira3, 10-13kV, 12-16nA, 10 mm working distance.
Laser ablation system	
Make, Model & type	Photon Machines, Analyte G2
Ablation cell & volume	HelEx II Active 2-volume
Laser wavelength	193 nm
Pulse width	>4 ns
Fluence	2.5 J/cm^{-2}
Repetition rate	11-13 Hz
Spot size	18 x 18, 25 x 13, 23 x 14 µm
Sampling mode / pattern	18 µm single spot analyses
Carrier gas	He 0,8 L/min, N^2 4 ml/min, Ar make-up gas combined using a Y-connector close to sample cell
Pre-ablation laser warm-up (background collection)	30 seconds
Ablation duration	30 seconds
Wash-out delay	2 seconds
Cell carrier gas flow	0.8 l/min He
ICP-MS Instrument	
Make, Model & type	Bruker Aurora M90 quadrupole ICP-MS
Sample introduction	Via conventional tubing (1814a) and squid tubing (1802, 1806, 1816)
RF power	1350 W
Make-up gas flow	1.0 l/min Ar
Detection system	Single collector secondary electron multiplier
Masses measured	202, 204, 206, 207, 208, 232, 238
Integration time per peak	4 ms
Total integration time per reading	Approx. 1 sec
Sensitivity	20000 cps/ppm Pb
Dead time	16 ns
Data Processing	
Gas blank	40 second on-peak
Calibration strategy	GJ-1 used as primary reference material, 91500 used as secondary reference material, possibly BB-16 as well.
Reference Material info	GJ-1 (Jackson et al. 2004) 91500 (Wiedenbeck et al. 1995)

Data processing package used / Correction for LIEF	Iolite Software: baseline correction, downhole fractionation correction and common Pb correction
Mass discrimination	Standard-sample bracketing with $^{207}Pb/^{206}Pb$ and $^{206}Pb/^{238}U$ normalized to reference material GJ-1
Uncertainty level & propagation	Ages are quoted at 2 sigma internal errors
Quality control / Validation	GJ-1: Wtd ave $^{207}Pb/^{206}Pb$ Age = 605 ± 5 Ma 91500: Wtd ave $^{207}Pb/^{206}Pb$ Age = 1068 ± 4 Ma
Other information	Detailed method description reported by Frei & Gerdes (2009)

Appendix III – Spot positions in representative zircons

Hälltorp, Median Segment

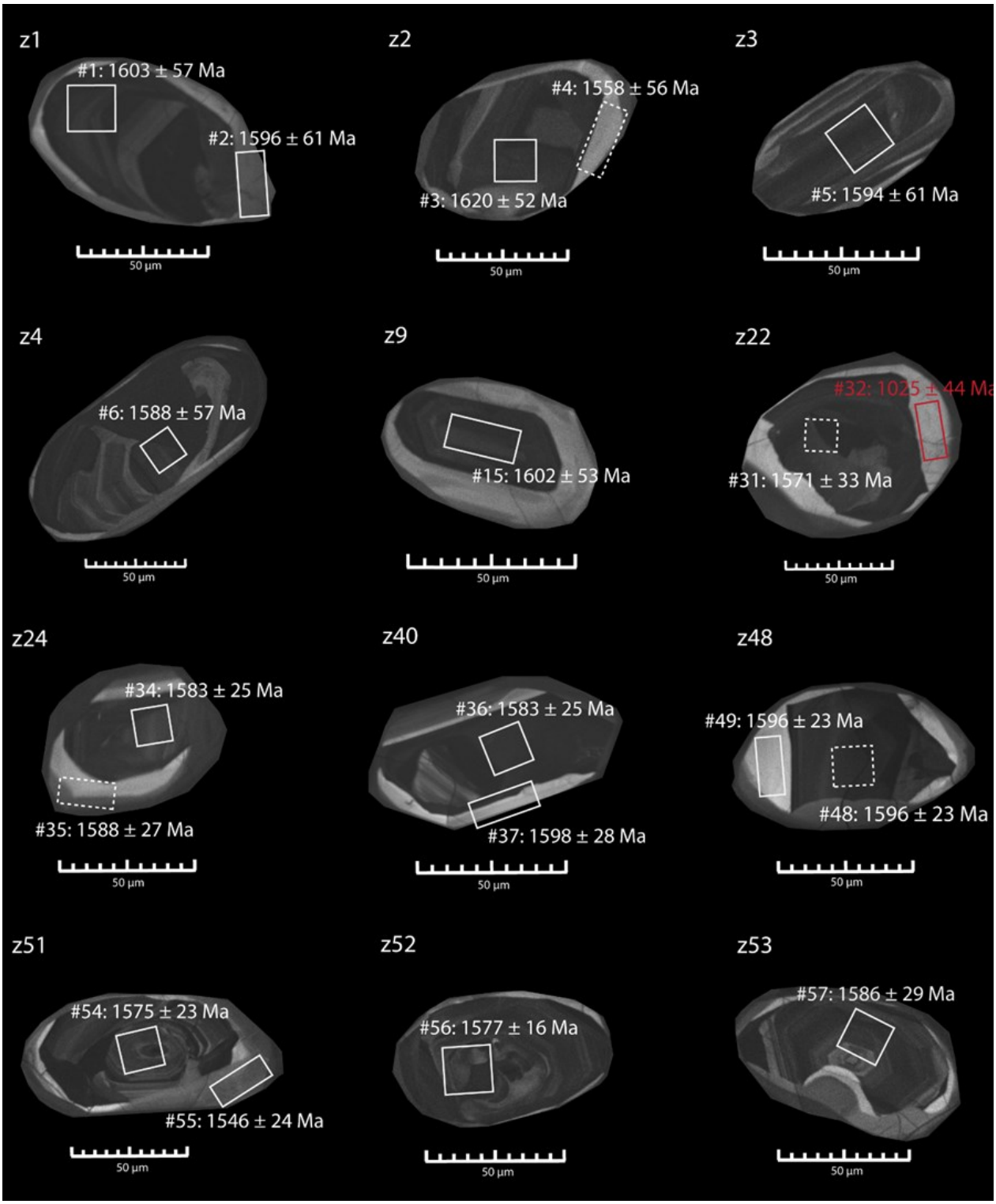

Fig. 1a. Hälltorp, Median Segment. CL-images of analysed zircons in MISE1814a, that gave concordant analyses. Concordant (<5% discordance) spots are shown with solid lines and discordant analyses with dotted lines (>5% discordance). White spots represent the older igneous population while red spots represent the younger metamorphic population. The zircon number is shown in the upper left corner of each image. The spot number is indicated with #, followed by the $^{207}Pb/^{206}Pb$ date with 2 standard errors.

Hälltorp, Median Segment

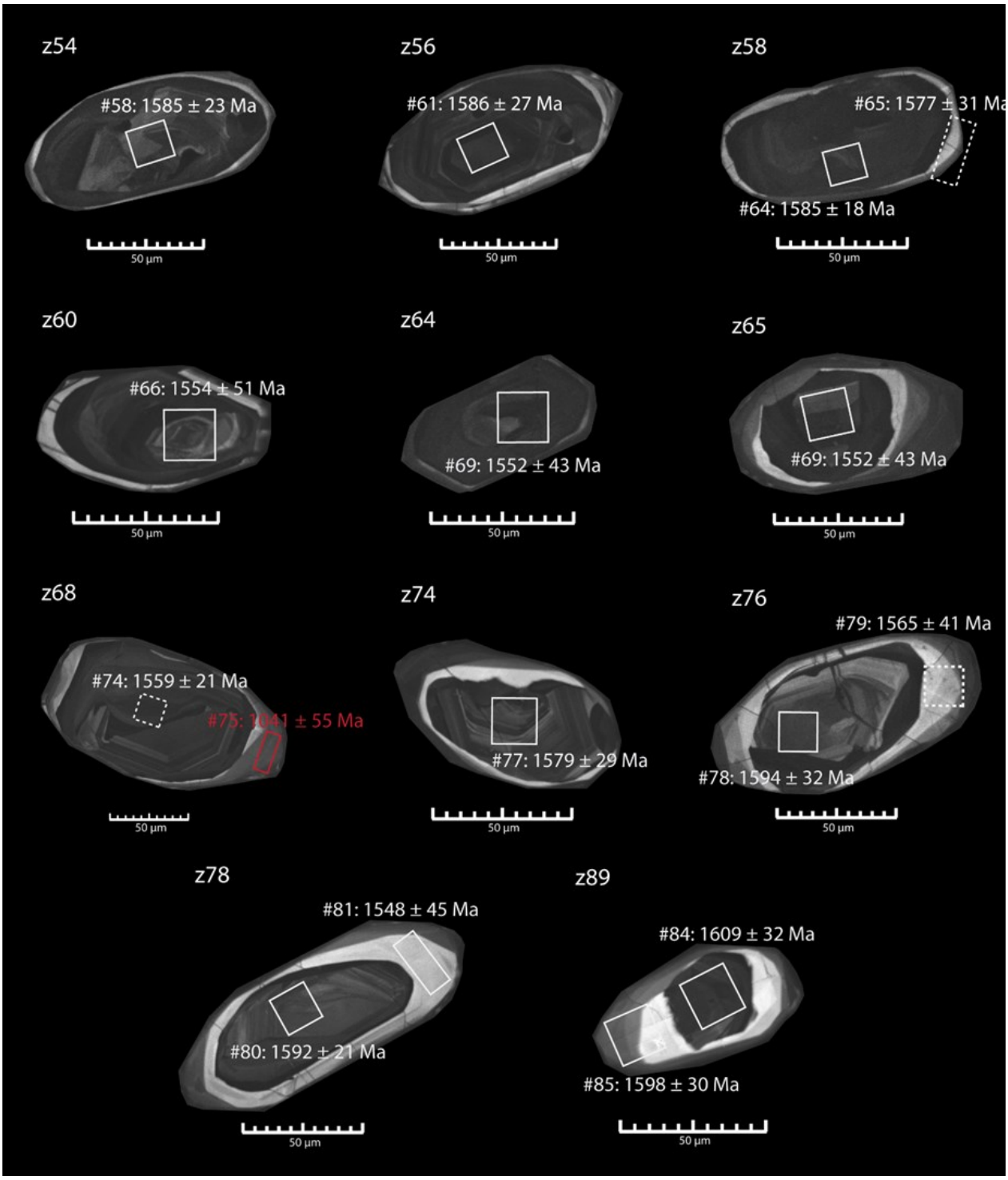

Fig. 1b. Hälltorp, Median Segment. CL-images of analysed zircons in MISE1814a, that gave concordant analyses. Concordant (<5% discordance) spots are shown with solid lines and discordant analyses with dotted lines (>5% discordance). White spots represent the older igneous population while red spots represent the younger metamorphic population. The zircon number is shown in the upper left corner of each image. The spot number is indicated with #, followed by the $^{207}Pb/^{206}Pb$ date with 2 standard errors.

Tösslanda, Göta Älv Shear Zone

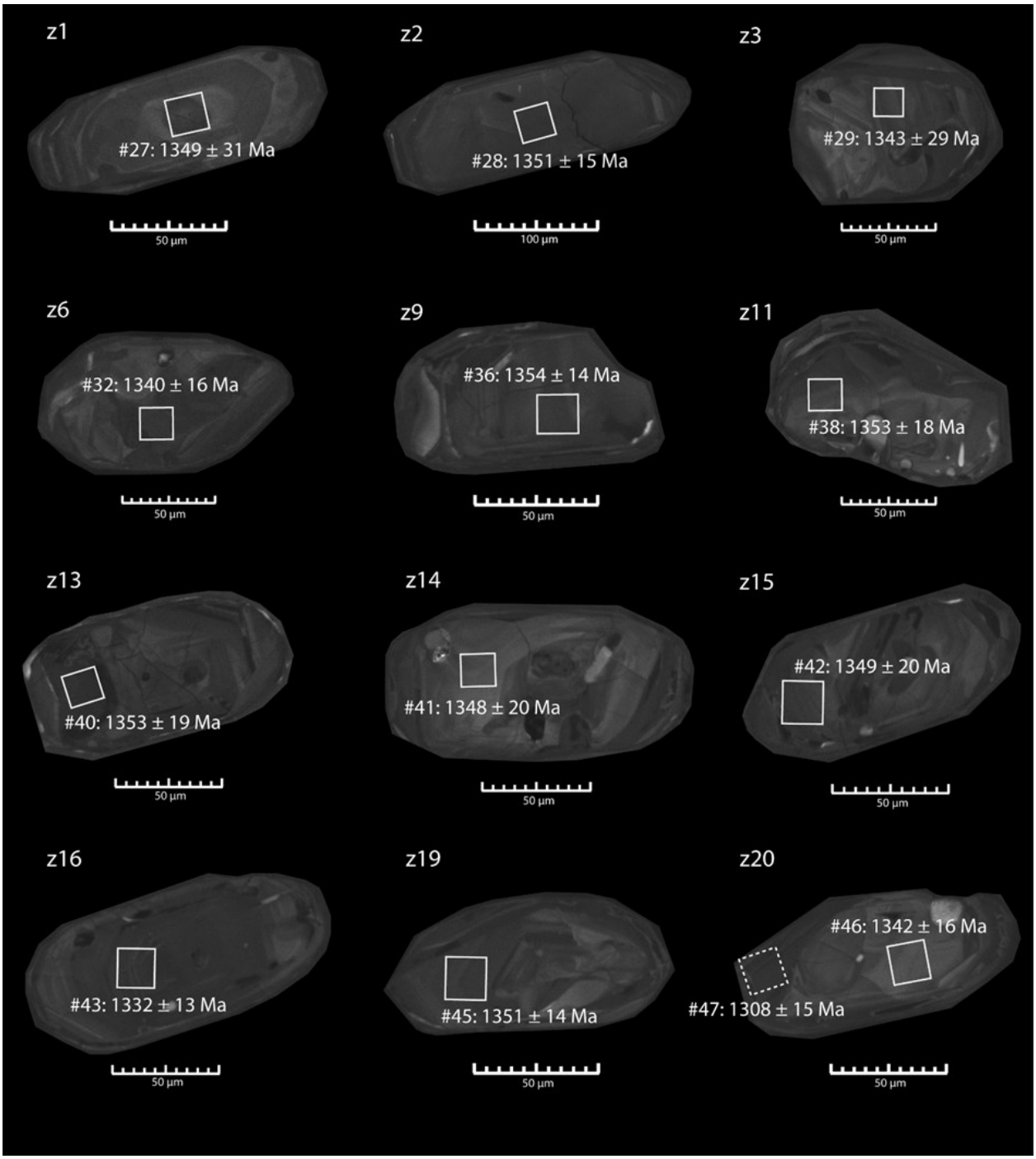

Fig. 2a. Tösslanda, Göta Älv Shear Zone. CL-images of analysed zircons in MISE1806 melanosome, that gave concordant analyses. Concordant (<5% discordance) spots are shown with solid lines and discordant analyses with dotted lines (>5% discordance). White spots represent the older igneous population. The zircon number is shown in the upper left corner of each image. The spot number is indicated with #, followed by the $^{207}Pb/^{206}Pb$ date with 2 standard errors.

Tösslanda, Göta Älv Shear Zone

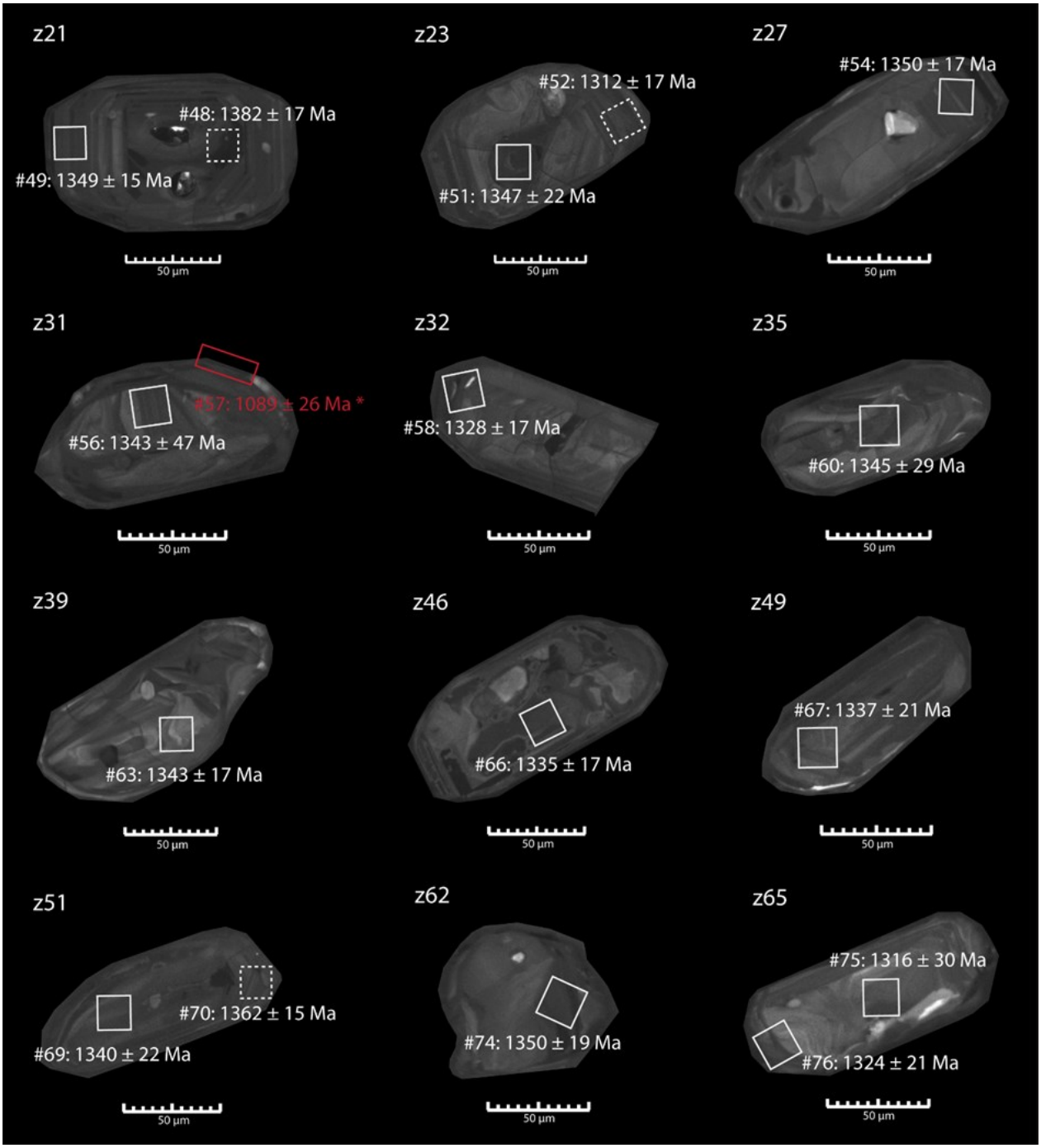

Fig. 2b. Tösslanda, Göta Älv Shear Zone. CL-images of analysed zircons in MISE1806 melanosome, that gave concordant analyses. Concordant (<5% discordance) spots are shown with solid lines and discordant analyses with dotted lines (>5% discordance). White spots represent the older igneous population while red spots represent the younger metamorphic population. The zircon number is shown in the upper left corner of each image. The spot number is indicated with #, followed by the $^{207}Pb/^{206}Pb$ date with 2 standard errors. The asterisk indicates an analysis used for age calculations with up to 10% discordance.

Tösslanda, Göta Älv Shear Zone

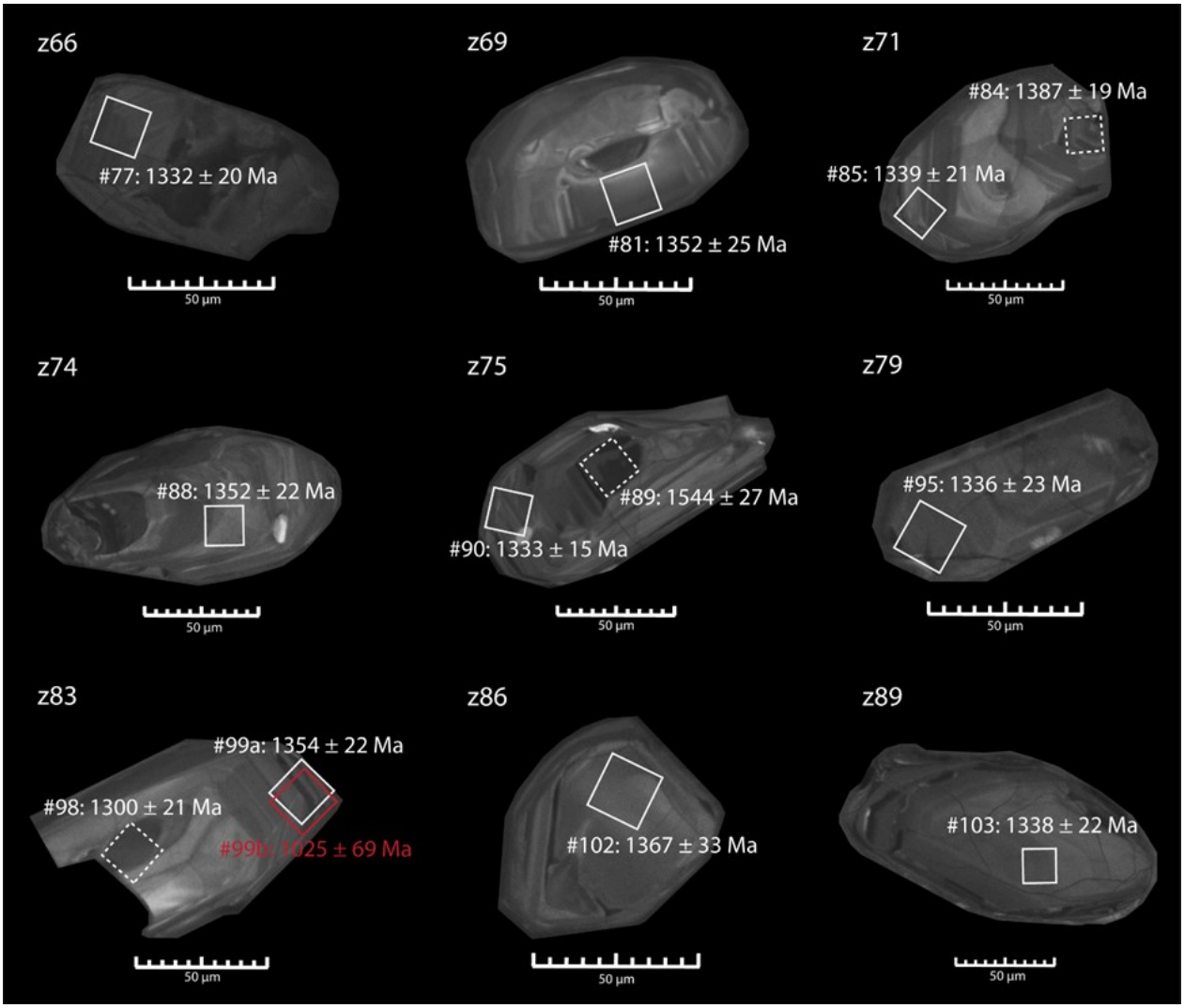

Fig. 2c. Tösslanda, Göta Älv Shear Zone. CL-images of analysed zircons in MISE1806 melanosome, that gave concordant analyses. Concordant (<5% discordance) spots are shown with solid lines and discordant analyses with dotted lines (>5% discordance). White spots represent the older igneous population while red spots represent the younger metamorphic population. Overlapping spots are split analyses. The zircon number is shown in the upper left corner of each image. The spot number is indicated with #, followed by the $^{207}Pb/^{206}Pb$ date with 2 standard errors.

Tösslanda, Göta Älv Shear Zone

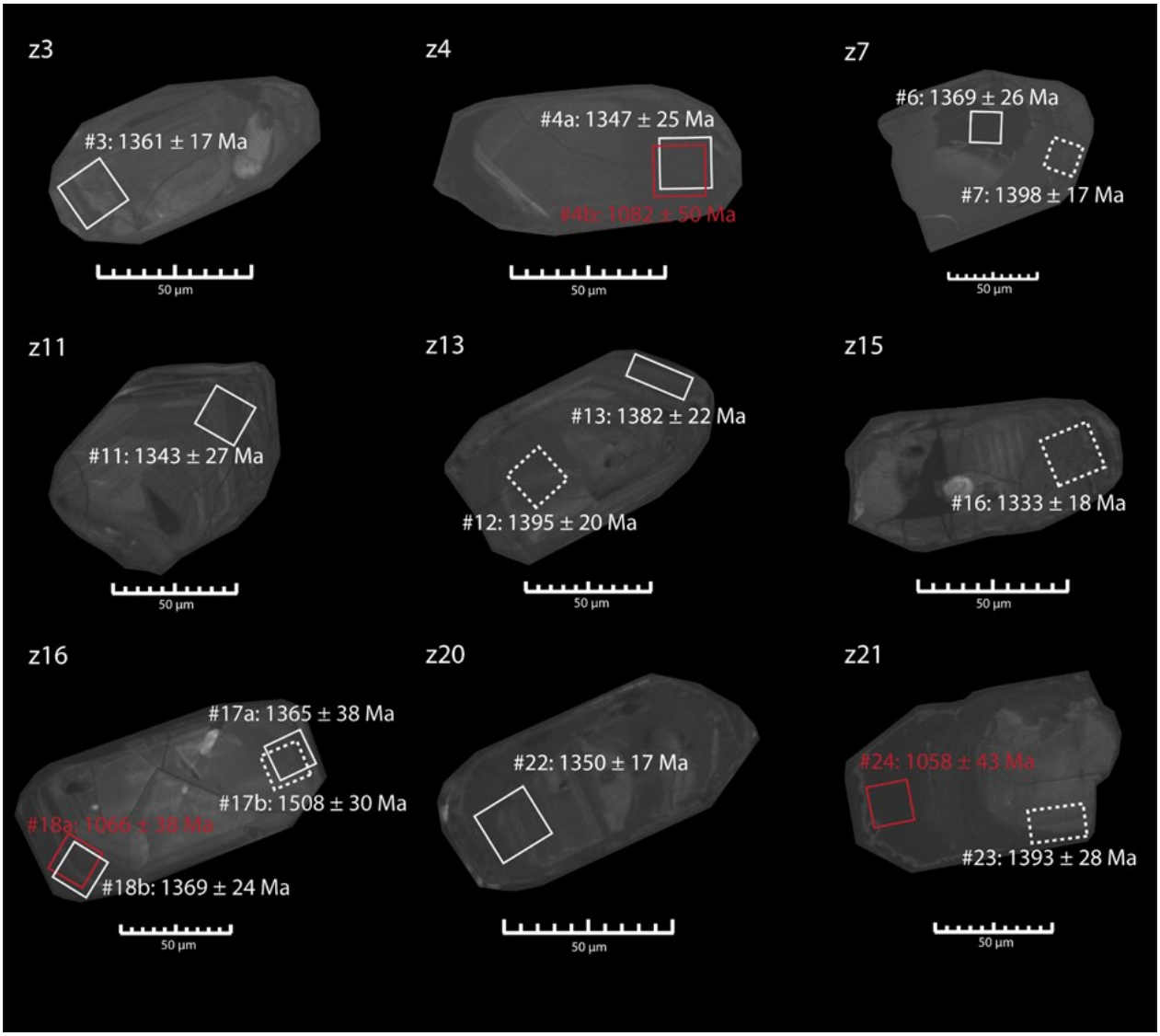

Fig. 3a. Tösslanda, Göta Älv Shear Zone. CL-images of analysed zircons in MISE1806 leucosome, that gave concordant analyses. Concordant (<5% discordance) spots are shown with solid lines and discordant analyses with dotted lines (>5% discordance). White spots represent the older igneous population while red spots represent the younger metamorphic population. Overlapping spots are split analyses. The zircon number is shown in the upper left corner of each image. The spot number is indicated with #, followed by the $^{207}Pb/^{206}Pb$ date with 2 standard errors.

Tösslanda, Göta Älv Shear Zone

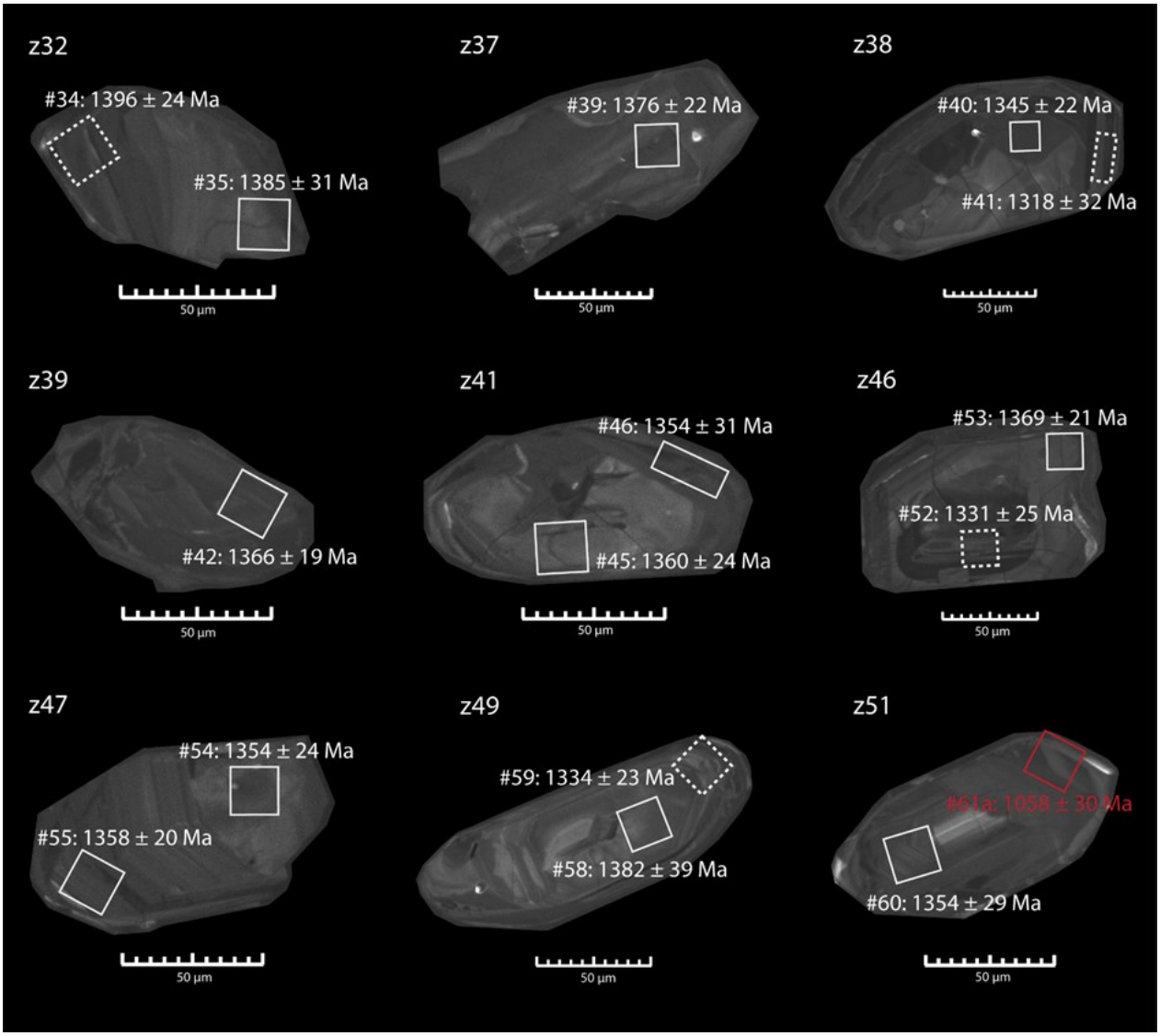

Fig. 3b. Tösslanda, Göta Älv Shear Zone. CL-images of analysed zircons in MISE1806 leucosome, that gave concordant analyses. Concordant (<5% discordance) spots are shown with solid lines and discordant analyses with dotted lines (>5% discordance). White spots represent the older igneous population while red spots represent the younger metamorphic population. The zircon number is shown in the upper left corner of each image. The spot number is indicated with #, followed by the $^{207}Pb/^{206}Pb$ date with 2 standard errors.

Tösslanda, Göta Älv Shear Zone

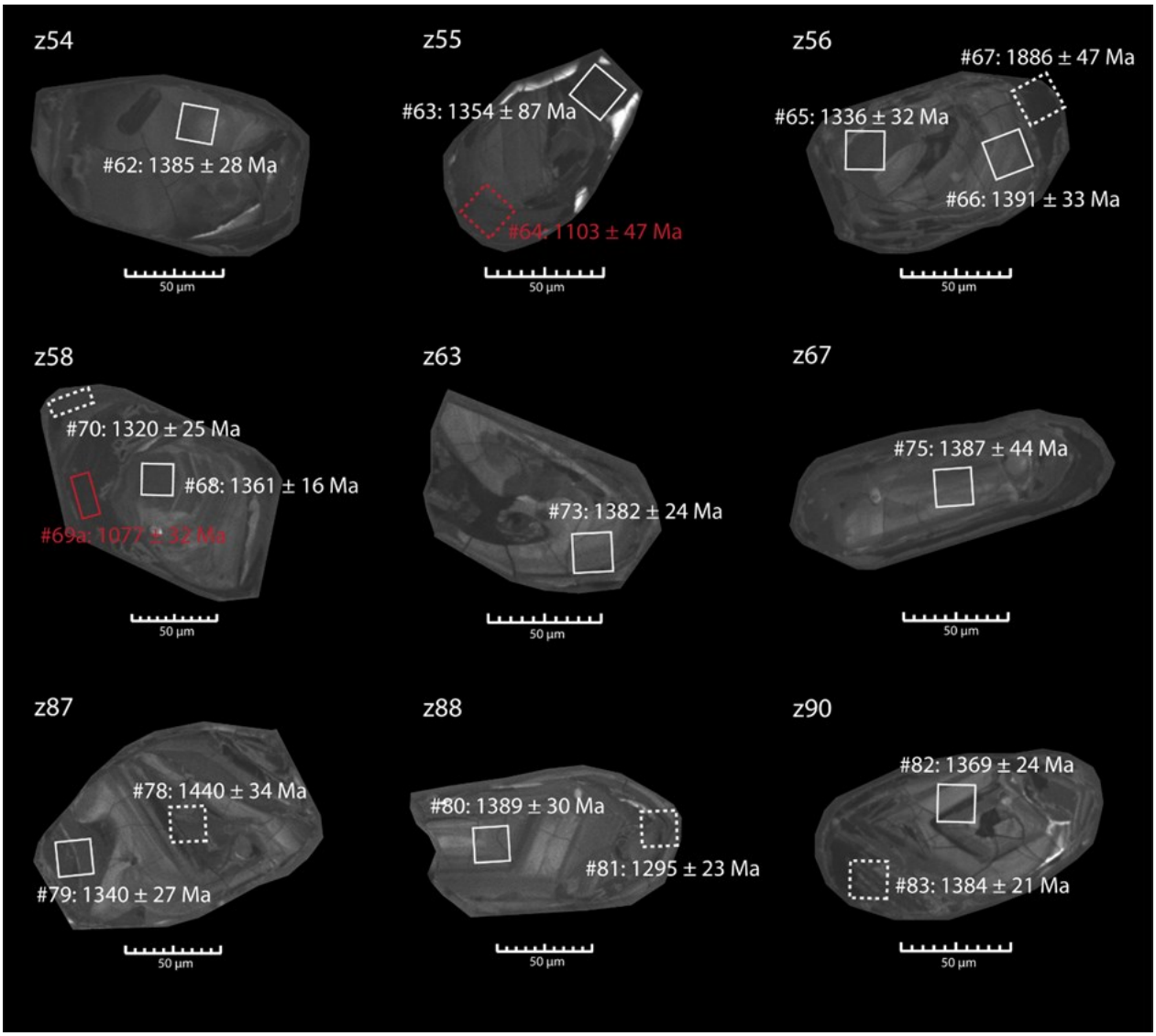

Fig. 3c. Tösslanda, Göta Älv Shear Zone. CL-images of analysed zircons in MISE1806 leucosome, that gave concordant analyses. Concordant (<5% discordance) spots are shown with solid lines and discordant analyses with dotted lines (>5% discordance). White spots represent the older igneous population while red spots represent the younger metamorphic population. The zircon number is shown in the upper left corner of each image. The spot number is indicated with #, followed by the $^{207}Pb/^{206}Pb$ date with 2 standard errors.

Hälltorp, Median Segment

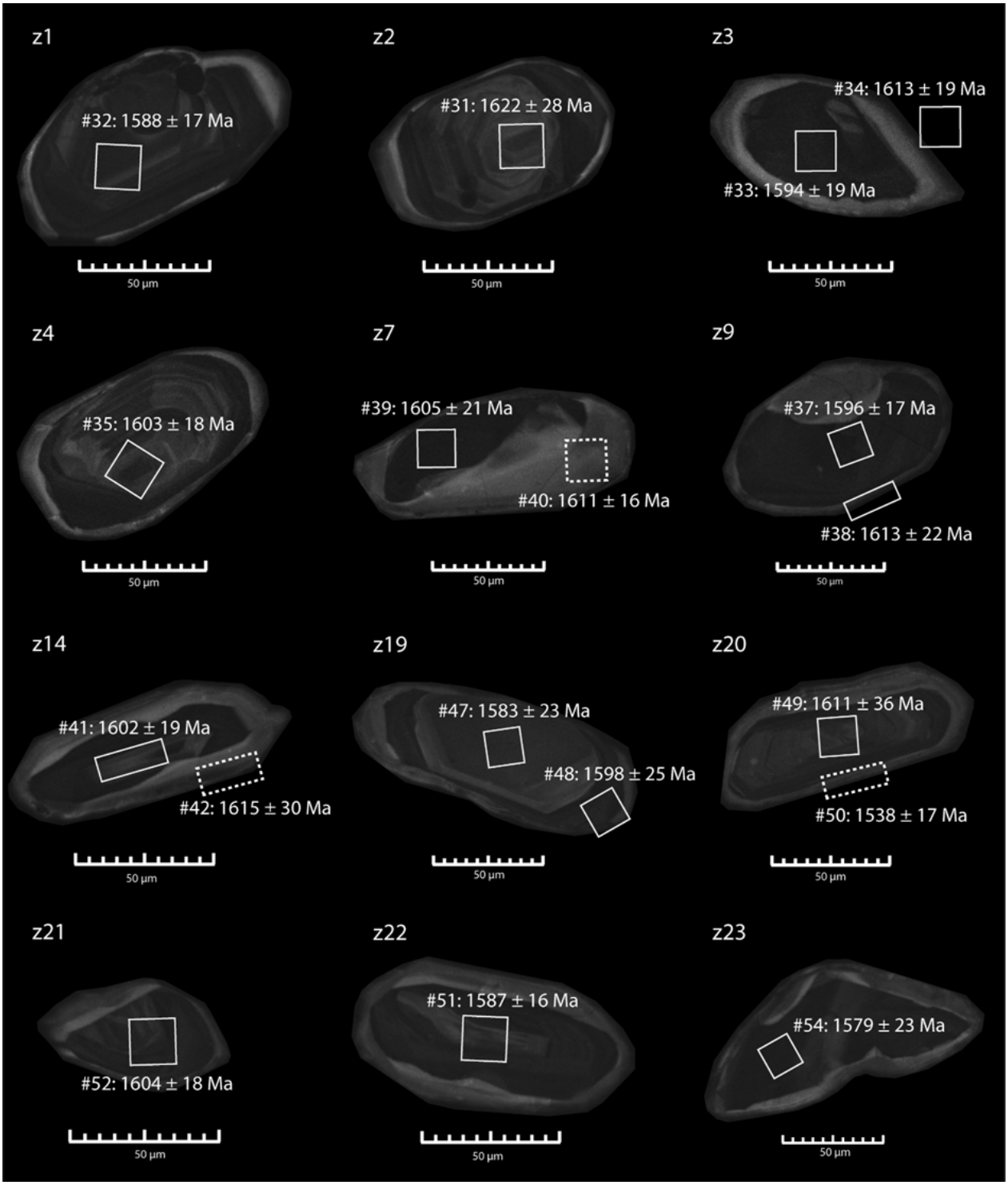

Fig. 4a. Hälltorp, Median Segment. CL-images of analysed zircons in MISE1816c melanosome, that gave concordant analyses. Concordant (<5% discordance) spots are shown with solid lines and discordant analyses with dotted lines (>5% discordance). White spots represent the older igneous population. The zircon number is shown in the upper left corner of each image. The spot number is indicated with #, followed by the $^{207}Pb/^{206}Pb$ date with 2 standard errors.

Hälltorp, Median Segment

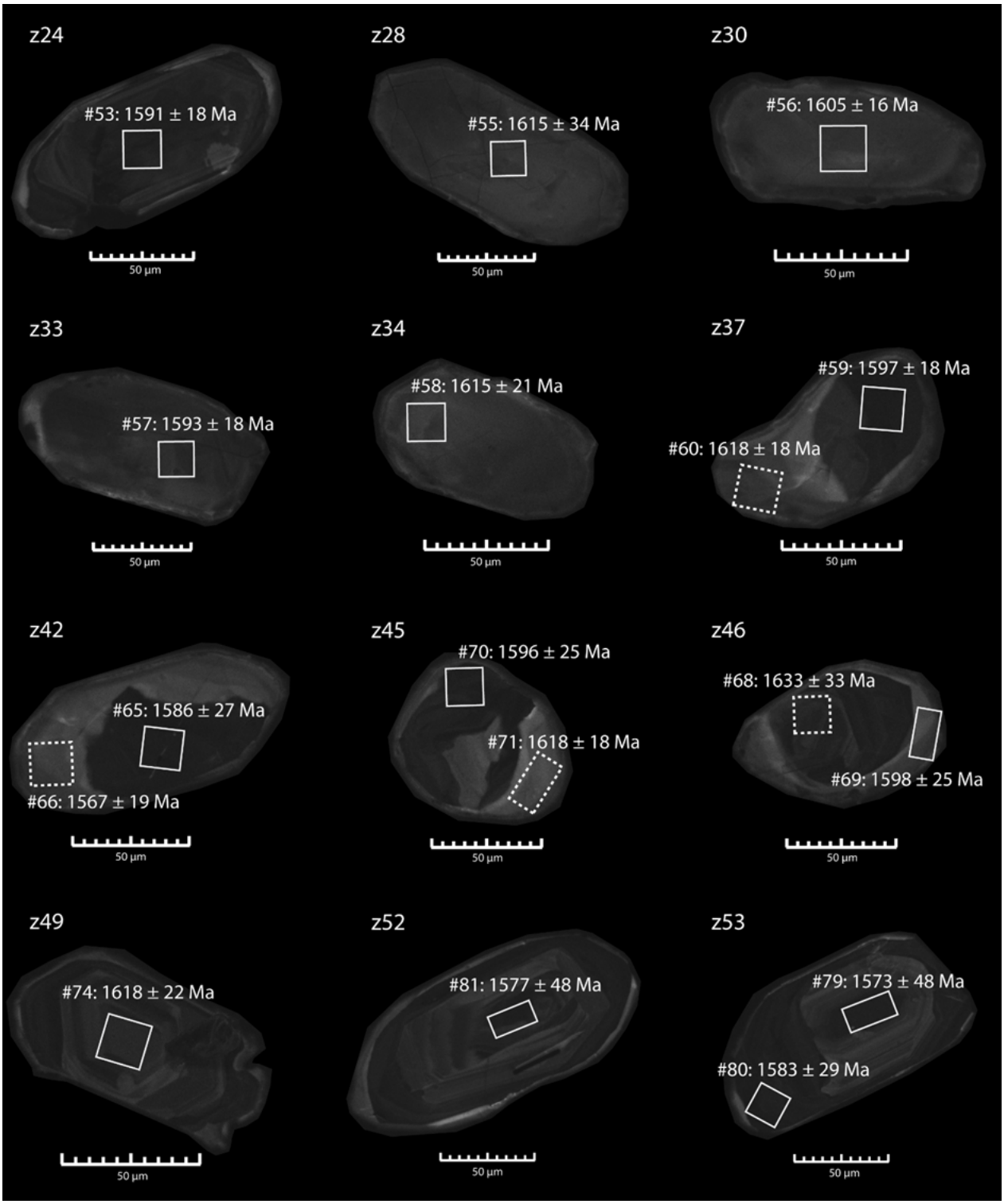

Fig. 4b. Hälltorp, Median Segment. CL-images of analysed zircons in MISE1816 melanosome, that gave concordant analyses. Concordant (<5% discordance) spots are shown with solid lines and discordant analyses with dotted lines (>5% discordance). White spots represent the older igneous population. The zircon number is shown in the upper left corner of each image. The spot number is indicated with #, followed by the $^{207}Pb/^{206}Pb$ date with 2 standard errors.

Hälltorp, Median Segment

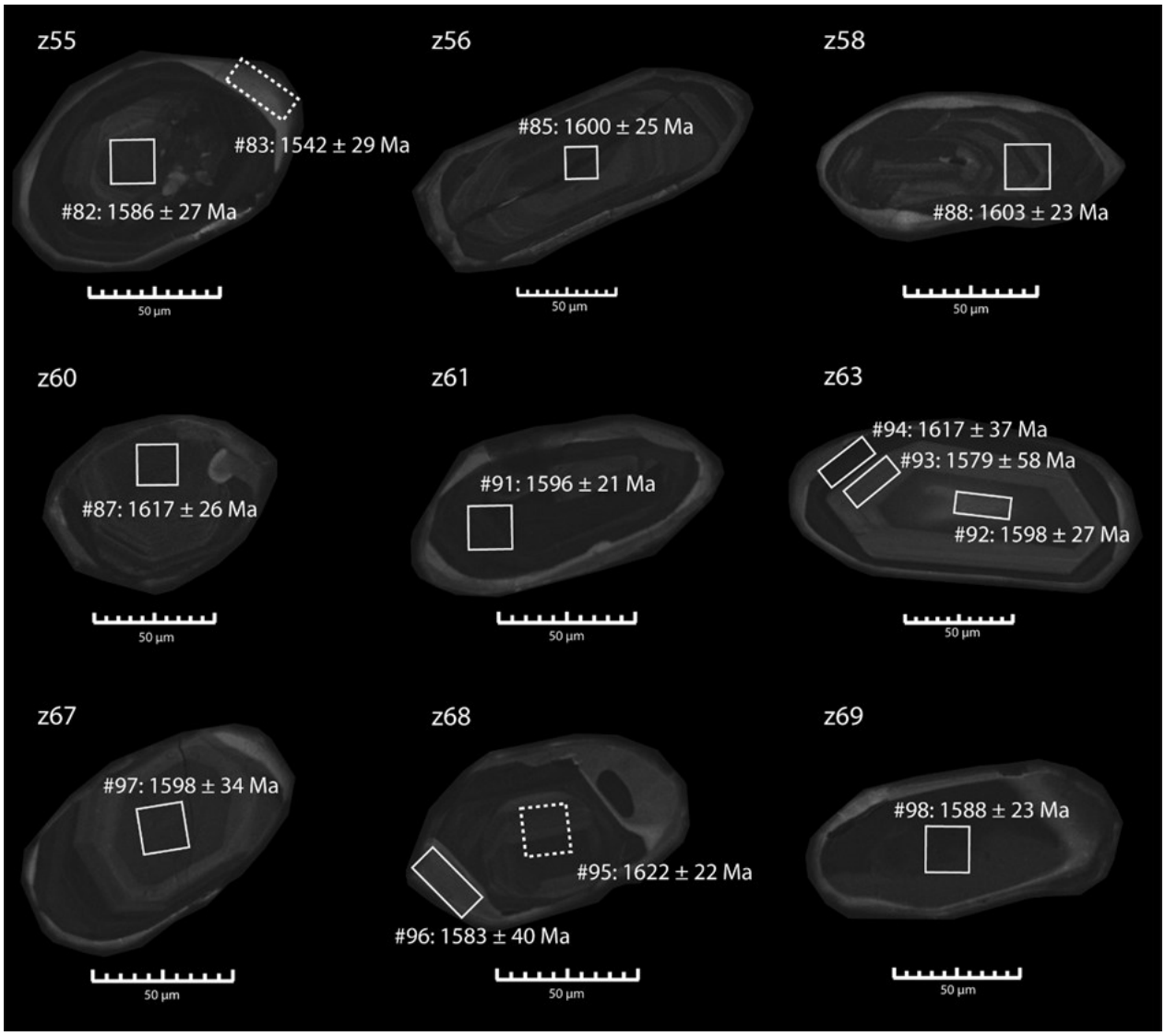

Fig. 4c. Hälltorp, Median Segment. CL-images of analysed zircons in MISE1816 melanosome, that gave concordant analyses. Concordant (<5% discordance) spots are shown with solid lines and discordant analyses with dotted lines (>5% discordance). White spots represent the older igneous population. The zircon number is shown in the upper left corner of each image. The spot number is indicated with #, followed by the $^{207}Pb/^{206}Pb$ date with 2 standard errors.

Hälltorp, Median Segment

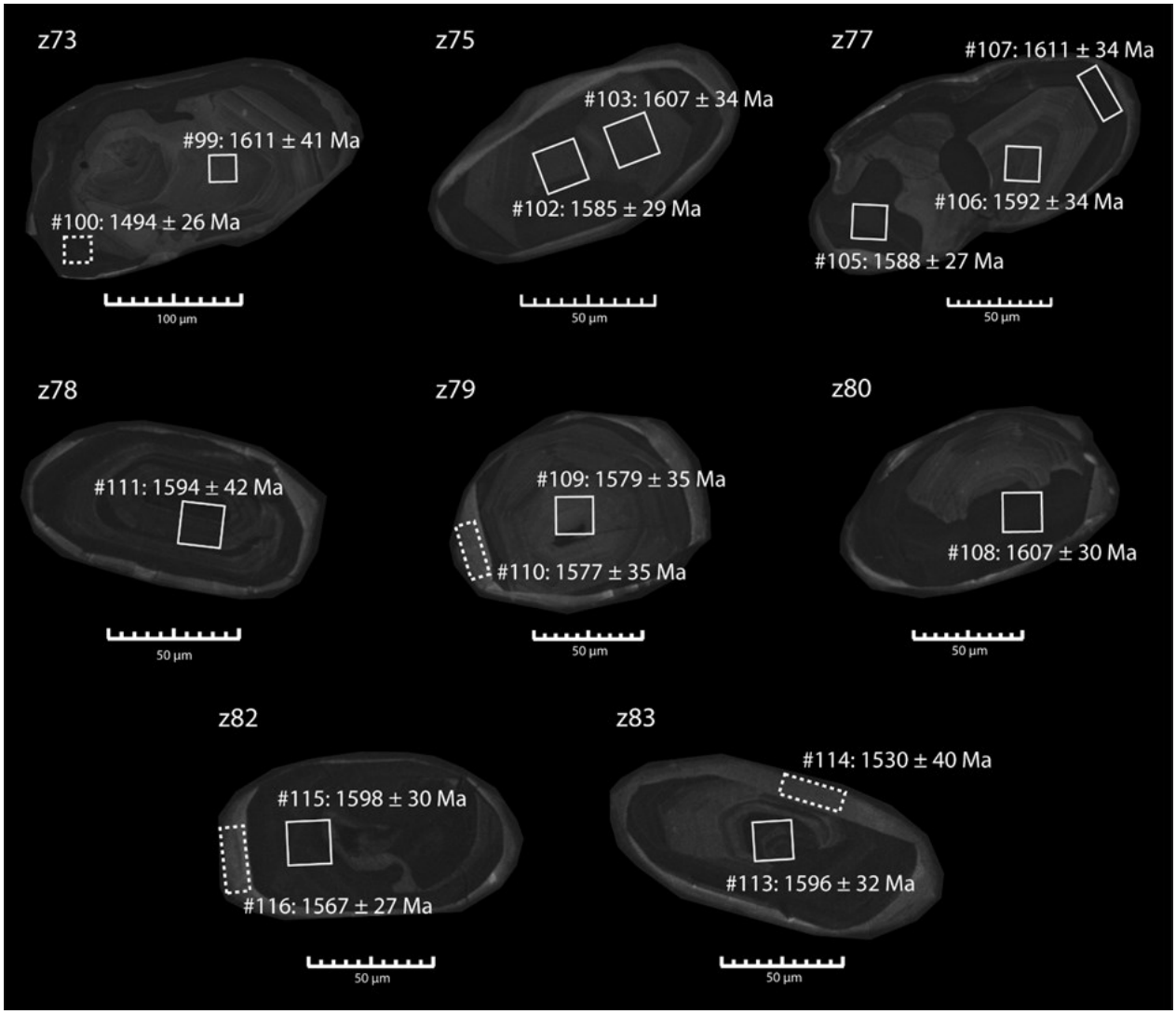

Fig. 4d. Hälltorp, Median Segment. CL-images of analysed zircons in MISE1816 melanosome, that gave concordant analyses. Concordant (<5% discordance) spots are shown with solid lines and discordant analyses with dotted lines (>5% discordance). White spots represent the older igneous population. The zircon number is shown in the upper left corner of each image. The spot number is indicated with #, followed by the $^{207}Pb/^{206}Pb$ date with 2 standard errors.

Hälltorp, Median Segment

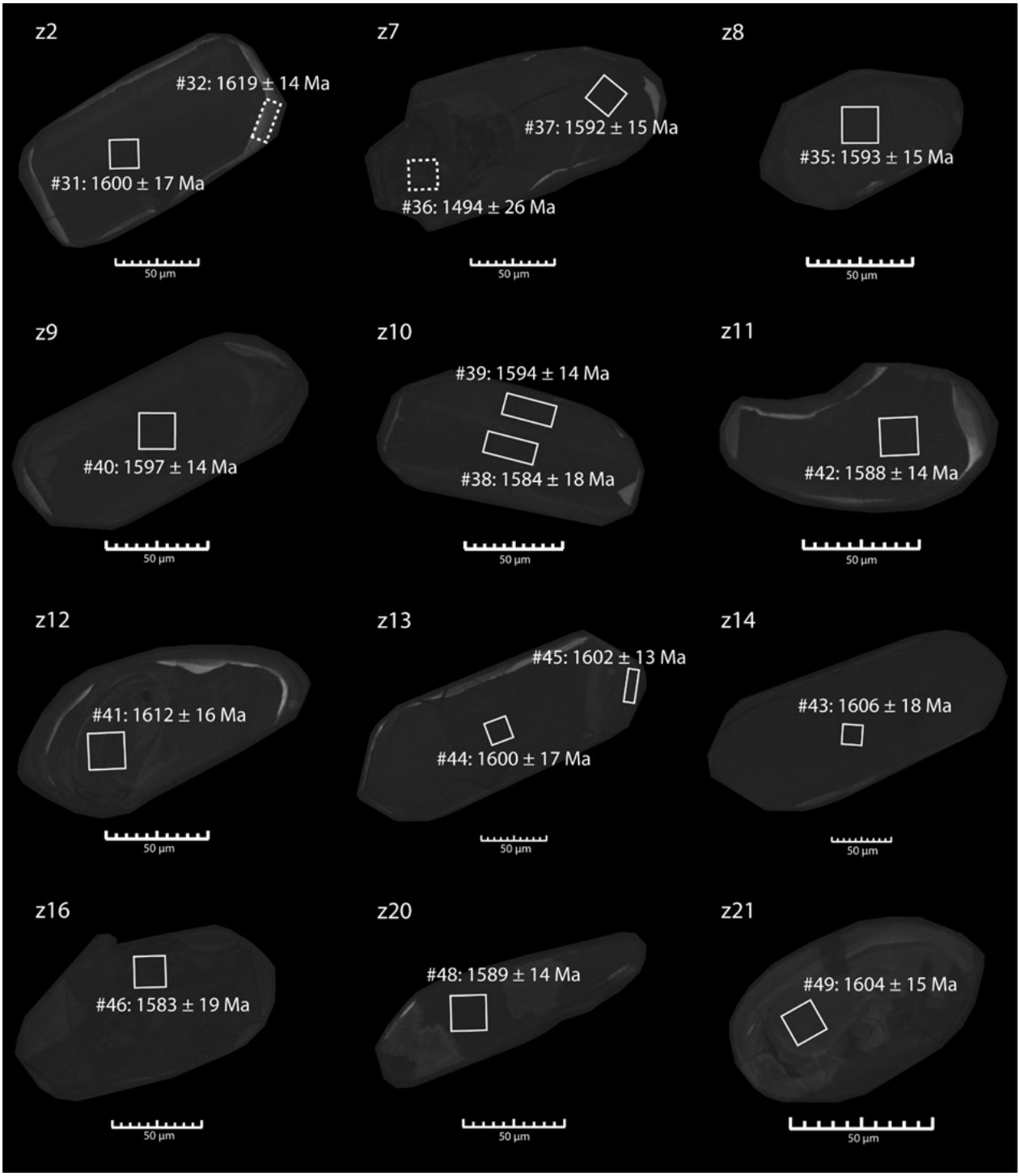

Fig. 5a. Hälltorp, Median Segment. CL-images of analysed zircons in MISE1816 leucosome, that gave concordant analyses. Concordant (<5% discordance) spots are shown with solid lines and discordant analyses with dotted lines (>5% discordance). White spots represent the older igneous population. The zircon number is shown in the upper left corner of each image. The spot number is indicated with #, followed by the $^{207}Pb/^{206}Pb$ date with 2 standard errors.

Hälltorp, Median Segment

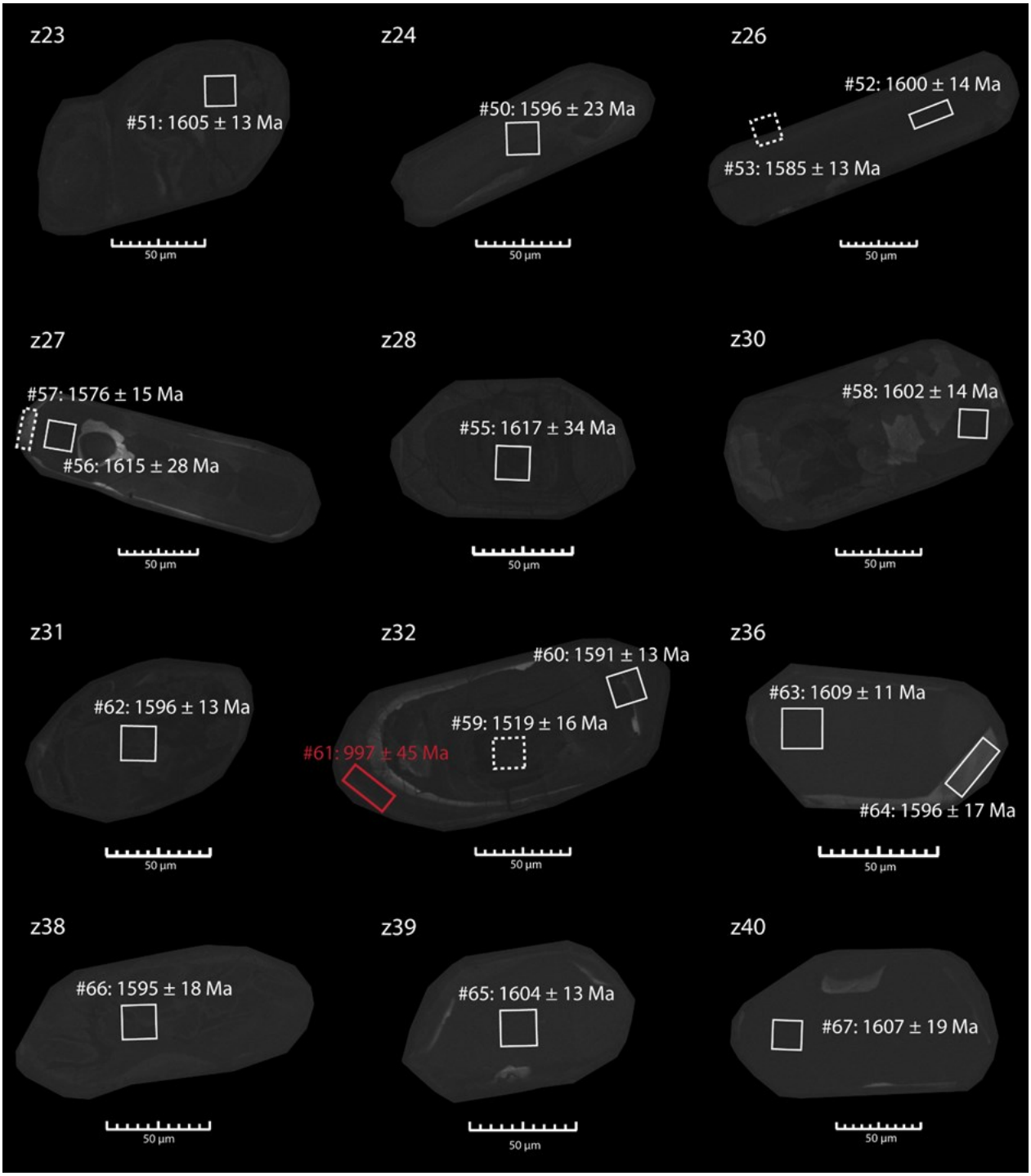

Fig. 5b. Hälltorp, Median Segment. CL-images of analysed zircons in MISE1816 leucosome, that gave concordant analyses. Concordant (<5% discordance) spots are shown with solid lines and discordant analyses with dotted lines (>5% discordance). White spots represent the older igneous population while red spots represent the younger metamorphic population. The zircon number is shown in the upper left corner of each image. The spot number is indicated with #, followed by the $^{207}Pb/^{206}Pb$ date with 2 standard errors.

Hälltorp, Median Segment

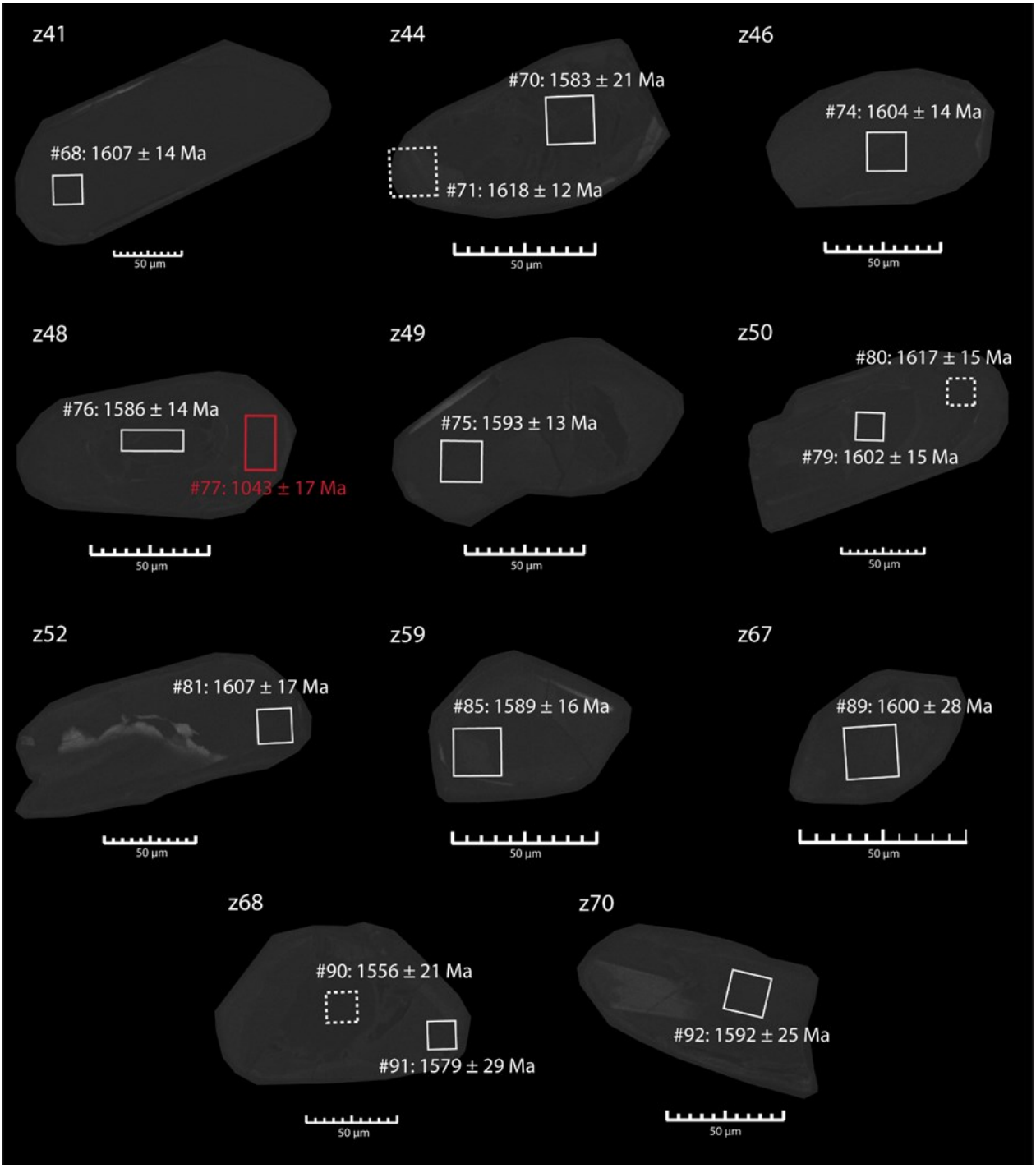

Fig. 5c. Hälltorp, Median Segment. CL-images of analysed zircons in MISE1816 leucosome, that gave concordant analyses. Concordant (<5% discordance) spots are shown with solid lines and discordant analyses with dotted lines (>5% discordance). White spots represent the older igneous population while red spots represent the younger metamorphic population. The zircon number is shown in the upper left corner of each image. The spot number is indicated with #, followed by the $^{207}Pb/^{206}Pb$ date with 2 standard errors.

Arsjön, Western Segment

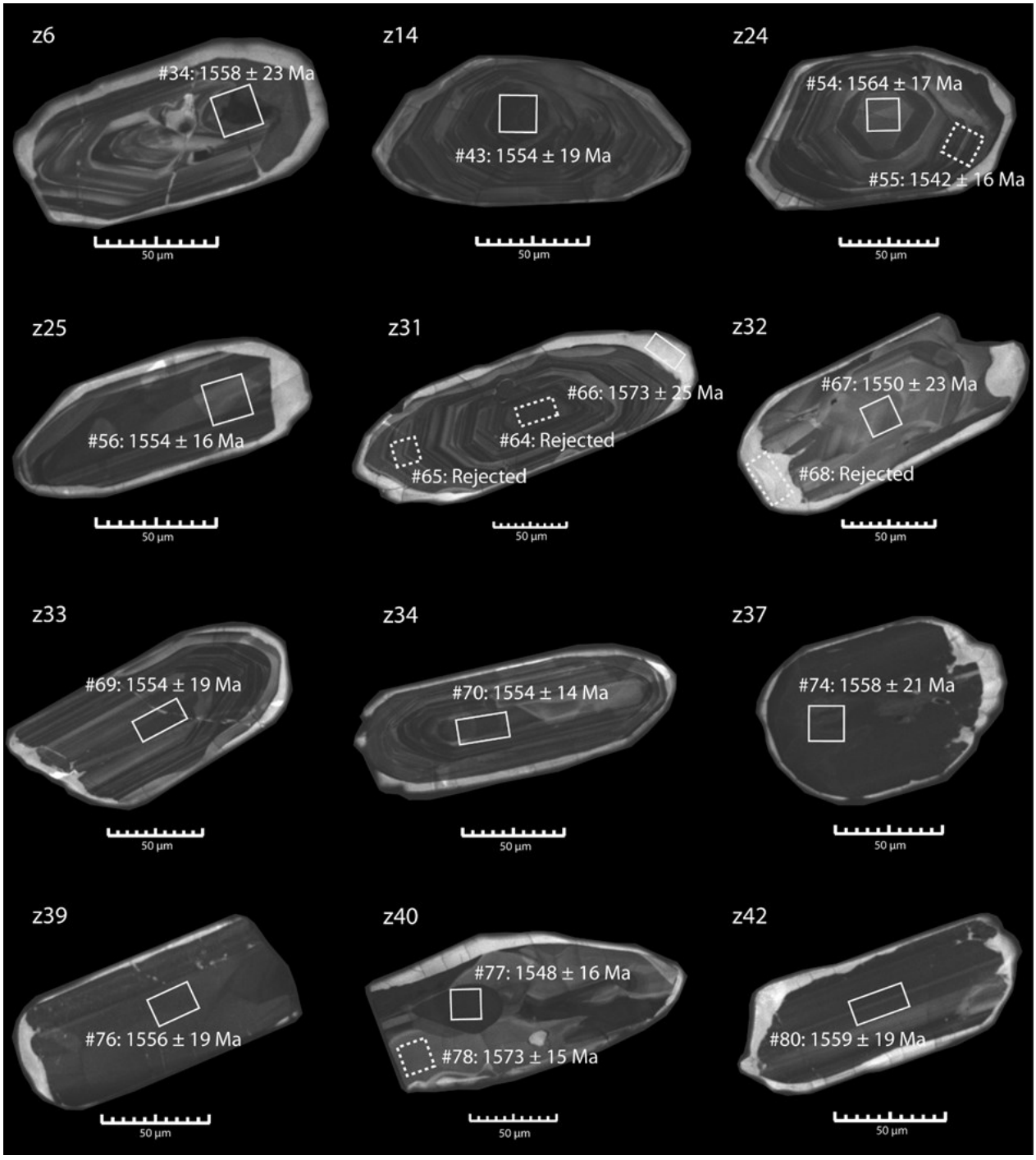

Fig. 6a. Arsjön, Western Segment. CL-images of analysed zircons in MISE1802a melanosome, that gave concordant analyses. Concordant (<5% discordance) spots are shown with solid lines and discordant analyses with dotted lines (>5% discordance). White spots represent the older igneous population. The zircon number is shown in the upper left corner of each image. The spot number is indicated with #, followed by the $^{207}Pb/^{206}Pb$ date with 2 standard errors.

Arsjön, Western Segment

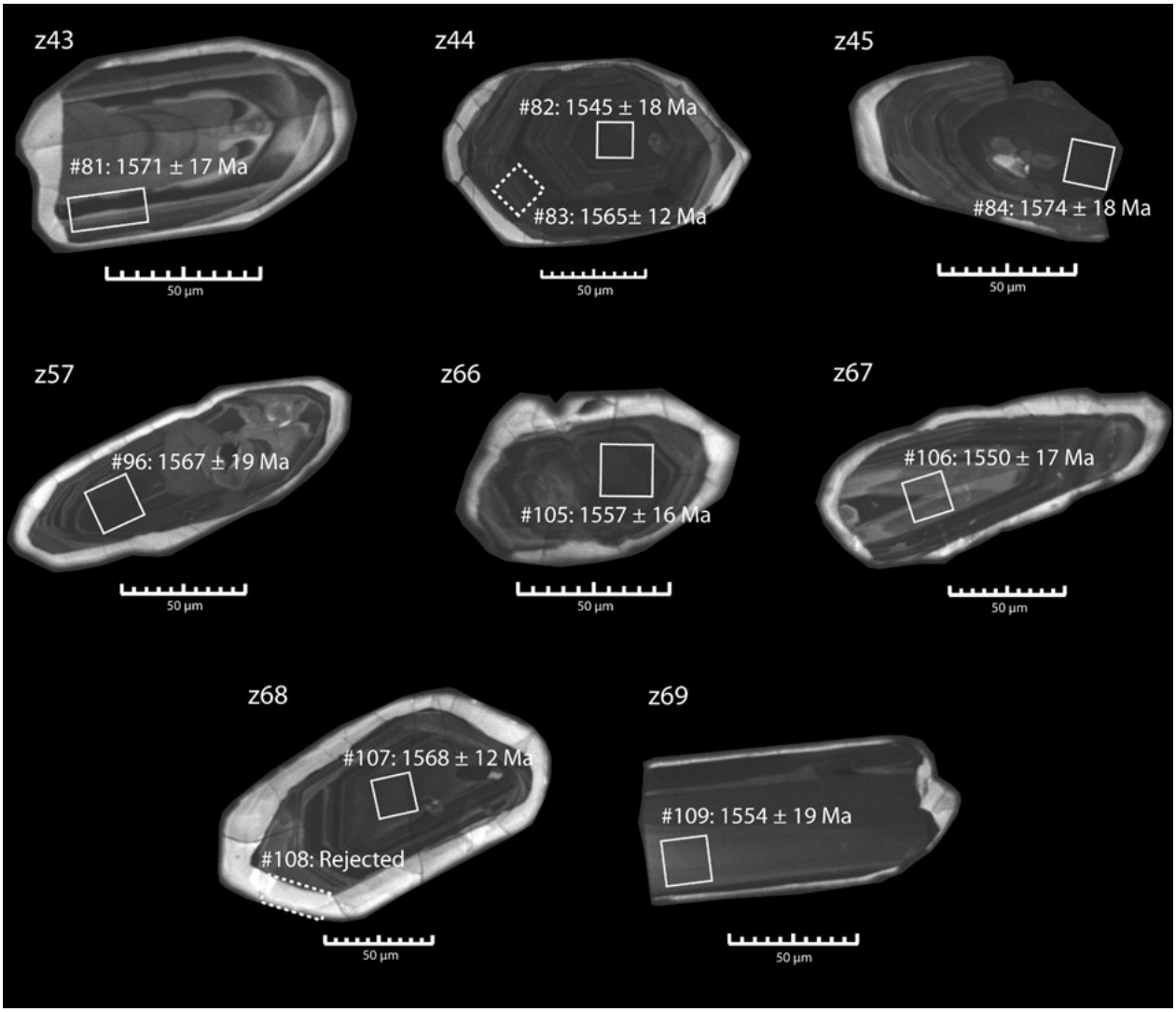

Fig. 6b. Arsjön, Western Segment. CL-images of analysed zircons in MISE1802a melanosome, that gave concordant analyses. Concordant (<5% discordance) spots are shown with solid lines and discordant analyses with dotted lines (>5% discordance). White spots represent the older igneous population. The zircon number is shown in the upper left corner of each image. The spot number is indicated with #, followed by the $^{207}Pb/^{206}Pb$ date with 2 standard errors.

Arsjön, Western Segment

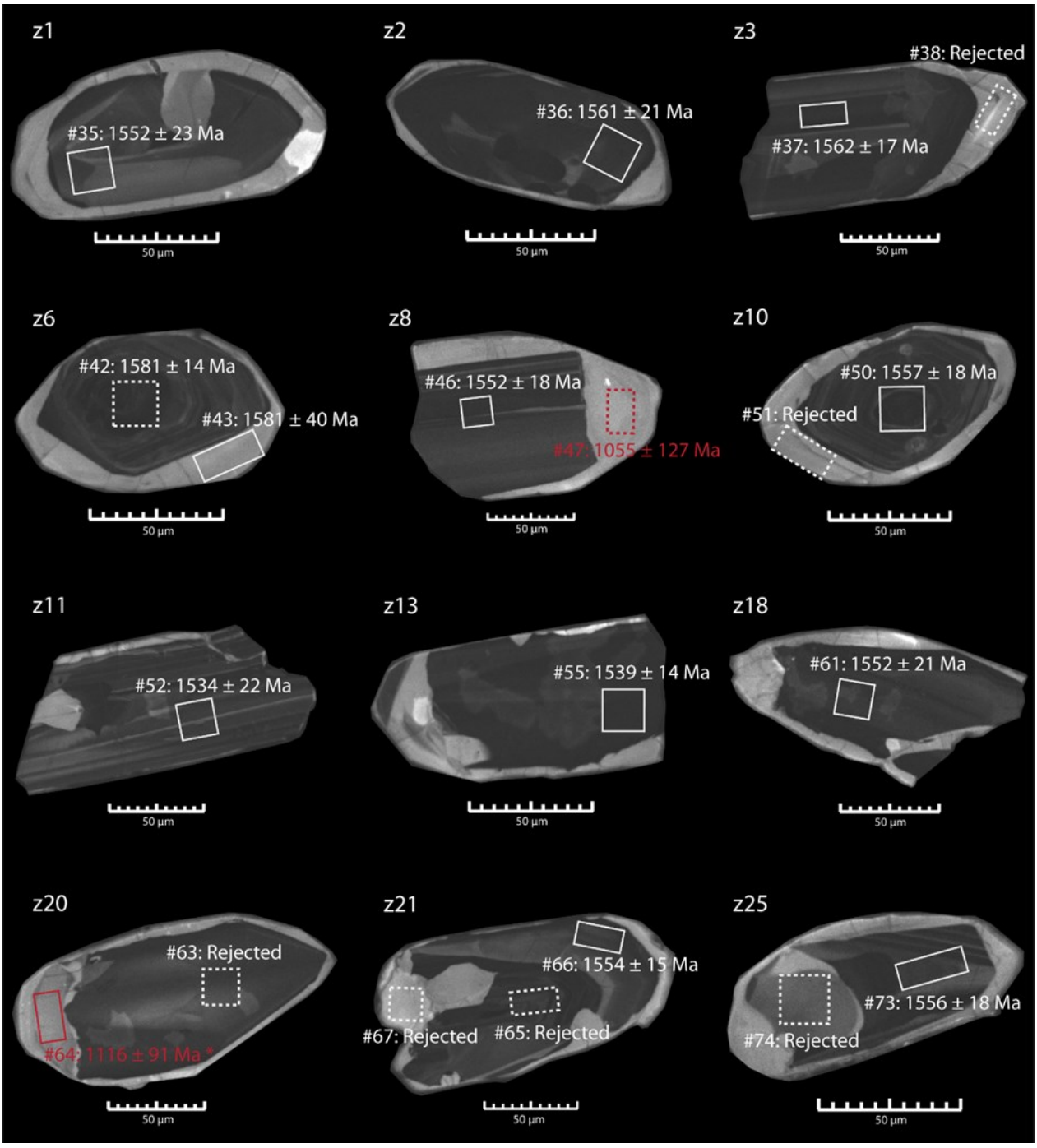

Fig. 7a. Arsjön, Western Segment. CL-images of analysed zircons in MISE1802a leucosome, that gave concordant analyses. Concordant (<5% discordance) spots are shown with solid lines and discordant analyses with dotted lines (>5% discordance). White spots represent the older igneous population while red spots represent the younger metamorphic population. The zircon number is shown in the upper left corner of each image. The spot number is indicated with #, followed by the $^{207}Pb/^{206}Pb$ date with 2 standard errors. The asterisk indicates an analysis used for age calculations with up to 10% discordance.

Arsjön, Western Segment

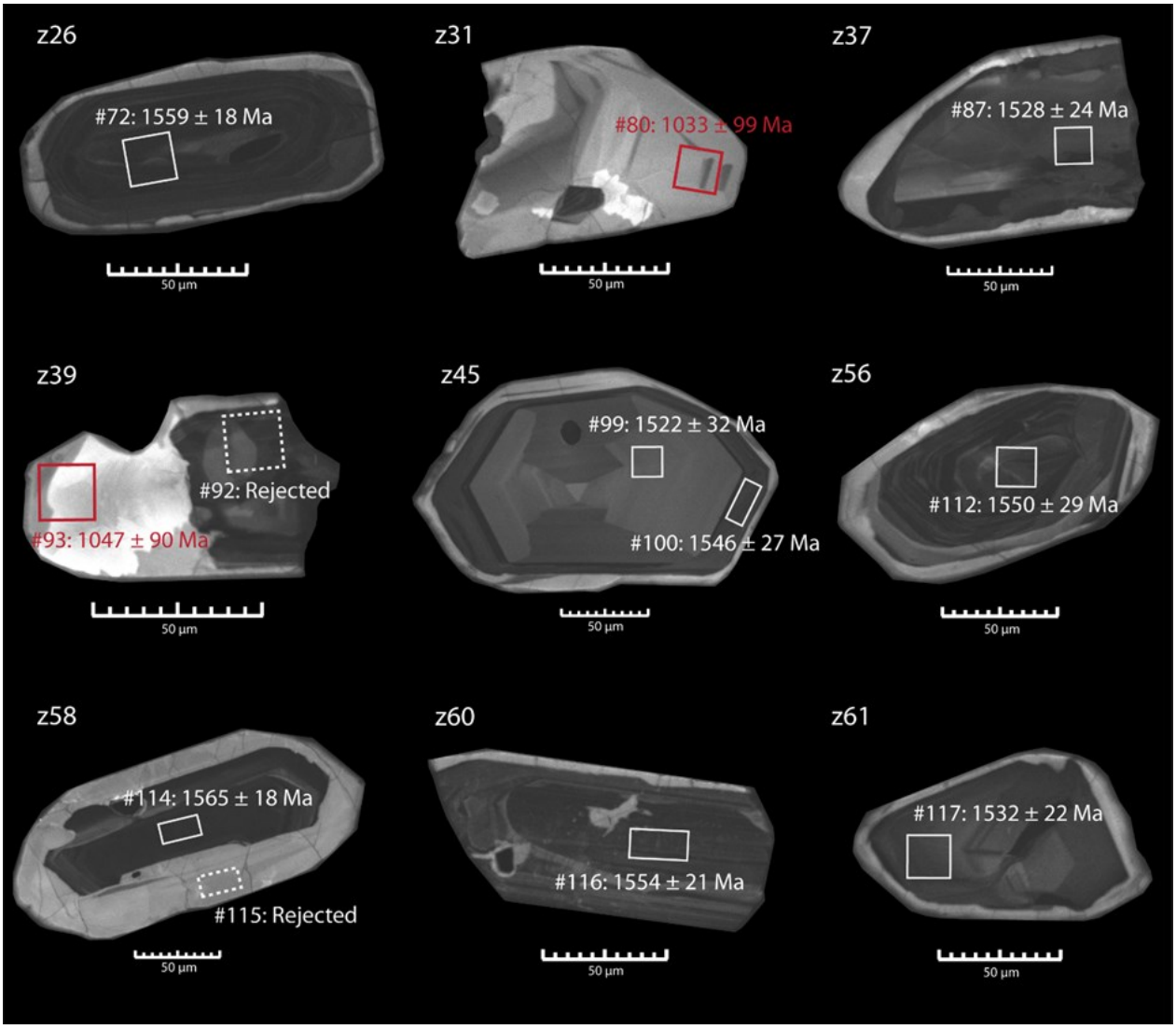

Fig. 7b. Arsjön, Western Segment. CL-images of analysed zircons in MISE1802a leucosome, that gave concordant analyses. Concordant (<5% discordance) spots are shown with solid lines and discordant analyses with dotted lines (>5% discordance). White spots represent the older igneous population while red spots represent the younger metamorphic population. The zircon number is shown in the upper left corner of each image. The spot number is indicated with #, followed by the $^{207}Pb/^{206}Pb$ date with 2 standard errors.

Arsjön, Western Segment

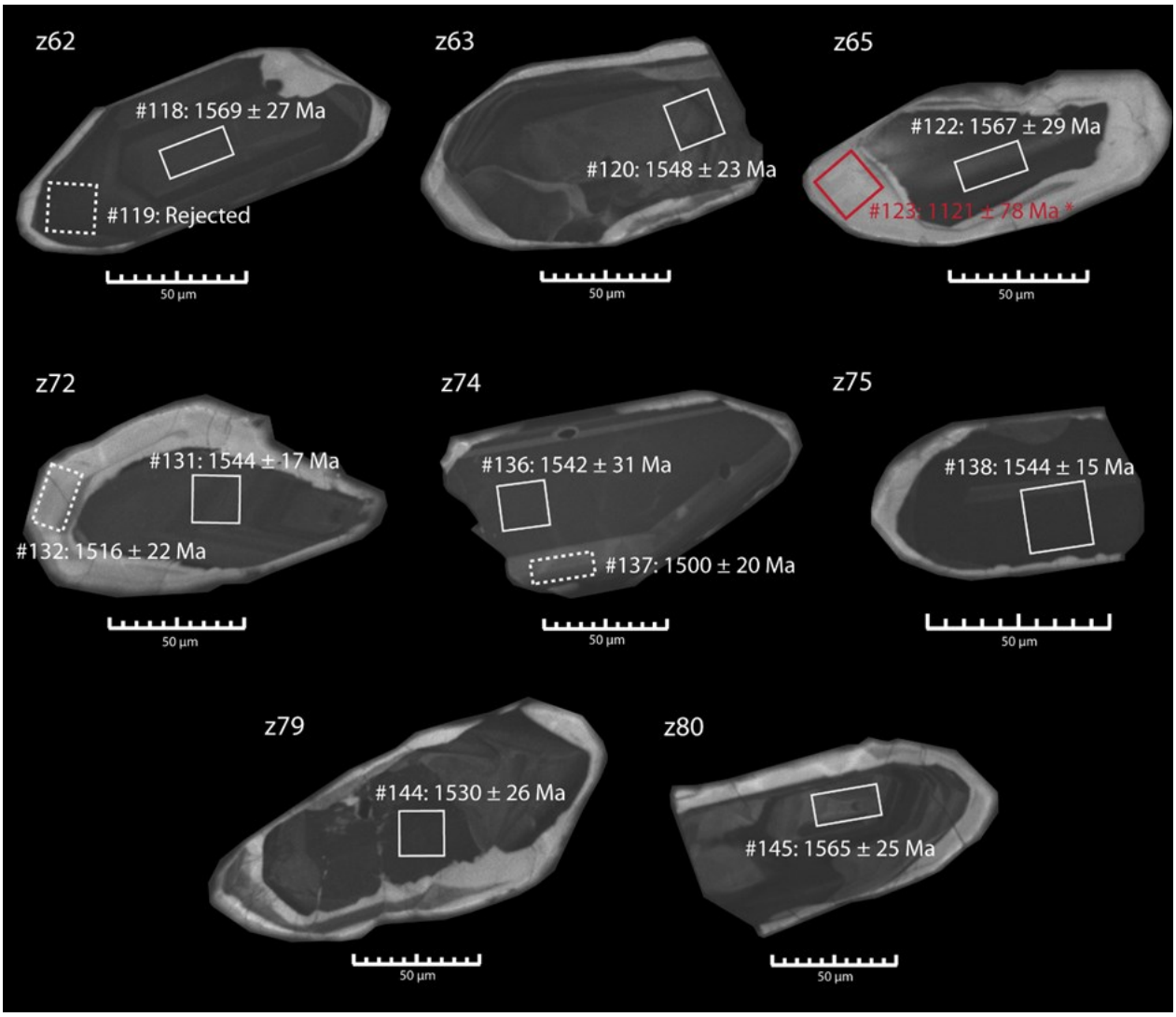

Fig. 7c. Arsjön, Western Segment. CL-images of analysed zircons in MISE1802a leucosome, that gave concordant analyses. Concordant (<5% discordance) spots are shown with solid lines and discordant analyses with dotted lines (>5% discordance). White spots represent the older igneous population while red spots represent the younger metamorphic population. The zircon number is shown in the upper left corner of each image. The spot number is indicated with #, followed by the $^{207}Pb/^{206}Pb$ date with 2 standard errors. The asterisk indicates an analysis used for age calculations with up to 10% discordance.

APPENDIX IV – Geochronology data

Table 1. LA-ICP-MS data for analysed zircons, includes all analyses except for rejected spots. Bold text indicates the concordant and filtered data at 5% discordance, out of which the mean average ages were calculated. Asterisk indicates measurements of up to 10% discordance in the younger population, used in the age calculations. Sq = square, Rec = rectangle.

Zircon	Spot	Spot geometry	Core/ Rim	U (ppm)	Th (ppm)	Th/U	$^{238}U/^{206}Pb$	± 2SE	$^{207}Pb/^{206}Pb$	± 2SE	$^{207}Pb/^{206}Pb$ age (Ma)	± 2SE	Conc. %
MISE1802a leucosome													
1	**Spot 35**	**Sq**	**Core**	**81**	**104**	**1.1806**	**3.5323**	**0.0374**	**0.0962**	**0.0012**	**1552**	**23**	**104**
2	**Spot 36**	**Sq**	**Core**	**278**	**87**	**0.2004**	**3.5236**	**0.0509**	**0.0967**	**0.0011**	**1561**	**21**	**103**
3	**Spot 37**	**Rec**	**Core**	**247**	**277**	**1.0604**	**3.5199**	**0.0335**	**0.0968**	**0.0009**	**1562**	**17**	**103**
4	**Spot 39**	**Sq**	**Core**	**404**	**488**	**1.1862**	**3.6232**	**0.0420**	**0.0989**	**0.0009**	**1604**	**18**	**98**
5	Spot 41	Rec	Rim	121	52	0.4146	4.1442	0.0979	0.0963	0.0020	1554	39	90
6	**Spot 42**	**Sq**	**Core**	**650**	**753**	**0.9804**	**3.7120**	**0.0427**	**0.0977**	**0.0007**	**1581**	**14**	**97**
6	**Spot 43**	**Rec**	**Rim**	**46**	**21**	**0.4421**	**3.5587**	**0.0608**	**0.0977**	**0.0021**	**1581**	**40**	**101**
7	**Spot 44**	**Sq**	**Core**	**163**	**26**	**0.1364**	**3.6364**	**0.0397**	**0.0976**	**0.0011**	**1579**	**21**	**99**
7	**Spot 45**	**Sq**	**Rim**	**12**	**0.01**	**0.0018**	**5.3619**	**0.0978**	**0.0749**	**0.0029**	**1066**	**78**	**103**
8	**Spot 46**	**Sq**	**Core**	**109**	**106**	**0.9390**	**3.5311**	**0.0324**	**0.0962**	**0.0009**	**1552**	**18**	**104**
8	Spot 47	Rec	Rim	8	0.02	0.0033	4.9826	0.1316	0.0745	0.0047	1055	127	112
9	**Spot 48**	**Sq**	**Core**	**104**	**23**	**0.2212**	**3.7679**	**0.0369**	**0.0980**	**0.0013**	**1586**	**25**	**96**
9	**Spot 49**	**Sq**	**Rim**	**12**	**1.06**	**0.0762**	**5.9067**	**0.1919**	**0.0745**	**0.0052**	**1055**	**141**	**96**
10	**Spot 50**	**Sq**	**Core**	**227**	**203**	**0.8150**	**3.6403**	**0.0477**	**0.0965**	**0.0009**	**1557**	**18**	**101**
11	**Spot 52**	**Sq**	**Core**	**193**	**168**	**0.8045**	**3.5461**	**0.0390**	**0.0953**	**0.0011**	**1534**	**22**	**104**
12	Spot 53	Rec	Core	332	260	0.7843	4.0917	0.0636	0.1075	0.0011	1757	19	80
12	**Spot 54**	**Rec**	**Rim**	**13**	**4**	**0.2688**	**3.6900**	**0.0899**	**0.0927**	**0.0032**	**1482**	**65**	**104**
13	**Spot 55**	**Sq**	**Core**	**253**	**272**	**1.0173**	**3.5039**	**0.0307**	**0.0955**	**0.0007**	**1539**	**14**	**105**
14	**Spot 56**	**Sq**	**Core**	**156**	**193**	**1.2022**	**3.6010**	**0.0415**	**0.0976**	**0.0010**	**1578**	**19**	**100**
18	**Spot 61**	**Sq**	**Core**	**187**	**111**	**0.5727**	**3.5997**	**0.0454**	**0.0962**	**0.0011**	**1552**	**21**	**102**
20	**Spot 64 ***	**Rec**	**Rim**	**9**	**0.03**	**0.0028**	**5.8005**	**0.1144**	**0.0768**	**0.0035**	**1116**	**91**	**92**
21	**Spot 66**	**Rec**	**Rim**	**140**	**78**	**0.5450**	**3.6536**	**0.0280**	**0.0963**	**0.0008**	**1554**	**15**	**100**
22	Spot 68	Sq	Core	289	239	0.8078	3.3014	0.0283	0.0944	0.0008	1516	15	113
24	**Spot 71**	**Sq**	**Core**	**231**	**327**	**1.2821**	**3.7037**	**0.0425**	**0.0946**	**0.0009**	**1521**	**19**	**101**
26	**Spot 72**	**Sq**	**Core**	**222**	**221**	**0.8921**	**3.4602**	**0.0383**	**0.0966**	**0.0009**	**1559**	**18**	**105**
25	**Spot 73**	**Rec**	**Core**	**176**	**144**	**0.7886**	**3.4734**	**0.0483**	**0.0964**	**0.0009**	**1556**	**18**	**105**
27	**Spot 75**	**Sq**	**Core**	**237**	**230**	**0.9452**	**3.6088**	**0.0313**	**0.0940**	**0.0007**	**1508**	**15**	**105**
27	Spot 76	Sq	Core	273	241	0.8666	3.4892	0.0317	0.0943	0.0008	1515	15	107
28	**Spot 77**	**Rec**	**Core**	**173**	**183**	**0.9191**	**3.7078**	**0.0344**	**0.0942**	**0.0010**	**1512**	**19**	**102**
29	**Spot 78**	**Sq**	**Core**	**87**	**115**	**1.2783**	**3.5829**	**0.0347**	**0.0947**	**0.0012**	**1522**	**24**	**104**
31	**Spot 80**	**Sq**	**Rim**	**12**	**0.04**	**0.0039**	**5.8241**	**0.1221**	**0.0737**	**0.0036**	**1033**	**99**	**99**
32	Spot 81	Sq	Core	215	190	0.8340	3.4352	0.0413	0.0941	0.0011	1510	22	109
33	Spot 82	Sq	Core	77	91	1.1249	3.5026	0.0368	0.0925	0.0010	1478	21	110
34	**Spot 83**	**Sq**	**Core**	**96**	**38**	**0.2825**	**3.7397**	**0.0392**	**0.0980**	**0.0011**	**1586**	**21**	**96**
35	Spot 84	Sq	Core	306	560	1.7995	3.3278	0.0399	0.0930	0.0009	1487	19	114
35	Spot 85	Rec	Rim	9	0.10	0.0333	5.9988	0.1475	0.0791	0.0050	1175	125	85
37	**Spot 87**	**Sq**	**Core**	**109**	**136**	**0.6711**	**3.6140**	**0.0379**	**0.0950**	**0.0012**	**1528**	**24**	**103**
38	**Spot 88**	**Sq**	**Core**	**147**	**241**	**1.6273**	**3.6010**	**0.0376**	**0.0936**	**0.0009**	**1499**	**19**	**105**
38	**Spot 89***	**Rec**	**Rim**	**5**	**0.17**	**0.0435**	**5.4885**	**0.1777**	**0.0792**	**0.0063**	**1177**	**157**	**92**
40	**Spot 90**	**Sq**	**Core**	**198**	**285**	**1.3441**	**3.6010**	**0.0467**	**0.0996**	**0.0008**	**1617**	**15**	**98**
39	**Spot 93**	**Sq**	**Rim**	**10**	**0.005**	**0.0018**	**6.0132**	**0.1193**	**0.0742**	**0.0033**	**1047**	**90**	**95**

42	Spot 95	Sq	Core	206	181	0.6250	3.4153	0.0397	0.0952	0.0009	1532	18	108
44	Spot 98	Sq	Rim	20	1.45	0.0645	5.6022	0.1287	0.0886	0.0034	1396	74	76
45	**Spot 99**	**Sq**	**Core**	**35**	**25**	**0.7102**	**3.6630**	**0.0416**	**0.0947**	**0.0016**	**1522**	**32**	**102**
45	**Spot 100**	**Rec**	**Rim**	**149**	**74**	**0.4566**	**3.7147**	**0.0580**	**0.0959**	**0.0014**	**1546**	**27**	**99**
49	Spot 104	Rec	Core	202	270	1.2870	3.3223	0.0596	0.0933	0.0016	1494	32	114
50	**Spot 105**	**Sq**	**Core**	**89**	**42**	**0.4439**	**3.7064**	**0.0495**	**0.0929**	**0.0014**	**1486**	**29**	**104**
50	Spot 106	Rec	Rim	109	26	0.2327	3.4130	0.0373	0.0894	0.0013	1413	28	117
51	**Spot 107**	**Sq**	**Core**	**165**	**297**	**1.7899**	**3.7636**	**0.0439**	**0.0939**	**0.0009**	**1506**	**19**	**101**
52	Spot 108	Sq	Core	125	104	0.7831	3.4698	0.0397	0.0946	0.0009	1519	18	107
53	**Spot 109**	**Sq**	**Core**	**104**	**129**	**1.2077**	**3.8183**	**0.0569**	**0.0932**	**0.0011**	**1492**	**22**	**101**
53	**Spot 110**	**Sq**	**Rim**	**10**	**0.33**	**0.1111**	**5.8651**	**0.1410**	**0.0729**	**0.0039**	**1011**	**108**	**100**
54	**Spot 111**	**Sq**	**Core**	**397**	**351**	**0.8432**	**3.8300**	**0.1085**	**0.0920**	**0.0008**	**1467**	**17**	**102**
56	**Spot 112**	**Sq**	**Core**	**167**	**58**	**0.3356**	**3.5461**	**0.0566**	**0.0961**	**0.0015**	**1550**	**29**	**103**
58	**Spot 114**	**Rec**	**Core**	**234**	**179**	**0.7657**	**3.7023**	**0.0411**	**0.0969**	**0.0009**	**1565**	**18**	**98**
60	**Spot 116**	**Rec**	**Core**	**124**	**116**	**0.7082**	**3.7147**	**0.0428**	**0.0963**	**0.0011**	**1554**	**21**	**99**
61	**Spot 117**	**Sq**	**Core**	**90**	**83**	**0.8977**	**3.8168**	**0.0495**	**0.0952**	**0.0011**	**1532**	**22**	**98**
62	**Spot 118**	**Rec**	**Core**	**184**	**190**	**1.0091**	**3.6900**	**0.0613**	**0.0971**	**0.0014**	**1569**	**27**	**99**
63	**Spot 120**	**Sq**	**Core**	**152**	**66**	**0.4203**	**3.7313**	**0.0557**	**0.0960**	**0.0012**	**1548**	**23**	**99**
65	**Spot 122**	**Rec**	**Core**	**59**	**23**	**0.2653**	**3.6350**	**0.0449**	**0.0970**	**0.0015**	**1567**	**29**	**100**
65	**Spot 123 ***	**Rec**	**Rim**	**12**	**0.02**	**0.0022**	**5.7770**	**0.1168**	**0.0770**	**0.0030**	**1121**	**78**	**92**
67	**Spot 124**	**Sq**	**Core**	**63**	**48**	**0.7663**	**3.7594**	**0.0438**	**0.0909**	**0.0013**	**1445**	**27**	**105**
69	Spot 127	Sq	Core	120	78	0.6382	3.3659	0.0521	0.0936	0.0012	1500	24	112
70	Spot 129	Sq	Rim	4	0.02	0.0065	5.1151	0.1622	0.0825	0.0070	1257	166	92
71	**Spot 130**	**Sq**	**Core**	**72**	**31**	**0.4329**	**3.7051**	**0.0398**	**0.0927**	**0.0013**	**1482**	**27**	**104**
72	**Spot 131**	**Sq**	**Core**	**192**	**113**	**0.5838**	**3.6684**	**0.0417**	**0.0958**	**0.0009**	**1544**	**17**	**101**
72	**Spot 132**	**Rec**	**Rim**	**97**	**40**	**0.4026**	**3.6550**	**0.0441**	**0.0944**	**0.0011**	**1516**	**22**	**103**
74	**Spot 136**	**Sq**	**Core**	**171**	**241**	**1.3928**	**3.6657**	**0.0699**	**0.0957**	**0.0016**	**1542**	**31**	**101**
74	**Spot 137**	**Rec**	**Rim**	**161**	**94**	**0.5482**	**3.7189**	**0.0567**	**0.0936**	**0.0010**	**1500**	**20**	**102**
75	**Spot 138**	**Sq**	**Core**	**313**	**343**	**1.0929**	**3.5026**	**0.0319**	**0.0958**	**0.0007**	**1544**	**15**	**105**
77	Spot 141	Sq	Core	239	216	0.8985	3.3411	0.0279	0.0950	0.0008	1527	16	110
79	**Spot 144**	**Sq**	**Core**	**215**	**218**	**1.0081**	**3.6523**	**0.0440**	**0.0951**	**0.0013**	**1530**	**26**	**102**
80	**Spot 145**	**Rec**	**Core**	**152**	**101**	**0.6570**	**3.6969**	**0.0547**	**0.0969**	**0.0013**	**1565**	**25**	**99**
81	Spot 146	Rec	Core	207	213	1.0267	3.3478	0.0426	0.0953	0.0011	1534	22	110
81	**Spot 147**	**Rec**	**Rim**	**12**	**0.03**	**0.0030**	**5.6593**	**0.1185**	**0.0742**	**0.0034**	**1047**	**92**	**100**
MISE1802a melanosome													
2	Spot 29	Rec	Core	375	10	0.0106	4.3029	0.0574	0.0975	0.0014	1577	27	85
3	Spot 30	Sq	Core	168	174	0.9980	4.1876	0.0649	0.0972	0.0013	1571	25	88
3	**Spot 31**	**Sq**	**Core**	**366**	**318**	**0.8368**	**3.9216**	**0.0400**	**0.0953**	**0.0010**	**1534**	**19**	**95**
5	Spot 33	Sq	Core	644	845	1.2005	3.9078	0.1252	0.1371	0.0042	2191	53	67
6	**Spot 34**	**Sq**	**Core**	**100**	**127**	**1.1614**	**3.8139**	**0.0407**	**0.0965**	**0.0012**	**1558**	**23**	**96**
7	**Spot 35**	**Sq**	**Core**	**311**	**226**	**0.6373**	**3.8183**	**0.0423**	**0.0953**	**0.0011**	**1534**	**22**	**98**
9	**Spot 37**	**Rec**	**Core**	**221**	**337**	**1.1765**	**3.8640**	**0.0358**	**0.0944**	**0.0010**	**1516**	**20**	**98**
11	Spot 39	Sq	Core	340	292	0.8621	3.7147	0.0400	0.1105	0.0012	1808	20	85
12	Spot 40	Sq	Core	307	405	1.0965	3.9463	0.0545	0.0969	0.0010	1564	19	93

13	Spot 41	Rec	Core	290	191	0.6725	3.5881	0.0438	0.1146	0.0023	1874	36	85
13	Spot 42	Rec	Rim	132	24	0.1883	3.9841	0.0381	0.1040	0.0012	1697	21	85
14	**Spot 43**	**Sq**	**Core**	**342**	**239**	**0.6807**	**3.7922**	**0.0618**	**0.0963**	**0.0010**	**1554**	**19**	**97**
15	Spot 45	Rec	Rim	161	84	0.5198	3.8506	0.0430	0.0981	0.0009	1588	17	94
17	Spot 47	Rec	Core	177	123	0.6468	3.4686	0.0469	0.1123	0.0025	1837	40	89
19	**Spot 49**	**Rec**	**Core**	**240**	**214**	**0.8150**	**3.6470**	**0.0306**	**0.0974**	**0.0009**	**1576**	**17**	**99**
20	Spot 50	Rec	Core	629	705	1.0235	3.6792	0.0338	0.1040	0.0010	1697	18	91
21	Spot 51	Rec	Core	302	16	0.0514	3.8820	0.0663	0.0971	0.0016	1569	31	94
22	**Spot 52**	**Rec**	**Core**	**388**	**730**	**1.7575**	**3.8226**	**0.0263**	**0.0958**	**0.0007**	**1544**	**14**	**97**
23	Spot 53	Sq	Core	442	413	0.8143	3.7979	0.0447	0.0987	0.0009	1599	17	94
24	**Spot 54**	**Sq**	**Core**	**222**	**217**	**0.8993**	**3.8300**	**0.0381**	**0.0968**	**0.0009**	**1564**	**17**	**96**
24	Spot 55	Sq	Rim	375	324	0.8104	3.9635	0.0346	0.0957	0.0008	1542	16	94
25	**Spot 56**	**Sq**	**Core**	**405**	**420**	**0.9355**	**3.7369**	**0.0363**	**0.0963**	**0.0008**	**1554**	**16**	**98**
26	Spot 57	Rec	Core	733	743	0.9533	4.2992	0.0684	0.1007	0.0010	1637	18	82
28	**Spot 60**	**Sq**	**Core**	**217**	**154**	**0.6826**	**3.7037**	**0.0398**	**0.0998**	**0.0012**	**1620**	**22**	**95**
29	**Spot 61**	**Sq**	**Core**	**287**	**254**	**0.9033**	**3.7722**	**0.0327**	**0.0955**	**0.0007**	**1538**	**14**	**99**
31	**Spot 66**	**Rec**	**Rim**	**61**	**29**	**0.5063**	**3.7010**	**0.0479**	**0.0973**	**0.0013**	**1573**	**25**	**98**
32	**Spot 67**	**Sq**	**Core**	**58**	**39**	**0.6949**	**3.7893**	**0.0359**	**0.0961**	**0.0012**	**1550**	**23**	**97**
33	**Spot 69**	**Rec**	**Core**	**197**	**247**	**1.2407**	**3.8139**	**0.0378**	**0.0963**	**0.0010**	**1554**	**19**	**97**
34	**Spot 70**	**Rec**	**Core**	**321**	**338**	**1.0101**	**3.8052**	**0.0333**	**0.0963**	**0.0007**	**1554**	**14**	**97**
35	**Spot 71**	**Sq**	**Core**	**477**	**381**	**0.7868**	**3.6792**	**0.0393**	**0.1002**	**0.0008**	**1627**	**15**	**95**
37	**Spot 74**	**Sq**	**Core**	**402**	**136**	**0.2740**	**3.6941**	**0.0478**	**0.0965**	**0.0011**	**1558**	**21**	**99**
39	**Spot 76**	**Rec**	**Core**	**385**	**28**	**0.0685**	**3.7722**	**0.0427**	**0.0964**	**0.0010**	**1556**	**19**	**97**
40	**Spot 77**	**Sq**	**Core**	**673**	**67**	**0.0932**	**3.7750**	**0.0328**	**0.0960**	**0.0008**	**1548**	**16**	**98**
40	Spot 78	Sq	Rim	325	355	0.7257	3.8895	0.0318	0.0973	0.0008	1573	15	94
41	**Spot 79**	**Rec**	**Core**	**755**	**652**	**0.7541**	**3.5524**	**0.0341**	**0.1009**	**0.0009**	**1641**	**17**	**97**
42	**Spot 80**	**Rec**	**Core**	**277**	**427**	**1.4388**	**3.7439**	**0.0378**	**0.0966**	**0.0010**	**1559**	**19**	**98**
43	**Spot 81**	**Rec**	**Core**	**306**	**584**	**1.8302**	**3.7313**	**0.0306**	**0.0972**	**0.0009**	**1571**	**17**	**97**
44	**Spot 82**	**Sq**	**Rim**	**342**	**244**	**0.7184**	**3.6711**	**0.0323**	**0.0959**	**0.0009**	**1545**	**18**	**101**
44	Spot 83	Sq	Rim	593	482	0.8140	4.0883	0.0318	0.0969	0.0006	1565	12	90
45	**Spot 84**	**Sq**	**Core**	**566**	**498**	**0.8857**	**3.6617**	**0.0429**	**0.0973**	**0.0009**	**1574**	**18**	**99**
46	Spot 85	Sq	Core	1022	830	0.5464	4.3328	0.1051	0.0955	0.0008	1538	15	87
47	Spot 86	Rec	Core	195	269	1.3439	3.8805	0.0301	0.0977	0.0010	1581	19	93
48	Spot 87	Sq	Core	402	319	0.7911	3.7495	0.0464	0.1006	0.0010	1636	18	93
49	Spot 88	Rec	Core	712	524	0.7310	4.1305	0.0546	0.1036	0.0011	1690	20	83
50	**Spot 89**	**Sq**	**Core**	**276**	**401**	**1.4209**	**3.7807**	**0.0300**	**0.0957**	**0.0008**	**1542**	**16**	**98**
51	Spot 90	Rec	Core	476	627	1.2804	3.6563	0.0455	0.1047	0.0019	1709	33	91
52	Spot 91	Sq	Core	535	536	0.9634	3.8760	0.0315	0.1015	0.0010	1652	18	90
53	Spot 92	Sq	Core	354	424	1.1723	3.8358	0.0427	0.1022	0.0015	1664	27	90
54	Spot 93	Sq	Core	669	649	0.9158	4.4053	0.0640	0.0991	0.0009	1608	17	82
55	**Spot 94**	**Sq**	**Core**	**205**	**103**	**0.4545**	**3.9573**	**0.0423**	**0.0939**	**0.0011**	**1506**	**22**	**96**
56	Spot 95	Sq	Core	489	396	0.8091	4.1859	0.0438	0.0975	0.0006	1578	12	88
57	**Spot 96**	**Sq**	**Core**	**345**	**474**	**1.3550**	**3.6232**	**0.0394**	**0.0970**	**0.0010**	**1567**	**19**	**100**
59	**Spot 98**	**Sq**	**Core**	**234**	**209**	**0.8576**	**3.7272**	**0.0306**	**0.0980**	**0.0009**	**1587**	**17**	**97**

62	**Spot 102**	**Rec**	**Rim**	**120**	**119**	**0.9434**	**3.6232**	**0.0473**	**0.0982**	**0.0009**	**1591**	**17**	**99**
66	**Spot 105**	**Sq**	**Core**	**410**	**430**	**1.0616**	**3.5817**	**0.0334**	**0.0965**	**0.0008**	**1557**	**16**	**102**
67	**Spot 106**	**Sq**	**Core**	**215**	**283**	**1.2240**	**3.6417**	**0.0345**	**0.0961**	**0.0009**	**1550**	**17**	**101**
68	**Spot 107**	**Sq**	**Core**	**576**	**581**	**0.9009**	**3.7216**	**0.0360**	**0.0970**	**0.0006**	**1568**	**12**	**98**
69	**Spot 109**	**Sq**	**Core**	**136**	**123**	**0.8368**	**3.5298**	**0.0361**	**0.0963**	**0.0010**	**1554**	**19**	**103**
70	**Spot 110**	**Sq**	**Core**	**576**	**506**	**0.8006**	**3.6140**	**0.0379**	**0.0973**	**0.0007**	**1573**	**13**	**100**
MISE1806 leucosome													
3	**Spot 3**	**Sq**	**Core**	**731**	**820**	**1.0893**	**4.1220**	**0.0561**	**0.0870**	**0.0008**	**1361**	**17**	**103**
4	**Spot 4a**	**Sq**	**Core**	**1102**	**854**	**0.7680**	**4.2248**	**0.0553**	**0.0864**	**0.0011**	**1347**	**25**	**102**
4	**Spot 4b**	**Sq**	**Core**	**728**	**45**	**0.0518**	**5.3648**	**0.1094**	**0.0755**	**0.0019**	**1082**	**50**	**102**
5	Spot 5	Sq	Core	854	2220	1.9841	5.7078	0.1662	0.0864	0.0007	1348	16	77
7	**Spot 6**	**Sq**	**Core**	**362**	**318**	**0.8432**	**4.2248**	**0.1321**	**0.0874**	**0.0012**	**1369**	**26**	**100**
7	Spot 7	Sq	Rim	980	732	0.7062	5.2110	0.1385	0.0887	0.0008	1398	17	81
8	Spot 8	Sq	Core	492	1890	3.8023	5.5249	0.0794	0.0916	0.0011	1459	23	73
8	Spot 9	Sq	Rim	547	2890	5.0531	4.7778	0.0776	0.0896	0.0013	1417	28	86
9	Spot 10	Sq	Core	612	468	0.7485	3.9620	0.0392	0.0853	0.0007	1323	17	110
11	**Spot 11**	**Sq**	**Core**	**820**	**768**	**0.7657**	**4.3085**	**0.0947**	**0.0862**	**0.0012**	**1343**	**27**	**100**
13	**Spot 12**	**Sq**	**Core**	**735**	**643**	**0.8475**	**4.1545**	**0.0501**	**0.0886**	**0.0009**	**1395**	**20**	**100**
13	**Spot 13**	**Rec**	**Rim**	**987**	**884**	**0.8591**	**4.2105**	**0.0762**	**0.0880**	**0.0010**	**1382**	**22**	**99**
14	Spot 14	Rec	Core	1060	1354	1.2422	3.8850	0.0664	0.0869	0.0010	1358	22	109
14	**Spot 15**	**Rec**	**Rim**	**403**	**283**	**0.6930**	**4.4683**	**0.0659**	**0.0848**	**0.0010**	**1311**	**23**	**99**
15	**Spot 16**	**Sq**	**Core**	**895**	**1427**	**1.7391**	**4.3783**	**0.0556**	**0.0858**	**0.0008**	**1333**	**18**	**99**
16	**Spot 17a**	**Sq**	**Core**	**636**	**754**	**1.1990**	**4.3271**	**0.1348**	**0.0872**	**0.0017**	**1365**	**38**	**98**
16	Spot 17b	Sq	Core	172	175	1.0352	3.4722	0.0603	0.0940	0.0015	1508	30	108
16	**Spot 18a**	**Sq**	**Rim**	**2005**	**83**	**0.0373**	**5.3163**	**0.1159**	**0.0749**	**0.0014**	**1066**	**38**	**104**
15	**Spot 18b**	**Sq**	**Rim**	**483**	**681**	**1.2019**	**4.2571**	**0.0598**	**0.0874**	**0.0011**	**1369**	**24**	**99**
17	Spot 19	Sq	Core	330	934	2.5510	4.6189	0.1088	0.0952	0.0015	1532	30	82
18	Spot 20	Sq	Core	845	1322	1.6393	4.7801	0.0708	0.0843	0.0013	1299	30	94
19	Spot 21	Sq	Core	816	1936	2.4213	4.5351	0.1070	0.0909	0.0016	1445	34	89
20	**Spot 22**	**Sq**	**Core**	**577**	**563**	**0.8613**	**4.2790**	**0.0604**	**0.0866**	**0.0008**	**1350**	**17**	**100**
21	**Spot 23**	**Rec**	**Core**	**292**	**128**	**0.4562**	**4.1169**	**0.0644**	**0.0885**	**0.0013**	**1393**	**28**	**101**
21	**Spot 24**	**Sq**	**Rim**	**2470**	**12**	**0.0051**	**5.3305**	**0.1478**	**0.0746**	**0.0016**	**1058**	**43**	**105**
22	**Spot 25**	**Sq**	**Core**	**344**	**184**	**0.5659**	**4.2553**	**0.0598**	**0.0849**	**0.0010**	**1313**	**22**	**104**
22	**Spot 26**	**Rec**	**Rim**	**1082**	**200**	**0.1499**	**5.5586**	**0.0865**	**0.0755**	**0.0010**	**1082**	**27**	**99**
24	Spot 27	Sq	Core	541	2680	4.8544	6.9444	0.7234	0.0984	0.0043	1594	82	54
23	Spot 28	Sq	Core	660	780	1.0707	4.2790	0.0641	0.0934	0.0013	1496	26	90
23	**Spot 29**	**Rec**	**Rim**	**204**	**90**	**0.4617**	**3.6127**	**0.0653**	**0.0937**	**0.0013**	**1502**	**26**	**105**
25	Spot 30	Sq	Core	759	1060	1.0787	5.2056	0.0867	0.0863	0.0010	1346	22	84
27	Spot 31	Sq	Core	788	797	1.0571	4.4033	0.1047	0.0927	0.0018	1482	37	89
28	Spot 32	Sq	Core	413	392	0.9634	4.0193	0.0630	0.0847	0.0008	1309	17	109
31	Spot 33	Rec	Core	261	304	0.8850	3.9246	0.0400	0.0855	0.0010	1326	22	110
32	Spot 34	Sq	Core	483	564	0.8703	5.8411	0.0716	0.0886	0.0011	1396	24	73
32	**Spot 35**	**Sq**	**Core**	**159**	**88**	**0.5488**	**4.0733**	**0.0498**	**0.0881**	**0.0014**	**1385**	**31**	**102**
34	Spot 36	Sq	Core	1087	697	0.6373	5.5006	0.0877	0.1103	0.0036	1804	59	60

36	Spot 37	Sq	Core	2800	33	0.0125	6.7250	0.0995	0.0733	0.0007	1021	18	88
36	Spot 38	Sq	Rim	2850	39	0.0129	6.8259	0.0978	0.0706	0.0007	945	19	93
37	**Spot 39**	**Sq**	**Core**	**651**	**787**	**0.9579**	**4.1754**	**0.0941**	**0.0877**	**0.0010**	**1376**	**22**	**101**
38	**Spot 40**	**Sq**	**Core**	**500**	**480**	**0.7092**	**4.3234**	**0.0542**	**0.0863**	**0.0010**	**1345**	**22**	**100**
38	**Spot 41**	**Rec**	**Rim**	**149**	**67**	**0.4589**	**4.3365**	**0.1222**	**0.0851**	**0.0014**	**1318**	**32**	**102**
39	**Spot 42**	**Sq**	**Core**	**533**	**435**	**0.8425**	**4.2212**	**0.0481**	**0.0873**	**0.0009**	**1366**	**19**	**100**
40	Spot 43	Sq	Core	1239	7240	5.7971	5.6306	0.2917	0.0880	0.0022	1382	48	76
40	Spot 44	Sq	Rim	304	1180	3.1546	5.0813	0.0826	0.0890	0.0016	1404	34	82
41	**Spot 45**	**Sq**	**Core**	**297**	**405**	**1.0776**	**4.2937**	**0.0627**	**0.0870**	**0.0011**	**1360**	**24**	**99**
41	**Spot 46**	**Rec**	**Rim**	**187**	**386**	**1.2821**	**4.2717**	**0.0839**	**0.0867**	**0.0014**	**1354**	**31**	**100**
42	Spot 47	Sq	Core	240	82	0.3106	4.7596	0.0793	0.0876	0.0015	1374	33	89
42	Spot 48	Rec	Rim	402	36	0.0871	6.4683	0.1171	0.0813	0.0014	1229	34	75
43	**Spot 49**	**Sq**	**Rim**	**332**	**180**	**0.4778**	**4.2626**	**0.0600**	**0.0842**	**0.0011**	**1297**	**25**	**105**
45	**Spot 50**	**Sq**	**Core**	**506**	**467**	**0.9033**	**4.1982**	**0.0846**	**0.0856**	**0.0014**	**1329**	**32**	**104**
45	Spot 51	Sq	Rim	637	2133	3.3898	5.2770	0.0668	0.0930	0.0011	1488	22	75
46	**Spot 52**	**Sq**	**Core**	**238**	**324**	**1.2180**	**4.5351**	**0.0864**	**0.0857**	**0.0011**	**1331**	**25**	**96**
46	**Spot 53**	**Sq**	**Rim**	**339**	**804**	**2.0790**	**4.2283**	**0.0518**	**0.0874**	**0.0010**	**1369**	**21**	**100**
47	**Spot 54**	**Sq**	**Core**	**358**	**471**	**1.3405**	**4.1964**	**0.0458**	**0.0867**	**0.0011**	**1354**	**24**	**102**
47	**Spot 55**	**Sq**	**Rim**	**775**	**575**	**0.7479**	**4.1391**	**0.0463**	**0.0869**	**0.0009**	**1358**	**20**	**103**
48	Spot 56	Sq	Core	557	495	0.8969	4.0568	0.0592	0.0858	0.0009	1333	21	107
48	**Spot 57**	**Rec**	**Rim**	**490**	**210**	**0.4115**	**4.7778**	**0.1370**	**0.0830**	**0.0013**	**1269**	**31**	**97**
49	**Spot 58**	**Sq**	**Core**	**447**	**357**	**0.7246**	**4.0783**	**0.0765**	**0.0880**	**0.0018**	**1382**	**39**	**102**
49	Spot 59	Sq	Rim	944	571	0.6135	6.5876	0.1128	0.0858	0.0010	1334	23	68
51	**Spot 60**	**Sq**	**Core**	**782**	**558**	**0.7380**	**4.2882**	**0.0883**	**0.0867**	**0.0013**	**1354**	**29**	**100**
51	**Spot 61a**	**Sq**	**Rim**	**1013**	**40**	**0.0333**	**5.4496**	**0.0891**	**0.0746**	**0.0011**	**1058**	**30**	**103**
51	Spot 61b	Sq	Rim	146	71	0.4926	3.9370	0.0450	0.0860	0.0016	1338	36	109
54	**Spot 62**	**Sq**	**Core**	**378**	**666**	**1.6920**	**4.2517**	**0.0868**	**0.0881**	**0.0013**	**1385**	**28**	**98**
55	**Spot 63**	**Sq**	**Core**	**204**	**402**	**1.5873**	**4.2194**	**0.1086**	**0.0867**	**0.0039**	**1354**	**87**	**101**
55	Spot 64	Sq	Rim	1168	833	0.7163	5.2301	0.1723	0.0763	0.0018	1103	47	102
56	**Spot 65**	**Sq**	**Core**	**753**	**383**	**0.5076**	**4.2159**	**0.0658**	**0.0859**	**0.0014**	**1336**	**32**	**103**
56	**Spot 66**	**Sq**	**Rim**	**481**	**337**	**0.6798**	**4.0339**	**0.0504**	**0.0884**	**0.0015**	**1391**	**33**	**103**
56	Spot 67	Sq	Rim	628	1730	2.2883	10.7411	0.2884	0.1154	0.0030	1886	47	30
58	**Spot 68**	**Sq**	**Core**	**754**	**648**	**0.8703**	**4.0634**	**0.0380**	**0.0870**	**0.0007**	**1361**	**16**	**104**
58	**Spot 69a**	**Rec**	**Rim**	**3680**	**37**	**0.0097**	**5.3967**	**0.1194**	**0.0753**	**0.0012**	**1077**	**32**	**102**
58	Spot 69b	Rec	Rim	418	296	0.6969	3.6403	0.0689	0.0835	0.0011	1281	26	122
58	Spot 70	Rec	RIm	665	87	0.1182	5.4645	0.0717	0.0852	0.0011	1320	25	82
59	**Spot 71**	**Sq**	**Core**	**1770**	**16**	**0.0057**	**5.7274**	**0.1082**	**0.0730**	**0.0007**	**1014**	**18**	**102**
62	**Spot 72**	**Sq**	**Rim**	**1810**	**29**	**0.0105**	**5.6338**	**0.0857**	**0.0736**	**0.0006**	**1032**	**17**	**102**
63	**Spot 73**	**Sq**	**Rim**	**462**	**1600**	**2.7933**	**4.2248**	**0.0803**	**0.0880**	**0.0011**	**1382**	**24**	**99**
66	Spot 74	Sq	Rim	1145	1119	0.9671	4.7148	0.0956	0.0881	0.0014	1385	31	90
67	**Spot 75**	**Sq**	**Core**	**1119**	**1105**	**0.9950**	**4.2553**	**0.1086**	**0.0882**	**0.0020**	**1387**	**44**	**98**
84	Spot 76	Sq	Core	2200	86	0.0403	10.3842	0.2157	0.0921	0.0020	1469	41	40
84	**Spot 77**	**Sq**	**Rim**	**1359**	**15**	**0.0115**	**6.1087**	**0.2202**	**0.0711**	**0.0011**	**960**	**32**	**102**
87	**Spot 78**	**Sq**	**Core**	**395**	**548**	**1.2837**	**3.9777**	**0.0665**	**0.0907**	**0.0016**	**1440**	**34**	**100**

87	**Spot 79**	**Sq**	**Rim**	**614**	**322**	**0.4651**	**4.3783**	**0.0537**	**0.0861**	**0.0012**	**1340**	**27**	**99**
88	**Spot 80**	**Sq**	**Core**	**624**	**2083**	**3.5002**	**4.3706**	**0.0669**	**0.0883**	**0.0014**	**1389**	**30**	**96**
88	**Spot 81**	**Sq**	**Rim**	**649**	**282**	**0.4456**	**4.4346**	**0.0629**	**0.0841**	**0.0010**	**1295**	**23**	**101**
90	**Spot 82**	**Sq**	**Core**	**435**	**576**	**1.3263**	**4.1632**	**0.0676**	**0.0874**	**0.0011**	**1369**	**24**	**101**
90	Spot 83	Sq	Rim	630	963	1.3004	4.9529	0.1006	0.0881	0.0010	1384	21	86
91	Spot 84	Sq	Rim	516	379	0.7348	3.8432	0.0384	0.0864	0.0008	1347	17	111
93	Spot 85	Sq	Rim	464	360	0.7955	3.7327	0.0488	0.0873	0.0010	1367	22	112
95	Spot 86	Rec	Core	1451	1260	0.9058	3.7608	0.0594	0.0870	0.0011	1360	24	112
95	Spot 87	Rec	Rim	1395	167	0.1149	6.6934	0.2867	0.0939	0.0019	1506	38	60
98	Spot 88	Sq	Core	1205	847	0.7402	3.8241	0.0380	0.0865	0.0008	1350	18	111
98	Spot 89	Rec	Rim	1510	322	0.1988	5.4705	0.0658	0.0916	0.0011	1459	23	74
98	**Spot 90**	**Sq**	**Core**	**1083**	**1257**	**1.1696**	**3.9952**	**0.0623**	**0.0932**	**0.0012**	**1492**	**24**	**97**
MISE1806 melanosome													
1	**Spot 27**	**Sq**	**Core**	**722**	**716**	**1.0040**	**4.3215**	**0.0840**	**0.0865**	**0.0014**	**1349**	**31**	**99**
2	**Spot 28**	**Sq**	**Core**	**547**	**480**	**0.8190**	**4.2445**	**0.0468**	**0.0866**	**0.0007**	**1351**	**15**	**101**
3	**Spot 29**	**Sq**	**Core**	**445**	**288**	**0.6506**	**4.4053**	**0.0543**	**0.0862**	**0.0013**	**1343**	**29**	**98**
4	**Spot 30**	**Sq**	**Core**	**382**	**663**	**1.3755**	**4.1946**	**0.0440**	**0.0879**	**0.0008**	**1381**	**17**	**100**
5	**Spot 31**	**Sq**	**Core**	**472**	**359**	**0.4608**	**4.2626**	**0.0382**	**0.0870**	**0.0007**	**1359**	**15**	**100**
6	**Spot 32**	**Sq**	**Core**	**721**	**367**	**0.5216**	**4.2517**	**0.0380**	**0.0861**	**0.0007**	**1340**	**16**	**102**
7	Spot 33	Sq	Core	306	459	1.3928	4.2827	0.0385	0.0914	0.0009	1455	19	93
7	Spot 34	Rec	Rim	598	3650	5.5991	7.7942	0.1458	0.1283	0.0021	2075	29	38
8	Spot 35	Sq	Core	873	779	0.8749	5.6054	0.1100	0.0853	0.0008	1322	17	80
9	**Spot 36**	**Sq**	**Core**	**682**	**721**	**0.9452**	**4.3178**	**0.0485**	**0.0867**	**0.0006**	**1354**	**14**	**99**
10	Spot 37	Sq	Core	1368	1124	0.7843	3.9777	0.0427	0.0862	0.0006	1342	13	108
11	**Spot 38**	**Sq**	**Core**	**478**	**263**	**0.5618**	**4.3649**	**0.0457**	**0.0867**	**0.0008**	**1353**	**18**	**98**
12	Spot 39	Sq	Core	463	1430	2.4752	5.0659	0.0821	0.0892	0.0012	1408	26	82
13	**Spot 40**	**Sq**	**Core**	**1362**	**509**	**0.3683**	**4.4924**	**0.0686**	**0.0867**	**0.0009**	**1353**	**19**	**96**
14	**Spot 41**	**Sq**	**Core**	**330**	**165**	**0.4885**	**4.3122**	**0.0465**	**0.0864**	**0.0009**	**1348**	**20**	**100**
15	**Spot 42**	**Sq**	**Core**	**667**	**324**	**0.4943**	**4.1615**	**0.0468**	**0.0865**	**0.0009**	**1349**	**20**	**103**
16	**Spot 43**	**Sq**	**Core**	**1476**	**1086**	**0.6964**	**4.1477**	**0.0516**	**0.0857**	**0.0006**	**1332**	**13**	**105**
18	**Spot 44**	**Sq**	**Core**	**487**	**320**	**0.6456**	**4.2753**	**0.0402**	**0.0883**	**0.0008**	**1389**	**17**	**98**
19	**Spot 45**	**Sq**	**Core**	**925**	**670**	**0.7194**	**4.1442**	**0.0429**	**0.0866**	**0.0006**	**1351**	**14**	**103**
20	**Spot 46**	**Sq**	**Core**	**457**	**384**	**0.7413**	**4.3159**	**0.0428**	**0.0862**	**0.0007**	**1342**	**16**	**100**
20	**Spot 47**	**Sq**	**Rim**	**972**	**233**	**0.2481**	**4.3215**	**0.0486**	**0.0847**	**0.0007**	**1308**	**15**	**103**
21	**Spot 48**	**Sq**	**Core**	**520**	**683**	**1.1364**	**4.0258**	**0.0421**	**0.0880**	**0.0008**	**1382**	**17**	**103**
21	**Spot 49**	**Sq**	**Rim**	**681**	**613**	**0.8795**	**4.2391**	**0.0431**	**0.0865**	**0.0007**	**1349**	**15**	**101**
22	**Spot 50**	**Sq**	**Core**	**501**	**378**	**0.7153**	**4.1477**	**0.0516**	**0.0853**	**0.0009**	**1322**	**21**	**105**
23	**Spot 51**	**Sq**	**Core**	**2004**	**1796**	**0.9302**	**4.2373**	**0.0700**	**0.0864**	**0.0010**	**1347**	**22**	**101**
23	**Spot 52**	**Sq**	**Rim**	**925**	**511**	**0.5653**	**4.5290**	**0.0595**	**0.0848**	**0.0007**	**1312**	**17**	**98**
25	Spot 53	Sq	Core	500	1370	2.7027	5.2356	0.0987	0.1398	0.0033	2225	41	51
27	**Spot 54**	**Sq**	**Core**	**643**	**376**	**0.5155**	**4.1511**	**0.0724**	**0.0866**	**0.0008**	**1350**	**17**	**103**
30	Spot 55	Sq	Core	745	1060	1.3351	4.6318	0.0601	0.0884	0.0007	1391	16	91
31	**Spot 56**	**Sq**	**Core**	**968**	**673**	**0.7158**	**4.2735**	**0.1479**	**0.0862**	**0.0021**	**1343**	**47**	**101**
31	**Spot 57***	**Rec**	**Rim**	**870**	**342**	**0.3731**	**6.0606**	**0.0955**	**0.0758**	**0.0010**	**1089**	**26**	**90**

32	**Spot 58**	**Sq**	**Core**	**796**	**604**	**0.7463**	**4.3384**	**0.0546**	**0.0855**	**0.0007**	**1328**	**17**	**101**
34	**Spot 59**	**Sq**	**Rim**	**732**	**590**	**0.8299**	**4.3215**	**0.0598**	**0.0852**	**0.0009**	**1321**	**20**	**102**
35	**Spot 60**	**Sq**	**Core**	**1114**	**802**	**0.7468**	**4.4326**	**0.0727**	**0.0863**	**0.0013**	**1345**	**29**	**98**
37	**Spot 61**	**Sq**	**Core**	**903**	**928**	**1.0215**	**4.3029**	**0.0555**	**0.0882**	**0.0009**	**1387**	**19**	**97**
38	**Spot 62**	**Sq**	**Core**	**426**	**249**	**0.5599**	**4.3178**	**0.0503**	**0.0851**	**0.0009**	**1317**	**21**	**102**
39	**Spot 63**	**Sq**	**Core**	**432**	**424**	**1.0235**	**4.3048**	**0.0463**	**0.0862**	**0.0008**	**1343**	**17**	**100**
45	**Spot 64**	**Sq**	**Core**	**556**	**505**	**0.7734**	**4.2517**	**0.0416**	**0.0870**	**0.0007**	**1360**	**16**	**100**
45	**Spot 65**	**Sq**	**Rim**	**436**	**585**	**1.3423**	**4.6577**	**0.0716**	**0.0842**	**0.0009**	**1296**	**20**	**97**
46	**Spot 66**	**Sq**	**Core**	**647**	**504**	**0.7508**	**4.1667**	**0.0451**	**0.0858**	**0.0008**	**1335**	**17**	**104**
49	**Spot 67**	**Sq**	**Core**	**632**	**482**	**0.7610**	**4.2808**	**0.0513**	**0.0859**	**0.0009**	**1337**	**21**	**101**
50	Spot 68	Sq	Rim	433	217	0.4941	4.6189	0.0512	0.0871	0.0008	1362	18	93
51	**Spot 69**	**Sq**	**Core**	**1657**	**1316**	**0.7734**	**4.2699**	**0.0656**	**0.0861**	**0.0010**	**1340**	**22**	**101**
51	**Spot 70**	**Sq**	**Rim**	**717**	**574**	**0.7479**	**4.1911**	**0.0474**	**0.0871**	**0.0007**	**1362**	**15**	**101**
56	Spot 71	Sq	Core	413	311	0.7479	3.9017	0.0731	0.0855	0.0010	1327	23	111
61	Spot 72	Rec	Rim	515	722	1.4164	5.1151	0.1727	0.0883	0.0011	1389	24	83
61	Spot 73	Rec	Core	1160	2950	2.6483	8.0645	0.2341	0.1940	0.0044	2776	37	27
62	**Spot 74**	**Sq**	**Core**	**476**	**268**	**0.5618**	**4.2808**	**0.0403**	**0.0865**	**0.0008**	**1350**	**19**	**100**
65	**Spot 75**	**Sq**	**Core**	**469**	**317**	**0.6394**	**4.4209**	**0.0919**	**0.0850**	**0.0013**	**1316**	**30**	**100**
65	**Spot 76**	**Sq**	**Rim**	**287**	**155**	**0.5580**	**4.1771**	**0.0366**	**0.0854**	**0.0009**	**1324**	**21**	**105**
66	**Spot 77**	**Sq**	**Core**	**731**	**798**	**0.9276**	**4.3516**	**0.0663**	**0.0857**	**0.0009**	**1332**	**20**	**100**
67	Spot 78	Sq	Core	281	208	0.7485	4.0766	0.0465	0.0854	0.0011	1325	25	107
68	Spot 79	Sq	Core	539	396	0.6545	4.0733	0.0431	0.0858	0.0008	1334	19	106
68	Spot 80	Sq	Rim	707	315	0.4883	4.0917	0.0486	0.0852	0.0009	1320	21	107
69	**Spot 81**	**Sq**	**Core**	**384**	**424**	**1.1442**	**4.1615**	**0.0623**	**0.0866**	**0.0011**	**1352**	**25**	**103**
70	Spot 82	Sq	Core	353	246	0.6562	4.0112	0.0531	0.0988	0.0017	1602	32	90
70	Spot 83	Sq	Rim	821	268	0.3180	5.0000	0.0825	0.0840	0.0006	1291	15	91
71	**Spot 84**	**Sq**	**Core**	**400**	**400**	**0.9191**	**4.3159**	**0.0522**	**0.0882**	**0.0009**	**1387**	**19**	**97**
71	**Spot 85**	**Sq**	**Rim**	**981**	**650**	**0.6588**	**4.2283**	**0.0518**	**0.0860**	**0.0009**	**1339**	**21**	**102**
72	Spot 86	Sq	Core	497	1030	2.2321	4.8146	0.0719	0.1328	0.0030	2135	40	57
72	Spot 87	Sq	Rim	448	308	0.7032	4.0601	0.0429	0.0854	0.0008	1325	18	107
74	**Spot 88**	**Sq**	**Core**	**544**	**385**	**0.6969**	**4.1964**	**0.0511**	**0.0866**	**0.0010**	**1352**	**22**	**102**
75	Spot 89	Sq	Core	545	1570	2.7450	7.8740	0.1612	0.0958	0.0014	1544	27	50
75	**Spot 90**	**Sq**	**Rim**	**734**	**870**	**1.1641**	**4.1339**	**0.0427**	**0.0858**	**0.0007**	**1333**	**15**	**105**
76	Spot 91	Rec	Core	638	1370	1.0417	4.9702	0.2050	0.0878	0.0010	1378	22	86
76	Spot 92	Rec	Rim	534	691	1.2594	5.1177	0.0943	0.0995	0.0026	1615	49	71
77	**Spot 93**	**Sq**	**Rim**	**852**	**349**	**0.3704**	**4.7192**	**0.0579**	**0.0837**	**0.0009**	**1287**	**20**	**96**
78	**Spot 94**	**Sq**	**Rim**	**666**	**1426**	**2.0661**	**4.1876**	**0.0631**	**0.0885**	**0.0015**	**1393**	**33**	**99**
79	**Spot 95**	**Sq**	**Core**	**519**	**541**	**0.9579**	**4.3649**	**0.0419**	**0.0859**	**0.0010**	**1336**	**23**	**100**
82	Spot 96	Sq	Core	332	1010	2.3419	5.8582	0.0789	0.0994	0.0018	1613	34	63
82	Spot 97	Rec	Rim	564	738	1.2690	4.8591	0.0614	0.0934	0.0012	1496	24	81
83	Spot 98	Sq	Core	341	128	0.4219	4.1859	0.0648	0.0843	0.0009	1300	21	106
83	**Spot 99a**	**Sq**	**Rim**	**903**	**557**	**0.6349**	**4.2337**	**0.0484**	**0.0867**	**0.0010**	**1354**	**22**	**101**
83	**Spot 99b**	**Sq**	**Rim**	**254**	**14**	**0.0476**	**5.6402**	**0.1209**	**0.0734**	**0.0025**	**1025**	**69**	**103**
85	**Spot 100**	**Sq**	**Core**	**494**	**509**	**1.0320**	**4.1632**	**0.0485**	**0.0887**	**0.0012**	**1398**	**26**	**99**

85	Spot 101	Rec	Rim	1009	843	0.7576	4.8239	0.0721	0.0850	0.0016	1316	37	92
86	**Spot 102**	**Sq**	**Core**	**846**	**583**	**0.6892**	**4.2373**	**0.0628**	**0.0873**	**0.0015**	**1367**	**33**	**100**
89	**Spot 103**	**Sq**	**Core**	**526**	**369**	**0.7435**	**4.1789**	**0.0471**	**0.0860**	**0.0010**	**1338**	**22**	**103**
MISE1814a													
1	**Spot 1**	**Sq**	**Core**	**311**	**94**	**0.2915**	**3.4130**	**0.1864**	**0.0989**	**0.0030**	**1603**	**57**	**103**
1	**Spot 2**	**Rec**	**Rim**	**180**	**97**	**0.5618**	**3.3898**	**0.1953**	**0.0985**	**0.0032**	**1596**	**61**	**104**
2	**Spot 3**	**Sq**	**Core**	**219**	**95**	**0.3922**	**3.4722**	**0.1567**	**0.0998**	**0.0028**	**1620**	**52**	**101**
2	Spot 4	Rec	Rim	42	2	0.0260	3.9683	0.1575	0.0965	0.0029	1558	56	93
3	**Spot 5**	**Sq**	**Core**	**155**	**203**	**1.2594**	**3.5211**	**0.1736**	**0.0984**	**0.0032**	**1594**	**61**	**101**
4	**Spot 6**	**Sq**	**Core**	**400**	**197**	**0.4545**	**3.4843**	**0.1821**	**0.0981**	**0.0030**	**1588**	**57**	**102**
5	**Spot 7**	**Rec**	**Core**	**219**	**208**	**0.8857**	**3.9432**	**0.1228**	**0.0950**	**0.0020**	**1528**	**40**	**95**
5	**Spot 8**	**Rec**	**Rim**	**73**	**56**	**0.7032**	**3.4965**	**0.1589**	**0.1009**	**0.0031**	**1641**	**57**	**99**
6	Spot 9	Sq	Core	228	311	1.3004	3.6805	0.1260	0.1010	0.0022	1643	40	94
6	Spot 10	Rec	Rim	231	96	0.4525	3.3223	0.1545	0.0986	0.0027	1598	51	106
7	Spot 11	Sq	Core	218	169	0.7194	3.8462	0.2811	0.1020	0.0047	1661	85	90
7	Spot 12	Rec	Rim	294	75	0.2653	4.0816	0.2166	0.1005	0.0034	1633	63	86
8	**Spot 13**	**Rec**	**Core**	**190**	**192**	**1.0194**	**3.6630**	**0.1610**	**0.1010**	**0.0028**	**1643**	**51**	**95**
9	**Spot 15**	**Rec**	**Core**	**186**	**270**	**1.4124**	**3.6232**	**0.1575**	**0.0988**	**0.0028**	**1602**	**53**	**98**
10	Spot 16	Sq	Core	264	174	0.6402	3.8926	0.1045	0.0992	0.0018	1609	34	92
11	Spot 17	Sq	Core	131	159	1.1806	4.2212	0.0659	0.0987	0.0013	1600	25	86
12	Spot 18	Rec	Core	236	499	1.9194	3.1456	0.0970	0.0992	0.0013	1609	24	111
12	Spot 19	Sq	Rim	398	66	0.1318	4.1288	0.0903	0.0986	0.0015	1598	28	88
14	Spot 20	Sq	Core	213	244	1.1099	4.0933	0.0754	0.0966	0.0013	1559	25	90
15	Spot 21	Sq	Core	521	99	0.1946	4.2735	0.2739	0.1028	0.0037	1675	67	81
15	Spot 22	Sq	Core	159	87	0.5405	3.9526	0.1875	0.0958	0.0026	1544	51	94
16	Spot 23	Sq	Core	222	111	0.5444	3.9032	0.1127	0.0978	0.0018	1583	34	93
17	Spot 24	Sq	Core	229	190	0.8264	3.8700	0.0794	0.0982	0.0015	1590	29	93
18	Spot 25	Rec	Core	198	194	0.9398	3.9573	0.0532	0.0974	0.0011	1575	21	92
18	Spot 26	Sq	Rim	276	76	0.3021	3.9262	0.0555	0.0972	0.0009	1572	18	93
20	Spot 27	Sq	Core	208	116	0.5879	4.0355	0.0489	0.0970	0.0011	1567	21	91
20	**Spot 28**	**Rec**	**Rim**	**197**	**97**	**0.5263**	**3.6670**	**0.0430**	**0.0995**	**0.0011**	**1615**	**21**	**96**
21	Spot 29	Sq	Core	246	294	1.1876	4.0112	0.0434	0.0977	0.0011	1581	21	91
21	Spot 30	Sq	Rim	68	0.41	0.0044	6.2383	0.0856	0.0770	0.0018	1121	47	85
22	Spot 31	Sq	Core	314	265	0.8110	4.2699	0.0802	0.0972	0.0017	1571	33	86
22	**Spot 32**	**Rec**	**Rim**	**214**	**1.07**	**0.0049**	**5.9242**	**0.1474**	**0.0734**	**0.0016**	**1025**	**44**	**98**
23	Spot 33	Sq	Core	344	200	0.5869	4.1649	0.1128	0.0992	0.0025	1609	47	86
24	**Spot 34**	**Sq**	**Core**	**162**	**245**	**1.4837**	**3.6430**	**0.0372**	**0.0978**	**0.0013**	**1583**	**25**	**99**
24	Spot 35	Rec	Rim	114	91	0.8382	3.8790	0.0497	0.0981	0.0014	1588	27	93
40	**Spot 36**	**Sq**	**Core**	**124**	**155**	**1.2438**	**3.6697**	**0.0417**	**0.0978**	**0.0013**	**1583**	**25**	**98**
40	**Spot 37**	**Rec**	**Rim**	**65**	**58**	**0.8688**	**3.6206**	**0.0551**	**0.0986**	**0.0015**	**1598**	**28**	**98**
41	Spot 38	Sq	Core	289	520	1.7857	3.7936	0.0432	0.0988	0.0012	1602	23	94
42	Spot 39	Sq	Core	235	67	0.2768	3.6536	0.0481	0.1021	0.0016	1663	29	94
42	Spot 40	Rec	Rim	487	109	0.2239	3.8971	0.0608	0.0987	0.0008	1600	16	92

43	Spot 41	Sq	Core	220	297	1.3298	3.8655	0.0359	0.0979	0.0011	1585	21	94
44	**Spot 42**	**Sq**	**Core**	**179**	**104**	**0.5774**	**3.9308**	**0.0525**	**0.0926**	**0.0014**	**1480**	**29**	**99**
45	Spot 43	Sq	Core	293	451	1.4934	3.7779	0.0385	0.0992	0.0010	1609	19	94
45	Spot 44	Rec	Rim	130	41	0.3008	5.2165	0.0735	0.0976	0.0013	1579	25	72
46	Spot 45	Sq	Core	572	531	0.9050	6.0314	0.2656	0.0984	0.0012	1594	23	62
47	**Spot 46**	**Sq**	**Core**	**562**	**600**	**1.0893**	**3.6496**	**0.0400**	**0.1000**	**0.0011**	**1624**	**20**	**96**
47	Spot 47	Rec	Rim	330	22	0.0629	4.8709	0.1613	0.0983	0.0013	1592	25	76
48	Spot 48	Sq	Core	587	187	0.3378	4.0437	0.0965	0.0985	0.0012	1596	23	89
48	**Spot 49**	**Rec**	**Rim**	**185**	**65**	**0.3621**	**3.6166**	**0.0471**	**0.0985**	**0.0012**	**1596**	**23**	**99**
49	**Spot 50**	**Sq**	**Core**	**238**	**242**	**0.9208**	**3.8655**	**0.0478**	**0.0966**	**0.0010**	**1558**	**19**	**95**
50	Spot 52	Sq	Core	312	179	0.5938	5.2301	0.1422	0.0994	0.0012	1613	22	70
50	Spot 53	Rec	Rim	612	78	0.0877	7.2993	0.6926	0.0988	0.0014	1602	26	52
51	**Spot 54**	**Sq**	**Core**	**168**	**208**	**1.2255**	**3.6324**	**0.0396**	**0.0974**	**0.0012**	**1575**	**23**	**100**
51	**Spot 55**	**Rec**	**Rim**	**328**	**51**	**0.1621**	**3.7425**	**0.0574**	**0.0959**	**0.0012**	**1546**	**24**	**99**
52	**Spot 56**	**Sq**	**Core**	**362**	**444**	**1.2658**	**3.7051**	**0.0357**	**0.0975**	**0.0008**	**1577**	**16**	**98**
53	**Spot 57**	**Sq**	**Core**	**255**	**269**	**1.0811**	**3.6350**	**0.0489**	**0.0980**	**0.0015**	**1586**	**29**	**99**
54	**Spot 58**	**Sq**	**Core**	**313**	**380**	**1.2034**	**3.8139**	**0.0495**	**0.0979**	**0.0012**	**1585**	**23**	**95**
55	**Spot 59**	**Rec**	**Core**	**136**	**73**	**0.5155**	**3.8521**	**0.0638**	**0.0955**	**0.0016**	**1538**	**32**	**97**
55	Spot 60	Sq	Rim	92	65	0.7358	4.7148	0.0978	0.0948	0.0016	1524	32	81
56	**Spot 61**	**Sq**	**Core**	**701**	**904**	**1.3106**	**3.5137**	**0.0778**	**0.0980**	**0.0014**	**1586**	**27**	**102**
57	Spot 62	Sq	Core	68	63	0.9268	4.1684	0.0521	0.0949	0.0016	1526	32	91
57	Spot 63	Sq	Core	403	146	0.3636	4.2337	0.0358	0.0933	0.0009	1494	18	92
58	**Spot 64**	**Sq**	**Core**	**245**	**360**	**1.4327**	**3.8124**	**0.0320**	**0.0979**	**0.0009**	**1585**	**18**	**95**
58	Spot 65	Rec	Rim	113	17	0.1522	3.9339	0.0805	0.0975	0.0016	1577	31	93
60	**Spot 66**	**Sq**	**Core**	**391**	**282**	**0.7225**	**3.5537**	**0.1048**	**0.0963**	**0.0026**	**1554**	**51**	**103**
62	**Spot 67**	**Sq**	**Core**	**135**	**136**	**0.8576**	**3.5765**	**0.0435**	**0.0967**	**0.0010**	**1561**	**19**	**102**
63	Spot 68	Sq	Core	645	360	0.5464	4.2863	0.1121	0.0978	0.0012	1583	23	85
64	**Spot 69**	**Sq**	**Core**	**478**	**184**	**0.3931**	**3.7608**	**0.0891**	**0.0962**	**0.0022**	**1552**	**43**	**98**
65	**Spot 70**	**Sq**	**Core**	**418**	**487**	**1.1710**	**3.7189**	**0.1259**	**0.0977**	**0.0023**	**1581**	**44**	**97**
66	Spot 71	Sq	Core	212	244	1.1682	3.9200	0.0415	0.0964	0.0009	1556	18	94
67	**Spot 72**	**Sq**	**Core**	**102**	**93**	**0.9470**	**3.7369**	**0.0559**	**0.0954**	**0.0013**	**1536**	**26**	**100**
67	Spot 73	Sq	Rim	92	0.97	0.0094	6.7659	0.1877	0.0729	0.0031	1011	86	88
68	**Spot 74**	**Sq**	**Core**	**208**	**214**	**1.0684**	**3.6088**	**0.0873**	**0.0966**	**0.0011**	**1559**	**21**	**101**
68	**Spot 75**	**Rec**	**Rim**	**57**	**0.24**	**0.0029**	**5.9701**	**0.1141**	**0.0740**	**0.0020**	**1041**	**55**	**96**
73	Spot 76	Sq	Rim	43	7	0.1385	8.0775	0.3328	0.1007	0.0059	1637	109	46
74	**Spot 77**	**Sq**	**Core**	**417**	**537**	**1.3038**	**3.6430**	**0.0956**	**0.0976**	**0.0015**	**1579**	**29**	**99**
76	**Spot 78**	**Sq**	**Core**	**423**	**634**	**1.3624**	**3.5575**	**0.0823**	**0.0984**	**0.0017**	**1594**	**32**	**100**
76	Spot 79	Sq	Rim	144	23	0.1605	4.6729	0.2620	0.0969	0.0021	1565	41	80
78	**Spot 80**	**Sq**	**Core**	**234**	**155**	**0.6293**	**3.7636**	**0.0623**	**0.0983**	**0.0011**	**1592**	**21**	**95**
78	**Spot 81**	**Rec**	**Rim**	**103**	**10**	**0.0709**	**3.4722**	**0.1326**	**0.0960**	**0.0023**	**1548**	**45**	**105**
82	Spot 82	Sq	Core	303	387	1.2987	4.2608	0.0890	0.0944	0.0014	1516	28	90
82	Spot 83	Sq	Rim	46	0.53	0.0085	9.3197	0.3127	0.1060	0.0041	1732	71	38
89	**Spot 84**	**Sq**	**Core**	**413**	**608**	**1.4841**	**3.5039**	**0.0994**	**0.0992**	**0.0017**	**1609**	**32**	**101**
89	**Spot 85**	**Sq**	**Rim**	**321**	**470**	**1.4948**	**3.5727**	**0.0945**	**0.0986**	**0.0016**	**1598**	**30**	**100**

MISE1816c leucosome

2	**Spot 31**	**Sq**	**Core**	**1499**	**754**	**0.4953**	**3.5174**	**0.0470**	**0.0987**	**0.0009**	**1600**	**17**	**101**
2	**Spot 32**	**Rec**	**Rim**	**522**	**274**	**0.5038**	**3.5162**	**0.0532**	**0.0997**	**0.0007**	**1619**	**14**	**100**
5	Spot 33	Sq	Core	2293	1069	0.4132	5.9067	0.1814	0.0893	0.0010	1411	21	71
5	**Spot 34**	**Rec**	**Rim**	**1072**	**169**	**0.1658**	**3.6153**	**0.0706**	**0.0964**	**0.0006**	**1556**	**12**	**101**
8	**Spot 35**	**Sq**	**Core**	**1225**	**607**	**0.4845**	**3.5499**	**0.0391**	**0.0984**	**0.0008**	**1593**	**15**	**100**
7	Spot 36	Sq	Core	2490	7040	2.1930	4.2105	0.1099	0.0933	0.0013	1494	26	92
7	**Spot 37**	**Sq**	**Rim**	**1770**	**510**	**0.2881**	**3.4602**	**0.0443**	**0.0983**	**0.0008**	**1592**	**15**	**103**
10	**Spot 38**	**Rec**	**Core**	**1491**	**1400**	**0.9328**	**3.5411**	**0.0439**	**0.0979**	**0.0010**	**1584**	**18**	**101**
10	**Spot 39**	**Rec**	**Rim**	**1016**	**492**	**0.4766**	**3.5587**	**0.0532**	**0.0984**	**0.0008**	**1594**	**14**	**100**
9	**Spot 40**	**Sq**	**Core**	**1540**	**1435**	**0.9390**	**3.3841**	**0.0389**	**0.0985**	**0.0008**	**1597**	**14**	**105**
12	**Spot 41**	**Sq**	**Core**	**1089**	**864**	**0.7918**	**3.4734**	**0.0374**	**0.0994**	**0.0009**	**1612**	**16**	**101**
11	**Spot 42**	**Sq**	**Core**	**1585**	**1528**	**0.9692**	**3.4211**	**0.0339**	**0.0981**	**0.0007**	**1588**	**14**	**104**
14	**Spot 43**	**Sq**	**Core**	**1844**	**1112**	**0.5999**	**3.4868**	**0.0426**	**0.0990**	**0.0010**	**1606**	**18**	**101**
13	**Spot 44**	**Sq**	**Core**	**1497**	**1148**	**0.7610**	**3.5398**	**0.0388**	**0.0987**	**0.0009**	**1600**	**17**	**100**
13	**Spot 45**	**Rec**	**Rim**	**765**	**446**	**0.5615**	**3.5298**	**0.0274**	**0.0988**	**0.0007**	**1602**	**13**	**100**
16	**Spot 46**	**Sq**	**Core**	**3700**	**683**	**0.1789**	**3.6140**	**0.0718**	**0.0978**	**0.0010**	**1583**	**19**	**100**
19	**Spot 47**	**Sq**	**Core**	**876**	**484**	**0.5333**	**3.5855**	**0.0347**	**0.0976**	**0.0007**	**1579**	**14**	**100**
20	**Spot 48**	**Sq**	**Core**	**1228**	**889**	**0.7215**	**3.4130**	**0.0373**	**0.0981**	**0.0007**	**1589**	**14**	**104**
21	**Spot 49**	**Sq**	**Core**	**1588**	**1002**	**0.6435**	**3.5323**	**0.0499**	**0.0989**	**0.0008**	**1604**	**15**	**100**
24	**Spot 50**	**Sq**	**Core**	**641**	**492**	**0.7485**	**3.5894**	**0.0606**	**0.0985**	**0.0012**	**1596**	**23**	**99**
23	**Spot 51**	**Sq**	**Core**	**1805**	**1026**	**0.5817**	**3.5286**	**0.0473**	**0.0990**	**0.0007**	**1605**	**13**	**100**
26	**Spot 52**	**Rec**	**Core**	**1239**	**806**	**0.6770**	**3.5336**	**0.0350**	**0.0987**	**0.0007**	**1600**	**14**	**100**
26	**Spot 53**	**Sq**	**Rim**	**581**	**238**	**0.4132**	**3.3944**	**0.0300**	**0.0979**	**0.0007**	**1585**	**13**	**105**
25	Spot 54	Sq	Core	2180	328	0.1499	5.2356	0.1480	0.0886	0.0010	1395	21	81
28	**Spot 55**	**Sq**	**Core**	**3050**	**1295**	**0.4257**	**3.5524**	**0.0946**	**0.0996**	**0.0018**	**1617**	**34**	**99**
27	**Spot 56**	**Sq**	**Core**	**1215**	**620**	**0.5171**	**3.5663**	**0.0687**	**0.0995**	**0.0015**	**1615**	**28**	**99**
27	**Spot 57**	**Rec**	**Rim**	**654**	**351**	**0.5260**	**3.5829**	**0.0398**	**0.0975**	**0.0008**	**1576**	**15**	**101**
30	**Spot 58**	**Sq**	**Core**	**786**	**475**	**0.6165**	**3.5361**	**0.0325**	**0.0988**	**0.0007**	**1602**	**14**	**100**
32	Spot 59	Sq	Core	3790	901	0.2353	4.3706	0.1356	0.0946	0.0008	1519	16	87
32	**Spot 60**	**Sq**	**Core**	**709**	**332**	**0.4941**	**3.5907**	**0.0374**	**0.0983**	**0.0007**	**1591**	**13**	**100**
32	**Spot 61**	**Rec**	**Rim**	**1385**	**64**	**0.0469**	**6.0643**	**0.1655**	**0.0724**	**0.0016**	**997**	**45**	**99**
31	**Spot 62**	**Sq**	**Core**	**1697**	**942**	**0.5219**	**3.5765**	**0.0499**	**0.0985**	**0.0007**	**1596**	**13**	**100**
36	**Spot 63**	**Sq**	**Core**	**1031**	**572**	**0.5528**	**3.5051**	**0.0270**	**0.0992**	**0.0006**	**1609**	**11**	**101**
36	**Spot 64**	**Rec**	**Rim**	**854**	**414**	**0.4562**	**3.5549**	**0.0354**	**0.0985**	**0.0009**	**1596**	**17**	**100**
39	**Spot 65**	**Sq**	**Core**	**698**	**482**	**0.6406**	**3.5199**	**0.0273**	**0.0989**	**0.0007**	**1604**	**13**	**100**
38	**Spot 66**	**Sq**	**Core**	**3030**	**1960**	**0.6640**	**3.5286**	**0.0647**	**0.0984**	**0.0009**	**1595**	**18**	**101**
40	**Spot 67**	**Sq**	**Core**	**987**	**685**	**0.6998**	**3.5162**	**0.0371**	**0.0991**	**0.0010**	**1607**	**19**	**100**
41	**Spot 68**	**Sq**	**Core**	**895**	**567**	**0.6365**	**3.5014**	**0.0306**	**0.0991**	**0.0008**	**1607**	**14**	**101**
42	**Spot 69**	**Sq**	**Core**	**412**	**228**	**0.5379**	**3.4200**	**0.0386**	**0.1006**	**0.0011**	**1635**	**20**	**101**
44	**Spot 70**	**Sq**	**Core**	**2620**	**1320**	**0.4737**	**3.6101**	**0.0508**	**0.0978**	**0.0011**	**1583**	**21**	**100**
44	**Spot 71**	**Sq**	**Rim**	**950**	**188**	**0.1838**	**3.4941**	**0.0293**	**0.0997**	**0.0006**	**1618**	**12**	**100**
45	**Spot 72**	**Sq**	**Core**	**533**	**236**	**0.3003**	**3.4650**	**0.0348**	**0.1004**	**0.0012**	**1632**	**22**	**100**
45	**Spot 73**	**Rec**	**Rim**	**670**	**485**	**0.7184**	**3.4795**	**0.0412**	**0.0996**	**0.0010**	**1617**	**18**	**101**

46	**Spot 74**	**Sq**	**Core**	**759**	**447**	**0.5952**	**3.5063**	**0.0332**	**0.0989**	**0.0008**	**1604**	**14**	**101**
49	**Spot 75**	**Sq**	**Core**	**715**	**427**	**0.5970**	**3.5842**	**0.0270**	**0.0984**	**0.0007**	**1593**	**13**	**100**
48	**Spot 76**	**Rec**	**Core**	**3420**	**685**	**0.1969**	**3.5740**	**0.0741**	**0.0980**	**0.0007**	**1586**	**14**	**100**
48	**Spot 77**	**Rec**	**Rim**	**841**	**9**	**0.0108**	**5.6593**	**0.0480**	**0.0741**	**0.0006**	**1043**	**17**	**101**
51	**Spot 78**	**Sq**	**Core**	**939**	**349**	**0.3413**	**3.2982**	**0.0457**	**0.1006**	**0.0012**	**1635**	**22**	**104**
50	**Spot 79**	**Sq**	**Core**	**759**	**408**	**0.5714**	**3.5448**	**0.0302**	**0.0988**	**0.0008**	**1602**	**15**	**100**
50	**Spot 80**	**Sq**	**Rim**	**1079**	**267**	**0.2653**	**3.4880**	**0.0304**	**0.0996**	**0.0008**	**1617**	**15**	**101**
52	**Spot 81**	**Sq**	**Core**	**903**	**583**	**0.6868**	**3.4928**	**0.0317**	**0.0991**	**0.0009**	**1607**	**17**	**101**
54	**Spot 82**	**Sq**	**Core**	**1076**	**446**	**0.4369**	**3.4783**	**0.0557**	**0.0999**	**0.0013**	**1622**	**24**	**100**
57	**Spot 83**	**Sq**	**Core**	**720**	**329**	**0.5051**	**3.4746**	**0.0471**	**0.1001**	**0.0010**	**1626**	**19**	**100**
58	Spot 84	Sq	Core	1208	144	0.1212	5.4885	0.1175	0.0926	0.0014	1480	29	73
59	**Spot 85**	**Sq**	**Core**	**810**	**505**	**0.6053**	**3.6127**	**0.0313**	**0.0981**	**0.0008**	**1589**	**16**	**99**
61	**Spot 86**	**Sq**	**Core**	**872**	**544**	**0.5928**	**3.4892**	**0.0414**	**0.1005**	**0.0010**	**1633**	**18**	**99**
60	Spot 87	Sq	Core	1113	217	0.1692	4.5517	0.1388	0.0891	0.0019	1406	41	91
66	Spot 88	Sq	Core	985	783	0.7348	3.3212	0.0397	0.0989	0.0010	1604	18	106
67	**Spot 89**	**Sq**	**Core**	**1475**	**841**	**0.5325**	**3.6245**	**0.0946**	**0.0987**	**0.0015**	**1600**	**28**	**98**
68	Spot 90	Sq	Core	4140	912	0.1361	3.3058	0.0514	0.0964	0.0011	1556	21	110
68	**Spot 91**	**Sq**	**Rim**	**3980**	**606**	**0.1066**	**3.4662**	**0.0709**	**0.0976**	**0.0015**	**1579**	**29**	**104**
70	**Spot 92**	**Sq**	**Core**	**12000**	**11030**	**1.0881**	**3.5727**	**0.0549**	**0.0983**	**0.0013**	**1592**	**25**	**100**
MISE1816c melanosome													
2	**Spot 31**	**Sq**	**Core**	**348**	**372**	**1.0989**	**3.4060**	**0.0568**	**0.0999**	**0.0015**	**1622**	**28**	**102**
1	**Spot 32**	**Sq**	**Core**	**428**	**372**	**0.8834**	**3.6337**	**0.0396**	**0.0981**	**0.0009**	**1588**	**17**	**99**
3	**Spot 33**	**Sq**	**Core**	**875**	**251**	**0.2899**	**3.4904**	**0.0439**	**0.0984**	**0.0010**	**1594**	**19**	**102**
3	**Spot 34**	**Rec**	**Rim**	**217**	**133**	**0.6831**	**3.3512**	**0.0416**	**0.0994**	**0.0010**	**1613**	**19**	**104**
4	**Spot 35**	**Sq**	**Core**	**215**	**260**	**1.2320**	**3.7244**	**0.0319**	**0.0989**	**0.0010**	**1603**	**18**	**96**
5	**Spot 36**	**Sq**	**Core**	**196**	**197**	**0.9718**	**3.7779**	**0.0343**	**0.0973**	**0.0009**	**1573**	**17**	**96**
9	**Spot 37**	**Sq**	**Core**	**635**	**356**	**0.5291**	**3.6377**	**0.0423**	**0.0985**	**0.0009**	**1596**	**17**	**98**
9	**Spot 38**	**Rec**	**Rim**	**187**	**63**	**0.3372**	**3.3693**	**0.0636**	**0.0994**	**0.0012**	**1613**	**22**	**104**
7	**Spot 39**	**Sq**	**Core**	**192**	**221**	**1.1198**	**3.6697**	**0.0391**	**0.0990**	**0.0011**	**1605**	**21**	**97**
7	Spot 40	Sq	Rim	355	152	0.4401	6.4851	0.0757	0.0993	0.0009	1611	16	57
14	**Spot 41**	**Rec**	**Core**	**247**	**127**	**0.5653**	**3.5436**	**0.0389**	**0.0988**	**0.0010**	**1602**	**19**	**100**
14	Spot 42	Rec	Rim	126	70	0.5637	3.2185	0.0622	0.0995	0.0016	1615	30	108
13	Spot 43	Rec	Core	227	234	0.9662	3.9463	0.0389	0.0963	0.0009	1553	18	94
13	**Spot 44**	**Rec**	**Rim**	**223**	**176**	**0.8078**	**3.6550**	**0.0441**	**0.1000**	**0.0011**	**1624**	**20**	**96**
17	Spot 45	Rec	Core	196	133	0.6748	5.6786	0.1193	0.0975	0.0017	1577	33	66
17	Spot 46	Rec	Rim	126	72	0.5672	5.1975	0.1567	0.0969	0.0025	1565	48	72
19	**Spot 47**	**Sq**	**Core**	**263**	**347**	**1.3278**	**3.6670**	**0.0484**	**0.0978**	**0.0012**	**1583**	**23**	**98**
19	**Spot 48**	**Sq**	**Rim**	**241**	**89**	**0.3727**	**3.6324**	**0.0449**	**0.0986**	**0.0013**	**1598**	**25**	**98**
20	**Spot 49**	**Sq**	**Core**	**331**	**339**	**1.0320**	**3.5298**	**0.0847**	**0.0993**	**0.0019**	**1611**	**36**	**100**
20	**Spot 50**	**Rec**	**Rim**	**242**	**257**	**1.0373**	**3.7397**	**0.0378**	**0.0955**	**0.0009**	**1538**	**17**	**99**
22	**Spot 51**	**Sq**	**Core**	**352**	**259**	**0.7077**	**3.5753**	**0.0524**	**0.0981**	**0.0008**	**1587**	**16**	**100**
21	**Spot 52**	**Sq**	**Core**	**390**	**381**	**0.9990**	**3.5575**	**0.0481**	**0.0989**	**0.0010**	**1604**	**18**	**100**
24	**Spot 53**	**Sq**	**Core**	**278**	**295**	**0.9980**	**3.5348**	**0.0462**	**0.0982**	**0.0010**	**1591**	**18**	**101**
23	**Spot 54**	**Sq**	**Core**	**260**	**266**	**1.0163**	**3.6417**	**0.0517**	**0.0976**	**0.0012**	**1579**	**23**	**99**

28	**Spot 55**	**Sq**	**Core**	**1153**	**465**	**0.3981**	**3.4095**	**0.0744**	**0.0995**	**0.0018**	**1615**	**34**	**103**
30	**Spot 56**	**Sq**	**Core**	**588**	**206**	**0.3488**	**3.4072**	**0.0488**	**0.0990**	**0.0009**	**1605**	**16**	**103**
33	**Spot 57**	**Sq**	**Core**	**342**	**155**	**0.4525**	**3.4892**	**0.0536**	**0.0983**	**0.0010**	**1593**	**18**	**102**
34	**Spot 58**	**Sq**	**Core**	**215**	**239**	**1.1001**	**3.4831**	**0.0461**	**0.0995**	**0.0011**	**1615**	**21**	**101**
37	**Spot 59**	**Sq**	**Core**	**599**	**168**	**0.2759**	**3.6657**	**0.0390**	**0.0985**	**0.0009**	**1597**	**18**	**97**
37	**Spot 60**	**Sq**	**Rim**	**291**	**101**	**0.3377**	**3.7078**	**0.0440**	**0.0997**	**0.0010**	**1618**	**18**	**95**
36	Spot 61	Sq	Core	194	173	0.8889	4.3309	4.3309	4.3309	0.0012	1520	24	88
36	**Spot 62**	**Sq**	**Rim**	**289**	**347**	**1.0406**	**3.6819**	**0.0664**	**0.0954**	**0.0010**	**1536**	**20**	**101**
39	**Spot 63**	**Sq**	**Core**	**579**	**172**	**0.2964**	**3.6390**	**0.0596**	**0.0972**	**0.0012**	**1571**	**23**	**100**
39	**Spot 64**	**Rec**	**Rim**	**368**	**101**	**0.2614**	**3.3990**	**0.0381**	**0.1002**	**0.0011**	**1628**	**20**	**102**
42	**Spot 65**	**Sq**	**Core**	**485**	**295**	**0.6161**	**3.6670**	**0.0605**	**0.0980**	**0.0014**	**1586**	**27**	**98**
42	**Spot 66**	**Sq**	**Rim**	**271**	**81**	**0.2982**	**3.5511**	**0.0593**	**0.0970**	**0.0010**	**1567**	**19**	**102**
44	**Spot 67**	**Sq**	**Core**	**294**	**348**	**1.1655**	**3.5273**	**0.0622**	**0.1011**	**0.0016**	**1644**	**29**	**98**
46	Spot 68	Sq	Core	226	171	0.7273	3.9324	0.0711	0.1005	0.0018	1633	33	89
46	**Spot 69**	**Rec**	**Rim**	**153**	**47**	**0.3027**	**3.4916**	**0.0402**	**0.0986**	**0.0013**	**1598**	**25**	**102**
45	**Spot 70**	**Sq**	**Core**	**245**	**109**	**0.5160**	**3.5361**	**0.0388**	**0.0985**	**0.0013**	**1596**	**25**	**101**
45	**Spot 71**	**Rec**	**Rim**	**274**	**125**	**0.4476**	**3.3333**	**0.0467**	**0.0997**	**0.0010**	**1618**	**18**	**105**
48	**Spot 72**	**Sq**	**Core**	**213**	**272**	**1.1933**	**3.5932**	**0.0465**	**0.1001**	**0.0013**	**1626**	**24**	**97**
48	**Spot 73**	**Rec**	**Rim**	**445**	**222**	**0.4912**	**3.7147**	**0.0414**	**0.1000**	**0.0010**	**1623**	**18**	**95**
49	**Spot 74**	**Sq**	**Core**	**193**	**201**	**1.0225**	**3.6166**	**0.0366**	**0.0997**	**0.0012**	**1618**	**22**	**97**
47	Spot 75	Sq	Core	587	1350	1.9608	3.7793	0.0743	0.0990	0.0012	1605	23	94
47	Spot 76	Rec	Rim	41	0.42	0.0081	5.6883	0.0841	0.0887	0.0030	1398	65	75
51	**Spot 77**	**Sq**	**Core**	**141**	**140**	**0.9747**	**3.7106**	**0.0413**	**0.1000**	**0.0012**	**1624**	**22**	**95**
51	Spot 78	Rec	Rim	108	26	0.2305	3.9510	0.0437	0.0961	0.0017	1550	33	94
53	**Spot 79**	**Rec**	**Core**	**356**	**404**	**1.1001**	**3.7175**	**0.1258**	**0.0973**	**0.0025**	**1573**	**48**	**98**
53	**Spot 80**	**Sq**	**Rim**	**476**	**128**	**0.2451**	**3.6510**	**0.0706**	**0.0978**	**0.0015**	**1583**	**29**	**99**
52	**Spot 81**	**Rec**	**Core**	**316**	**384**	**1.1534**	**3.6928**	**0.1159**	**0.0975**	**0.0025**	**1577**	**48**	**98**
55	**Spot 82**	**Sq**	**Core**	**189**	**230**	**1.1507**	**3.7523**	**0.0507**	**0.0980**	**0.0014**	**1586**	**27**	**96**
55	**Spot 83**	**Rec**	**Rim**	**210**	**73**	**0.3318**	**3.6778**	**0.0636**	**0.0957**	**0.0015**	**1542**	**29**	**101**
54	**Spot 84**	**Rec**	**Core**	**108**	**93**	**0.8110**	**3.5186**	**0.0483**	**0.1001**	**0.0015**	**1626**	**28**	**99**
56	**Spot 85**	**Sq**	**Core**	**266**	**202**	**0.7072**	**3.5625**	**0.0558**	**0.0987**	**0.0013**	**1600**	**25**	**100**
59	**Spot 86**	**Sq**	**Core**	**197**	**183**	**0.8913**	**3.3613**	**0.0429**	**0.1009**	**0.0013**	**1641**	**24**	**102**
60	**Spot 87**	**Sq**	**Core**	**508**	**664**	**1.2484**	**3.3102**	**0.0581**	**0.0996**	**0.0014**	**1617**	**26**	**105**
58	**Spot 88**	**Sq**	**Core**	**185**	**185**	**0.9615**	**3.5039**	**0.0393**	**0.0989**	**0.0012**	**1603**	**23**	**101**
62	**Spot 89**	**Sq**	**Core**	**219**	**250**	**1.0672**	**3.6510**	**0.0760**	**0.0967**	**0.0019**	**1561**	**37**	**100**
62	**Spot 90**	**Rec**	**Rim**	**107**	**88**	**0.7924**	**3.6166**	**0.0589**	**0.0971**	**0.0016**	**1569**	**31**	**100**
61	**Spot 91**	**Sq**	**Core**	**367**	**278**	**0.7752**	**3.5186**	**0.0371**	**0.0985**	**0.0011**	**1596**	**21**	**101**
63	**Spot 92**	**Rec**	**Core**	**183**	**258**	**1.3280**	**3.5051**	**0.0491**	**0.0986**	**0.0014**	**1598**	**27**	**101**
63	**Spot 93**	**Rec**	**Rim**	**125**	**102**	**0.7746**	**3.6778**	**0.1123**	**0.0976**	**0.0030**	**1579**	**58**	**98**
63	**Spot 94**	**Rec**	**Rim**	**101**	**79**	**0.7570**	**3.4037**	**0.0660**	**0.0996**	**0.0020**	**1617**	**37**	**103**
68	**Spot 95**	**Sq**	**Core**	**333**	**462**	**1.3298**	**3.4188**	**0.0468**	**0.0999**	**0.0012**	**1622**	**22**	**102**
68	**Spot 96**	**Rec**	**Rim**	**153**	**86**	**0.5280**	**3.4376**	**0.0756**	**0.0978**	**0.0021**	**1583**	**40**	**104**
67	**Spot 97**	**Sq**	**Core**	**151**	**182**	**1.0672**	**3.4928**	**0.0561**	**0.0986**	**0.0018**	**1598**	**34**	**102**
69	**Spot 98**	**Sq**	**Core**	**148**	**148**	**0.9355**	**3.5689**	**0.0420**	**0.0981**	**0.0012**	**1588**	**23**	**100**

73	**Spot 99**	**Sq**	**Core**	**83**	**76**	**0.8749**	**3.5817**	**0.0577**	**0.0993**	**0.0022**	**1611**	**41**	**99**
73	Spot 100	Sq	Rim	374	132	0.3461	4.1186	0.0577	0.0933	0.0013	1494	26	94
72	**Spot 101**	**Sq**	**Core**	**300**	**313**	**0.9606**	**3.4638**	**0.0576**	**0.1006**	**0.0017**	**1635**	**31**	**100**
75	**Spot 102**	**Sq**	**Core**	**195**	**212**	**1.0384**	**3.5261**	**0.0547**	**0.0979**	**0.0015**	**1585**	**29**	**102**
75	**Spot 103**	**Sq**	**Core**	**146**	**119**	**0.7862**	**3.4990**	**0.0502**	**0.0991**	**0.0018**	**1607**	**34**	**101**
74	**Spot 104**	**Sq**	**Core**	**175**	**50**	**0.2770**	**3.6536**	**0.0801**	**0.0953**	**0.0018**	**1534**	**36**	**102**
77	**Spot 105**	**Sq**	**Core**	**171**	**68**	**0.3925**	**3.4990**	**0.0477**	**0.0981**	**0.0014**	**1588**	**27**	**102**
77	**Spot 106**	**Sq**	**Rim**	**113**	**96**	**0.8368**	**3.5829**	**0.0591**	**0.0983**	**0.0018**	**1592**	**34**	**100**
77	**Spot 107**	**Rec**	**Rim**	**322**	**133**	**0.3986**	**3.4317**	**0.0683**	**0.0993**	**0.0018**	**1611**	**34**	**102**
80	**Spot 108**	**Sq**	**Core**	**229**	**87**	**0.3846**	**3.5398**	**0.0564**	**0.0991**	**0.0016**	**1607**	**30**	**100**
79	**Spot 109**	**Sq**	**Core**	**262**	**446**	**1.1737**	**3.5791**	**0.0807**	**0.0976**	**0.0018**	**1579**	**35**	**101**
79	Spot 110	Rec	Rim	134	46	0.3401	4.0161	0.0532	0.0975	0.0018	1577	35	91
78	**Spot 111**	**Sq**	**Core**	**270**	**323**	**1.0341**	**3.4258**	**0.0704**	**0.0984**	**0.0022**	**1594**	**42**	**104**
84	**Spot 112**	**Sq**	**Core**	**55**	**43**	**0.7800**	**3.7965**	**0.0692**	**0.0934**	**0.0022**	**1496**	**45**	**101**
83	**Spot 113**	**Sq**	**Core**	**215**	**193**	**0.8576**	**3.6298**	**0.0606**	**0.0985**	**0.0017**	**1596**	**32**	**98**
83	**Spot 114**	**Rec**	**Rim**	**63**	**52**	**0.7806**	**3.8008**	**0.0737**	**0.0951**	**0.0020**	**1530**	**40**	**98**
82	**Spot 115**	**Sq**	**Core**	**294**	**122**	**0.4153**	**3.7327**	**0.0711**	**0.0986**	**0.0016**	**1598**	**30**	**96**
82	**Spot 116**	**Rec**	**Rim**	**257**	**64**	**0.2088**	**3.7411**	**0.0462**	**0.0970**	**0.0014**	**1567**	**27**	**97**

Appendix V - Concordia diagrams and histograms of all analyses

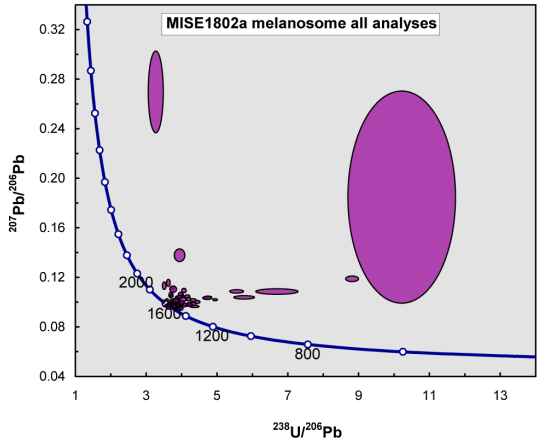

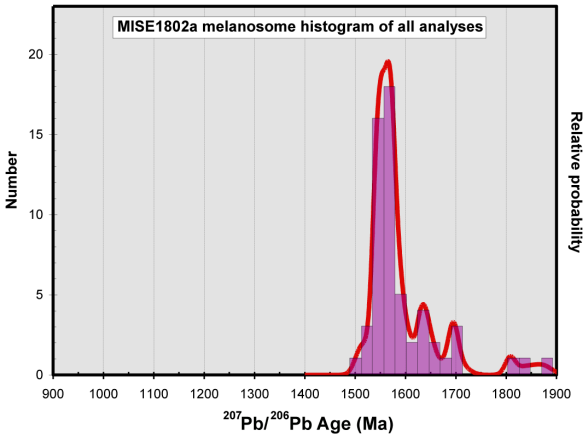

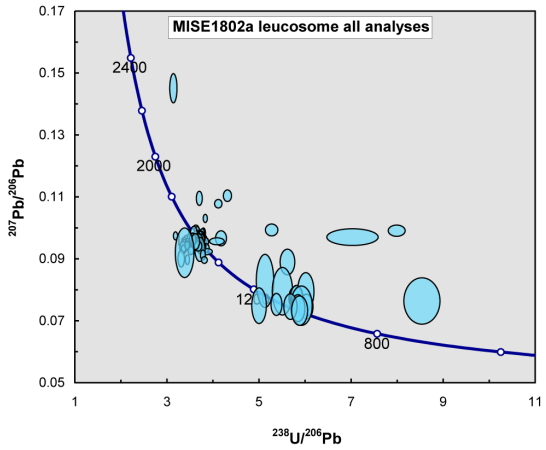

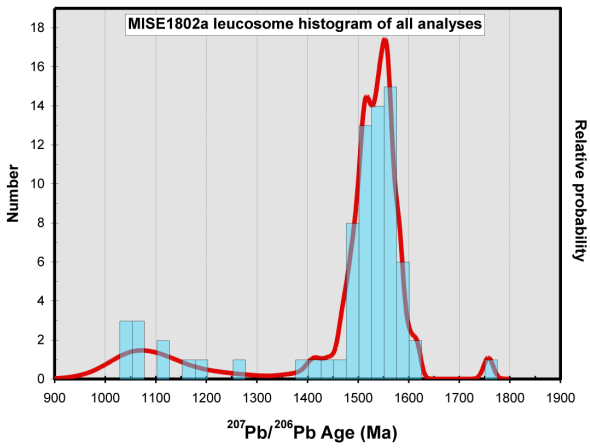

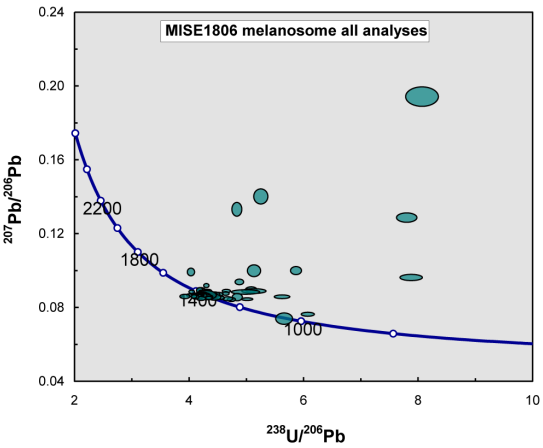

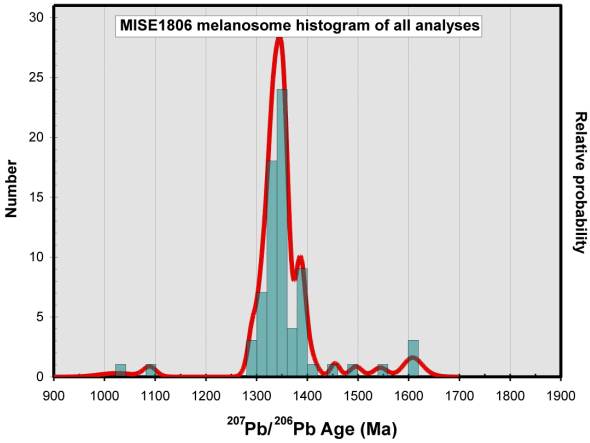

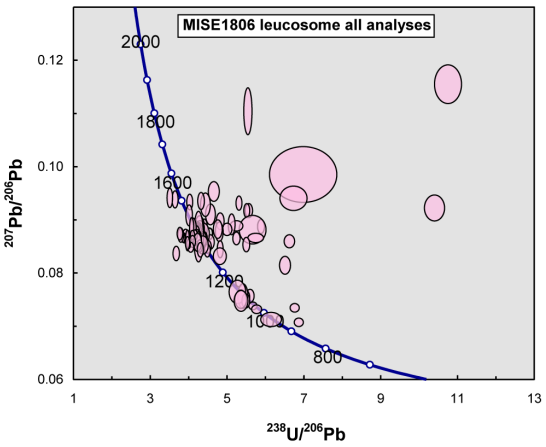

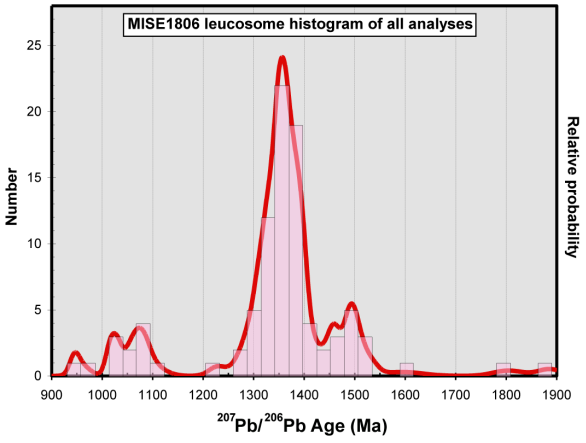

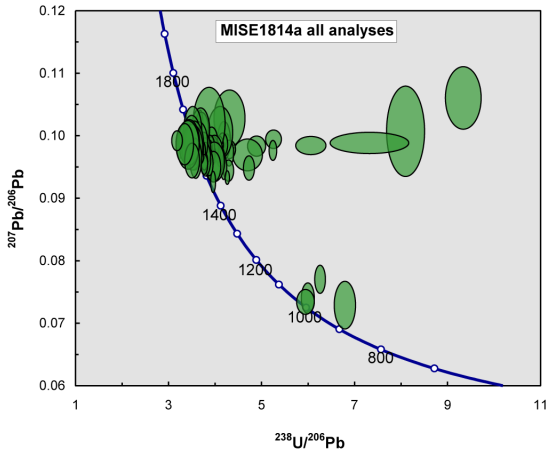
MISE1814a all analyses
1800
1400
1200
1000
800
0.12
0.11
0.10
0.09
0.08
0.07
0.06
1
3
5
7
9
11
207Pb/206Pb
238U/206Pb

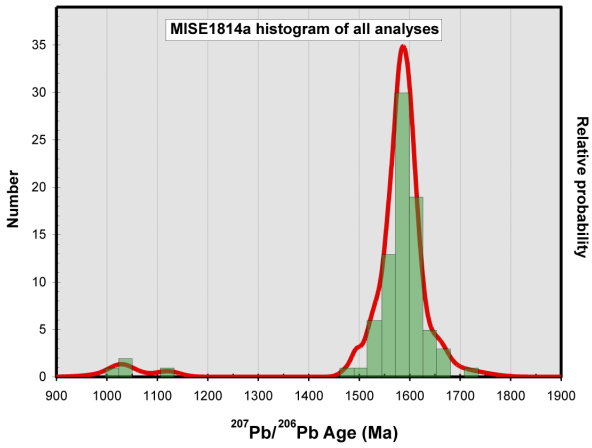
MISE1814a histogram of all analyses
Number
Relative probability
35
30
25
20
15
10
5
0
900
1000
1100
1200
1300
1400
1500
1600
1700
1800
1900
207Pb/206Pb Age (Ma)

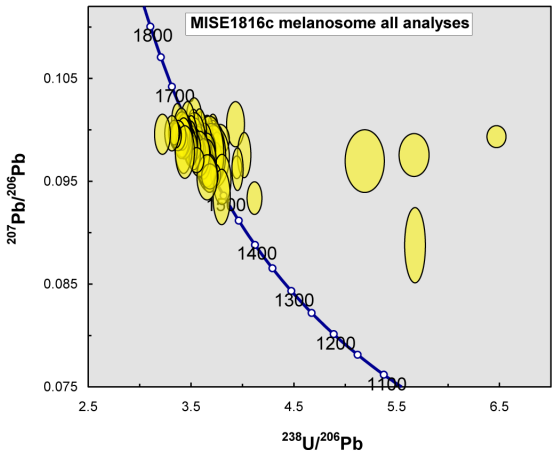
MISE1816c melanosome all analyses
1800
1700
1500
1400
1300
1200
1100
0.105
0.095
0.085
0.075
2.5
3.5
4.5
5.5
6.5
207Pb/206Pb
238U/206Pb

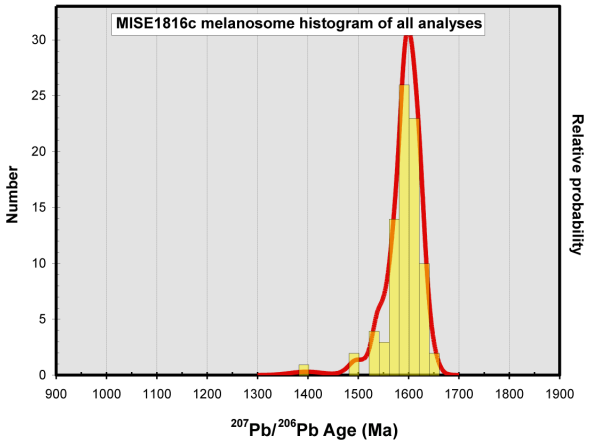
MISE1816c melanosome histogram of all analyses
Number
Relative probability
30
25
20
15
10
5
0
900
1000
1100
1200
1300
1400
1500
1600
1700
1800
1900
207Pb/206Pb Age (Ma)

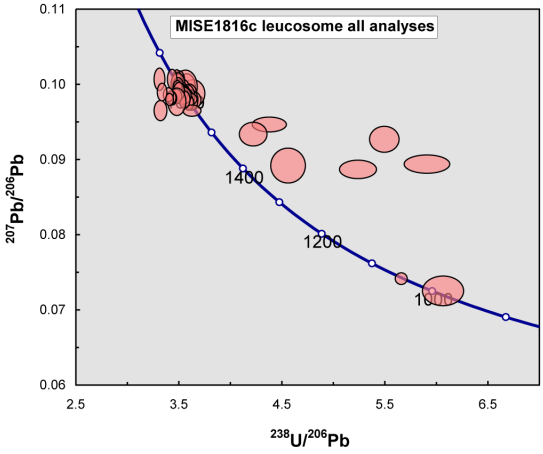
MISE1816c leucosome all analyses
1400
1200
1000
0.11
0.10
0.09
0.08
0.07
0.06
2.5
3.5
4.5
5.5
6.5
207Pb/206Pb
238U/206Pb

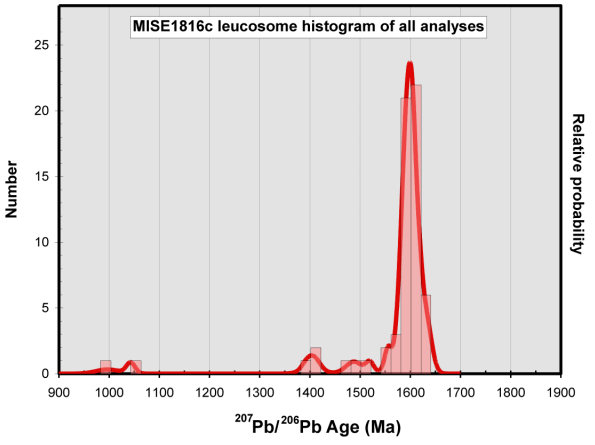
MISE1816c leucosome histogram of all analyses
Number
Relative probability
25
20
15
10
5
0
900
1000
1100
1200
1300
1400
1500
1600
1700
1800
1900
207Pb/206Pb Age (Ma)

Appendix VI - Th/U plots of all samples

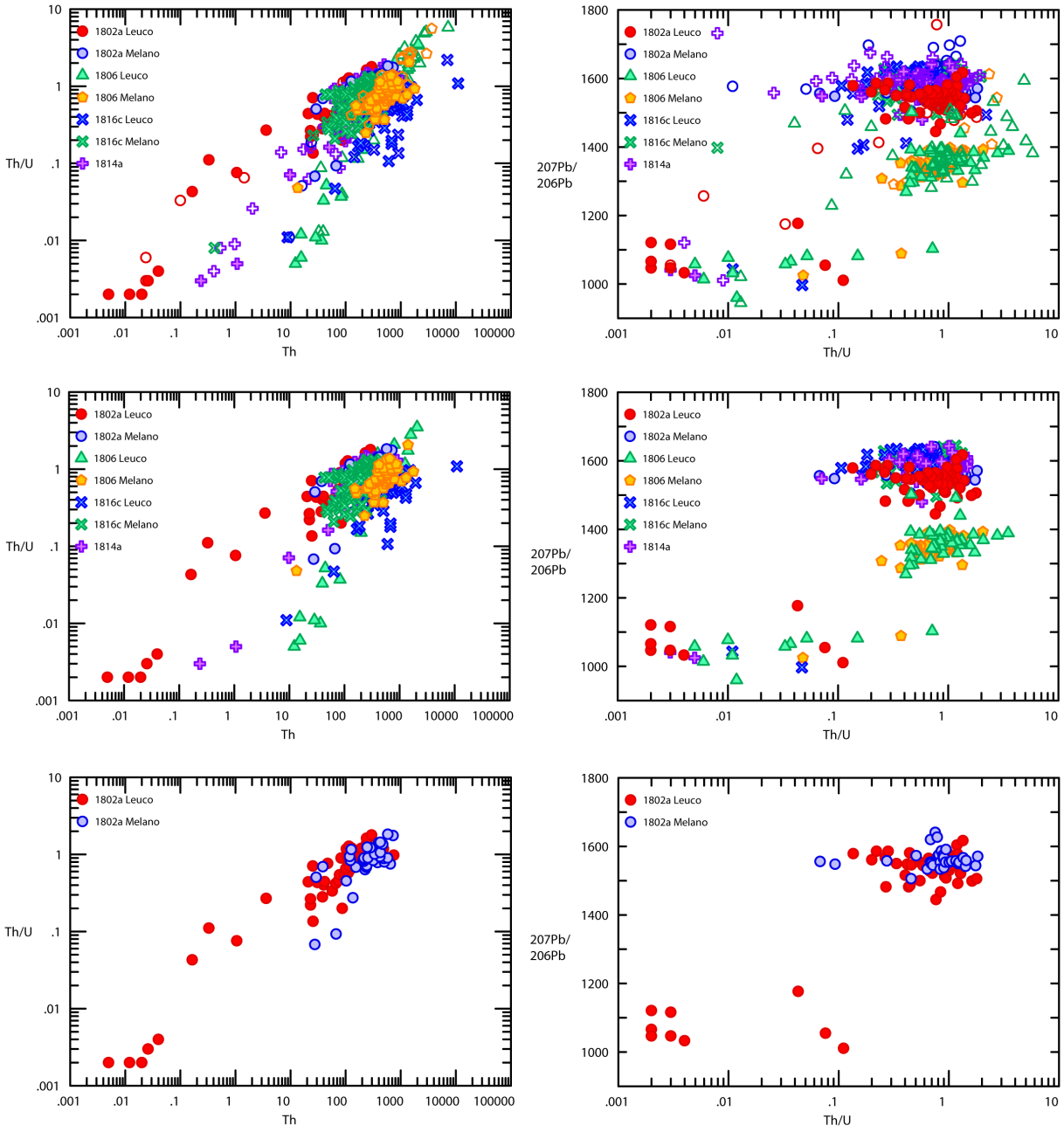

Fig. 1a. Igpet diagrams showing Th/U plotted against Th to the left and $^{207}Pb/^{206}Pb$ age (Ma) plotted against Th/U to the right. Filled symbols indicate concordant analyses (<5% discordance) used to calculate weighted average dates. Hollow symbols indicate discordant analyses (>5% discordance). Legend of samples is shown in the upper left corner of each diagram.

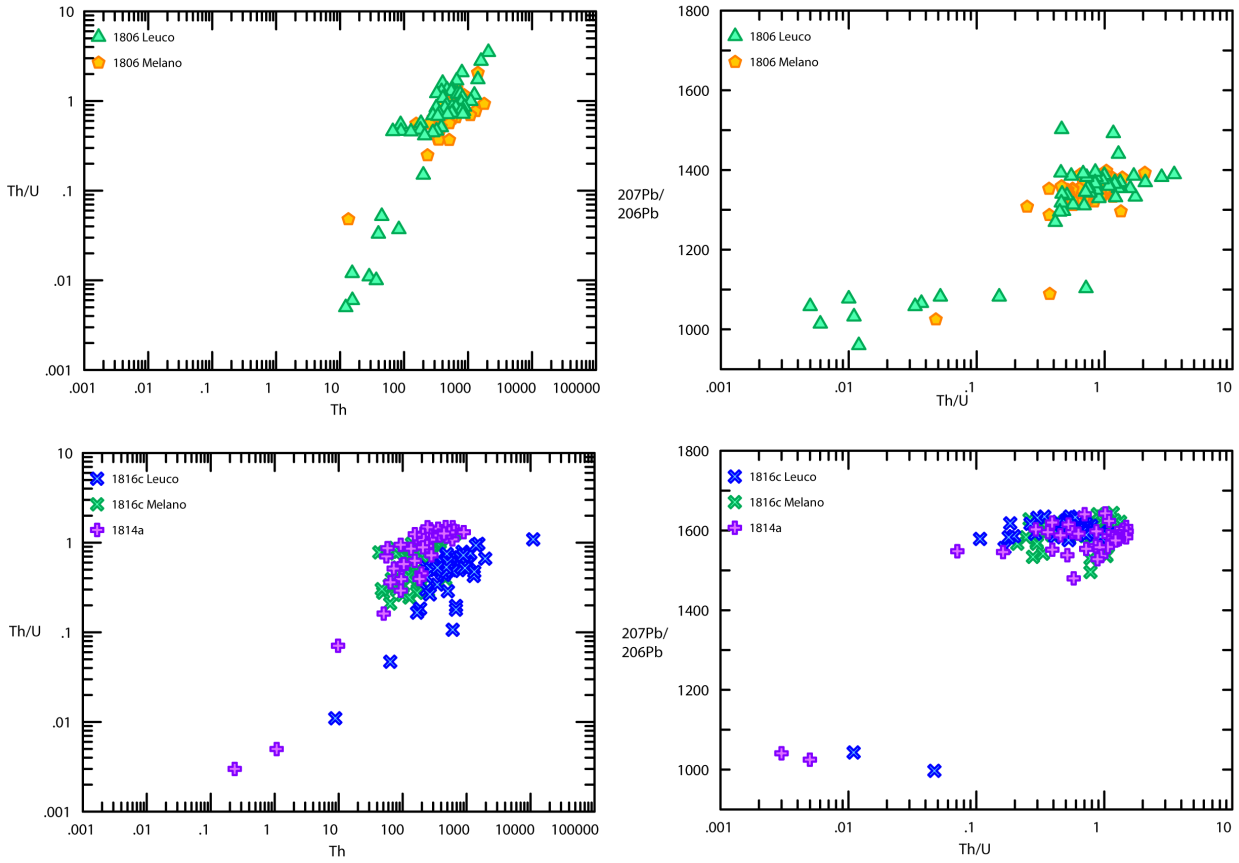

Fig. 1b. Igpet diagrams showing Th/U plotted against Th to the left and $^{207}Pb/^{206}Pb$ age (Ma) plotted against Th/U to the right. Filled symbols indicate concordant analyses (<5% discordance) used to calculate weighted average dates. Legend of samples is shown in the upper left corner of each diagram.

Tidigare skrifter i serien ”Examensarbeten i Geologi vid Lunds universitet”:

503. Sällström, Oskar, 2017: Tolkning av geofysiska mätningar i hammarborrhål på södra Gotland. (15 hp)
504. Ahrenstedt, Viktor, 2017: Depositional history of the Neoproterozoic Visingsö Group, south-central Sweden. (15 hp)
505. Schou, Dagmar Juul, 2017: Geometry and faulting history of the Long Spur fault zone, Castle Hill Basin, New Zealand. (15 hp)
506. Andersson, Setina, 2017: Skalbärande marina organismer och petrografi av tidigcampanska sediment i Kristianstadsbassängen – implikationer på paleomiljö. (15 hp)
507. Kempengren, Henrik, 2017: Föroreningsspridning från kustnära deponi: Applicering av Landsim 2.5 för modellering av lakvattentransport till Östersjön. (15 hp)
508. Ekborg, Charlotte, 2017: En studie på samband mellan jordmekaniska egenskaper och hydrodynamiska processer när erosion påverkar släntstabiliteten vid ökad nederbörd. (15 hp)
509. Silvén, Björn, 2017: LiDARstudie av glaciala landformer sydväst om Söderåsen, Skåne, Sverige. (15 hp)
510. Rönning, Lydia, 2017: Ceratopsida dinosauriers migrationsmönster under krittiden baserat på paleobiogeografi och fylogeni. (15 hp)
511. Engleson, Kristina, 2017: Miljökonsekvensbeskrivning Revinge brunnsfält. (15 hp)
512. Ingered, Mimmi, 2017: U-Pb datering av zirkon från migmatitisk gnejs i Delsjöområdet, Idefjordenterrängen. (15 hp)
513. Kervall, Hanna, 2017: EGS - framtidens geotermiska system. (15 hp)
514. Walheim, Karin, 2017: Kvartsmineralogins betydelse för en lyckad luminiscensdatering. (15 hp)
515. Aldenius, Erik, 2017: Lunds Geotermisystem, en utvärdering av 30 års drift. (15 hp)
516. Aulin, Linda, 2017: Constraining the duration of eruptions of the Rangitoto volcano, New Zealand, using paleomagnetism. (15 hp)
517. Hydén, Christina Engberg, 2017: Drumlinerna i Löberöd - Spår efter flera isrörelseriktningar i mellersta Skåne. (15 hp)
518. Svantesson, Fredrik, 2017: Metodik för kartläggning och klassificering av erosion och släntstabilitet i vattendrag. (45 hp)
519. Stjern, Rebecka, 2017: Hur påverkas luminiscenssignaler från kvarts under laboratorieförhållanden? (15 hp)
520. Karlstedt, Filippa, 2017: P-T estimation of the metamorphism of gabbro to garnet amphibolite at Herrestad, Eastern Segment of the Sveconorwegian orogen. (45 hp)
521. Önnervik, Oscar, 2017: Ooider som naturliga arkiv för förändringar i havens geokemi och jordens klimat. (15 hp)
522. Nilsson, Hanna, 2017: Kartläggning av sand och naturgrus med hjälp av resistivitetsmätning på Själland, Danmark. (15 hp)
523. Christensson, Lisa, 2017: Geofysisk undersökning av grundvattenskydd för planerad reservvattentäkt i Mjölkalånga, Hässleholms kommun. (15 hp)
524. Stamsnijder, Joaen, 2017: New geochronological constraints on the Klipriviersberg Group: defining a new Neoarchean large igneous province on the Kaapvaal Craton, South Africa. (45 hp)
525. Becker Jensen, Amanda, 2017: Den eocena Furformationen i Danmark: exceptionella bevaringstillstånd har bidragit till att djurs mjukdelar fossiliserats.(15 hp)
526. Radomski, Jan, 2018: Carbonate sedimentology and carbon isotope stratigraphy of the Tallbacken-1 core, early Wenlock Slite Group, Gotland, Sweden. (45 hp)
527. Pettersson, Johan, 2018: Ultrastructure and biomolecular composition of sea turtle epidermal remains from the Campanian (Upper Cretaceous) North Sulphur River of Texas. (45 hp)
528. Jansson, Robin, 2018: Multidisciplinary perspective on a natural attenuation zone in a PCE contaminated aquifer. (45 hp)
529. Larsson, Alfred, 2018: Rb-Sr sphalerite data and implications for the source and timing of Pb-Zn deposits at the Caledonian margin in Sweden. (45 hp)
530. Balija, Fisnik, 2018: Stratigraphy and pyrite geochemistry of the Lower–Upper Ordovician in the Lerhamn and Fågelsång -3 drill cores, Scania, Sweden. (45 hp)
531. Höglund, Nikolas, 2018: Groundwater chemistry evaluation and a GIS-based approach for determining groundwater potential in Mörbylånga, Sweden. (45 hp)
532. Haag, Vendela, 2018: Studie av mikrostrukturer i karbonatslagkäglor från nedslagsstrukturen Charlevoix, Kanada. (15 hp)
533. Hebrard, Benoit, 2018: Antropocen – vad, när och hur? (15 hp)
534. Jancsak, Nathalie, 2018: Åtgärder mot kusterosion i Skåne, samt en fallstudie av erosionsskydden i Löderup, Ystad kommun. (15 hp)

535. Zachén, Gabriel, 2018: Mesosideriter – redogörelse av bildningsprocesser samt SEM-analys av Vaca Muertameteoriten. (15 hp)
536. Fägersten, Andreas, 2018: Lateral variability in the quantification of calcareous nannofossils in the Upper Triassic, Austria. (15 hp)
537. Hjertman, Anna, 2018: Förutsättningar för djupinfiltration av ytvatten från Ivösjön till Kristianstadbassängen. (15 hp)
538. Lagerstam, Clarence, 2018: Varför svalde svanödlor (Reptilia, Plesiosauria) stenar? (15 hp)
539. Pilser, Hannes, 2018: Mg/Ca i bottenlevande foraminiferer, särskilt med avseende på temperaturer nära 0°C. (15 hp)
540. Christiansen, Emma, 2018: Mikroplast på och i havsbotten - Utbredningen av mikroplaster i marina bottensediment och dess påverkan på marina miljöer. (15 hp)
541. Staahlnacke, Simon, 2018: En sammanställning av norra Skånes prekambriska berggrund. (15 hp)
542. Martell, Josefin, 2018: Shock metamorphic features in zircon grains from the Mien impact structure - clues to conditions during impact. (45 hp)
543. Chitindingu, Tawonga, 2018: Petrological characterization of the Cambrian sandstone reservoirs in the Baltic Basin, Sweden. (45 hp)
544. Chonewicz, Julia, 2018: Dimensionerande vattenförbrukning av grundvatten samt alternativa vattenkvaliteter. (15 hp)
545. Adeen, Lina, 2018: Hur lämpliga är de geofysiska metoderna resistivitet och IP för kartläggning av PFOS? (15 hp)
546. Nilsson Brunlid, Anette, 2018: Impact of southern Baltic sea-level changes on landscape development in the Verkeån River valley at Haväng, southern Sweden, during the early and mid Holocene. (45 hp)
547. Perälä, Jesper, 2018: Dynamic Recrystallization in the Sveconorwegian Frontal Wedge, Småland, southern Sweden. (45 hp)
548. Artursson, Christopher, 2018: Stratigraphy, sedimentology and geophysical assessment of the early Silurian Halla and Klinteberg formations, Altajme core, Gotland, Sweden. (45 hp)
549. Kempengren, Henrik, 2018: Att välja den mest hållbara efterbehandlingsmetoden vid sanering: Applicering av beslutsstödsverktyget SAMLA. (45 hp)
550. Andreasson, Dagnija, 2018: Assessment of using liquidity index for the approximation of undrained shear strength of clay tills in Scania. (45 hp)
551. Ahrenstedt, Viktor, 2018: The Neoproterozoic Visingsö Group of southern Sweden: Lithology, sequence stratigraphy and provenance of the Middle Formation. (45 hp)
552. Berglund, Marie, 2018: Basaltkuppen - ett spel om mineralogi och petrologi. (15 hp)
553. Hernnäs, Tove, 2018: Garnet amphibolite in the internal Eastern Segment, Sveconorwegian Province: monitors of metamorphic recrystallization at high temperature and pressure during Sveconorwegian orogeny. (45 hp)
554. Halling, Jenny, 2019: Characterization of black rust in reinforced concrete structures: analyses of field samples from southern Sweden. (45 hp)
555. Stevic, Marijana, 2019: Stratigraphy and dating of a lake sediment record from Lyngsjön, eastern Scania - human impact and aeolian sand deposition during the last millennium. (45 hp)
556. Rabanser, Monika, 2019: Processes of Lateral Moraine Formation at a Debris-covered Glacier, Suldenferner (Vedretta di Solda), Italy. (45 hp)
557. Nilsson, Hanna, 2019: Records of environmental change and sedimentation processes over the last century in a Baltic coastal inlet. (45 hp)
558. Ingered, Mimmi, 2019: Zircon U-Pb constraints on the timing of Sveconorwegian migmatite formation in the Western and Median Segments of the Idefjorden terrane, SW Sweden. (45 hp)

LUNDS UNIVERSITET

Geologiska institutionen
Lunds universitet
Sölvegatan 12, 223 62 Lund